Russian Original Vol. 30, No. 4, April, 1971

Translation published November, 1971

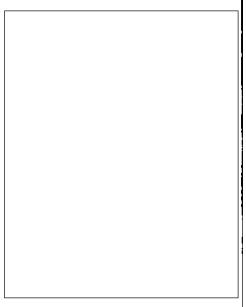

ILLEGIB

SOVIET ATOMIC ENERGY

АТОМНАЯ ЭНЕРГИЯ
(ATOMNAYA ÉNERGIYA)

TRANSLATED FROM RUSSIAN

CONSULTANTS BUREAU, NEW YORK

SOVIET ATOMIC ENERGY

Soviet Atomic Energy is a cover-to-cover translation of *Atomnaya Énergiya*, a publication of the Academy of Sciences of the USSR.

An arrangement with Mezhdunarodnaya Kniga, the Soviet book export agency, makes available both advance copies of the Russian journal and original glossy photographs and artwork. This serves to decrease the necessary time lag between publication of the original and publication of the translation and helps to improve the quality of the latter. The translation began with the first issue of the Russian journal.

Consultants Bureau journals appear about six months after the publication of the original Russian issue. For bibliographic accuracy, the English issue published by Consultants Bureau carries the same number and date as the original Russian from which it was translated. For example, a Russian issue published in December will appear in a Consultants Bureau English translation about the following June, but the translation issue will carry the December date. When ordering any volume or particular issue of a Consultants Bureau journal, please specify the date and, where applicable, the volume and issue numbers of the original Russian. The material you will receive will be a translation of that Russian volume or issue.

Subscription
$67.50 per volume (6 Issues)
2 volumes per year
(Add $5 for orders outside the United States and Canada.)

Single Issue: $30
Single Article: $15

CONSULTANTS BUREAU, NEW YORK AND LONDON

227 West 17th Street
New York, New York 10011

Davis House
8 Scrubs Lane
Harlesden, NW10 6SE
England

Second-class postage paid at Jamaica, New York 11431.

SOVIET ATOMIC ENERGY

A translation of *Atomnaya Énergiya*
Translation published November, 1971

Volume 30, Number 4 April, 1971

CONTENTS

CONTENTS

(continued)

CONTENTS

(continued)

The Russian press date (podpisano k pechati) of this issue was 4/2/1971. Publication therefore did not occur prior to this date, but must be assumed to have taken place reasonably soon thereafter.

ON THE EXPEDIENCY OF OPERATING AN ATOMIC-POWER STATION AT A REDUCED POWER BEFORE RECHARGING

Yu. I. Mityaev

UDC 621.039.566

The majority of atomic-power-station reactors have a negative power coefficient of reactivity α, ensuring the safe and stable operation of the reactors. Hence on reducing the power of the reactor a certain amount of reactivity is released, and this may be used for the production of additional electrical energy and for increasing the extent of fuel burn-up. Clearly this kind of operation is only possible for atomic-power stations working in the basic mode, a reduction in power only being expedient after the exhaustion of the reserve of reactivity for burn-up, i.e., immediately before the recharging of the fuel.

Certain atomic-power stations are in fact now operated with a reduced power prior to recharging [1, 2]. Usually in this case the operation of the reactor is conducted as follows. After extracting all the absorbers, the reactor is changed to the self-regulating mode of operation, in which the reduction in reactivity due to the burn-up of the fuel is compensated by a spontaneous reduction in reactor power. Thus the atomic-power station of the "Yankee Atomic" company (electrical power 200 MW) was regularly operated at a reduced power before recharging in 1961-1965 (four times). The maximum power reduction was 75 MW (electrical). Altogether more than 1 billion kW · h of electrical power was developed in the low-power mode over this period [1]. In the fourth operation of the Novo-Voronezh atomic-power station, an additional 110 million kW · h of electrical power were developed by reducing the power from 210 to 160 MW [2].

Let us determine the conditions under which the operation of an atomic-power station in the mode under consideration will be economically desirable, understanding this to mean a reduction in the net cost of producing electrical energy C. For this purpose we may consider the operation of the atomic-power station under conditions of regular partial fuel recharging, with and without reducing the power from N_0 to N_n before each recharging (Fig. 1). In order to simplify the problem let us assume the following: 1) the reactor is charged with identical fuel channels, the construction and manufacturing technology of which admit a certain increase in the extent of burn-up of the fuel; 2) the neutron breeding factor k_{eff} is a linear function of the burn-up of the fuel channels: $k_{eff} = K_0 - K_1 S$; this is quite frequently the case in the practice of reactor building [3] (the notation is also that of the earlier paper [3]); 3) the operation of the atomic-power station does not require any additional store of reactivity in order to avoid the "iodine depression," smoothing of the power distribution of the fuel channels, and so on; 4) the atomic power station is operated without the reprocessing and secondary use of the burnt-up fuel, which is a characteristic feature of modern nuclear-power techniques.

In contrast to an earlier paper [4], we shall compare the operation of the atomic-power station with and without a reduction in power before recharging for the two cases of greatest practical interest: for the same production of electrical power between rechargings, and for the same proportion of recharged fuel channels.

Case 1. Production of Electrical Power between Rechargings (with and without Reducing the Power of the Atomic-Power Station) Kept Constant and Equal to E_0 GW · h. In the reduced-power mode, $(E_0 - \Delta E)$ GW · h of electrical energy are produced with the atomic-power station working at a power of N_0, and ΔE GW · h are produced with the power station working at a power of ΔN lower than this, the difference being $\Delta N = N_0 - N_p$ MW; here $\Delta E = \Delta N \alpha$, where the coefficient α may be expressed as the amount of electrical energy developed by the power station on reducing its power by 1 MW (electrical). For example, in the case of the Novo-Voronezh and "Yankee Atomic" power stations, the value of α is 2.2 and 5.5 GW · h/MW

Translated from Atomnaya Énergiya, Vol. 30, No. 4, pp. 339-343, April, 1971. Original article submitted August 10, 1970.

TABLE 1. Reduction in the Net Cost of Electrical Energy $\Delta C/C$ and Increase in the Burn-Up of the Discharged Fuel $(S'_{max}-S_{max})/S_{max}$ on Operating an Atomic-Power Station with the Optimum Reduction in Power before Fuel Recharging, for N_0 = 200 MW, E_0 = 1200 GW·h, and $\eta = 1/3$

$c_т$	Characteristics	α = 2 GW·h/MW		α = 4 GW·h/MW		α = 6 GW·h/MW	
		case 1	case 2	case 1	case 2	case 1	case 2
$2C_p$	$\frac{\Delta C}{C}$, %	4,99	3,48	8,47	6,41	11,1	8,93
	ΔN_{opt}, MW	~ 120	113,4	~ 107	110,1	~ 98	107,2
	$\frac{S'_{max}-S_{max}}{S_{max}}$, %	13,3	9,45	23,8	18,4	32,7	26,8
C_p	$\frac{\Delta C}{C}$, %	2,41	1,59	4,26	3,01	5,76	4,29
	ΔN_{opt}, MW	~ 80	71,7	~ 73	70,1	~ 67	68,6
	$\frac{S'_{max}-S_{max}}{S_{max}}$, %	8,9	6,0	16,2	11,7	22,3	17,2
$0,5C_p$	$\frac{\Delta C}{C}$, %	0,96	0,60	1,76	1,16	2,45	1,68
	ΔN_{opt}, MW	~ 49	41,6	~ 46	41,0	~ 43	40,4
	$\frac{S'_{max}-S_{max}}{S_{max}}$, %	5,4	3,5	10,2	6,8	14,3	10,1

(electrical) respectively [1, 2]. In the operating mode without a reduction in power, the burn-up of the discharged fuel channels [3] is equal to

$$S_{max} = S_0 \frac{2}{1+\eta},$$

where η is the proportion of recharged fuel channels, $S_0 = (K_0-1)/K_1$ is the burn-up of the fuel channels for the complete recharging of the reactor, i.e., for $\eta = 1$. The changes in the burn-up and k_{eff} in recharging will [3] be equal to $\Delta S = S_{max}\eta$ and $\Delta k_{eff} = K_1 S_{max}\eta$. The operation of the atomic-power station at a reduced power is equivalent to an increase of δk_{eff} in the neutron-breeding coefficient, proportional to ΔE. In this mode of operation (indicated by a prime), the burn-up of the discharged fuel channels equals

$$S'_{max} = S'_0 \frac{2}{1+\eta'} = \frac{K_0-1+\delta k_{eff}}{K_1} \cdot \frac{2}{1+\eta'} = \left(S_0 + \frac{\delta k_{eff}}{K_1}\right) \frac{2}{1+\eta'}$$

$$= S_0 \left(1 + \frac{\delta k_{eff}}{\Delta k_{eff}} \cdot \frac{2\eta}{1+\eta}\right) \frac{2}{1+\eta'} = S_0 \left(1 + \frac{\Delta E}{E_0} \cdot \frac{2\eta}{1+\eta}\right) \frac{2}{1+\eta'}.$$

Since the two modes of operation are being compared for the same production of electrical energy, we have $\Delta S' = \Delta S$ or $\Delta S = S_{max}\eta = S_0(2\eta/1+\eta)$ and $\Delta S' = S'_{max}\eta' = S_0(1 + (\Delta E/E_0)(2\eta/1+\eta))(2\eta'/1+\eta')$. It follows from the latter two relationships that

$$\eta' = \eta \frac{E_0}{E_0 + 2\Delta E\eta};$$

$$S'_{max} = S_{max}\left(1 + 2\frac{\Delta E}{E_0}\eta\right).$$

The ratio of the fuel components of the net cost of the electrical energy is inversely proportional to the burn-up of the discharged fuel channels; hence

$$\frac{C'_т}{C_т} = \frac{S'_{max}}{S_{max}} = 1 + 2\frac{\Delta E}{E_0}\eta$$

and the reduction in the fuel component is

$$\Delta C_т = C_т - C'_т = C_т \frac{2\Delta E\eta}{E_0 + 2\Delta E\eta} = C_т \frac{2\Delta N\alpha\eta}{E_0 + 2\Delta N\alpha\eta}.$$

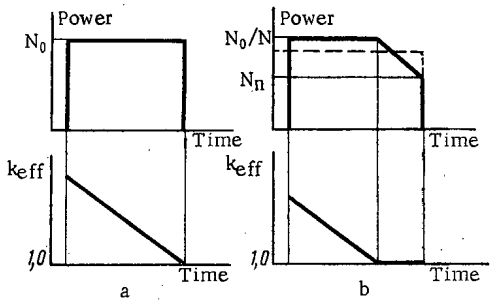

Fig. 1

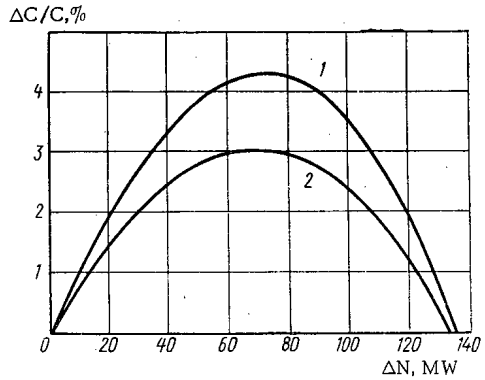

Fig. 2

Fig. 1. Loading graph and change in the effective neutron-breading factor k_{eff} during the operation of an atomic-power station between fuel rechargings, with and without reducing the power before recharging (b and a respectively).

Fig. 2. Relative change in the net cost of electrical energy $\Delta C/C$ as a function of the reduction in power before recharging ΔN for the first (1) and second (2) cases with $C_T = C_p$; $\eta = 1/3$; $E_0 = 1200$ GW · h; $N_0 = 200$ MW; $\alpha = 4$ GW · h/MW.

However, on working at a reduced power, the constant component of the cost of the electrical energy increases and is equal to

$$C'_p = C_p \frac{N_0}{\overline{N}},$$

where $\overline{N} = E_0/[(E_0-\Delta E)/N_0 + 2\Delta E/(2N_0-\Delta N)]$ is the average power of the reactor in the reduced-power mode. Here we allow for the fact that, in this mode, the reduction in power from N_0 to N_p takes place almost in accordance with a linear law [1, 2]. The increase in the constant component is

$$\Delta C_p = C_p \frac{\Delta N \alpha}{E_0} \cdot \frac{\Delta N}{2N_0 - \Delta N}.$$

Thus the reduction in the total net cost of the electrical energy is given by the equation

$$\Delta C = \Delta C_T - \Delta C_p = \alpha \Delta N \left(\frac{2C_T \eta}{E_0 + 2\Delta N \alpha \eta} - \frac{C_p}{E_0} \frac{\Delta N}{2N_0 - \Delta N} \right). \quad (1)$$

Case 2. Proportion of Recharged Fuel Channels (with or without Reducing the Power of the Atomic-Power Station) Kept Constant and Equal to η. In this case the burn-up of the discharged fuel channels will also be greater in the reduced-power mode S'_{max} than in the absence of power reduction (S_{max}):

$$\frac{S'_{max}}{S_{max}} = \frac{S'_0}{S_0} = \frac{S_0 + \frac{\delta k_{eff}}{K_1}}{S_0} = 1 + \frac{1}{S_0} \cdot \frac{\delta k_{eff}}{\Delta k_{eff}} \cdot S_{max} \eta = 1 + \frac{\delta k_{eff}}{\Delta k_{eff}} \cdot \frac{2\eta}{1+\eta} = 1 + \frac{\Delta E}{E_0} \cdot \frac{2\eta}{1+\eta}.$$

Hence the reduction in the fuel component is equal to

$$\Delta C_T = C_T - C'_T = C_T - \frac{C_T}{1 + \frac{\Delta E}{E_0} \cdot \frac{2\eta}{1+\eta}} = C_T \frac{2\Delta N \alpha \eta}{E_0(1+\eta) + 2\Delta N \alpha \eta}.$$

Since the proportion of the recharged fuel channels is the same for both modes of operation, the production of electrical energy between the rechargings will be proportional to the burn-up of the discharged fuel channels:

$$\frac{E'_0}{E_0} = \frac{S'_{max}}{S_{max}} = 1 + \frac{\Delta E}{E_0} \cdot \frac{2\eta}{1+\eta}.$$

Hence the average power in the reduced-power mode will be given by the equation

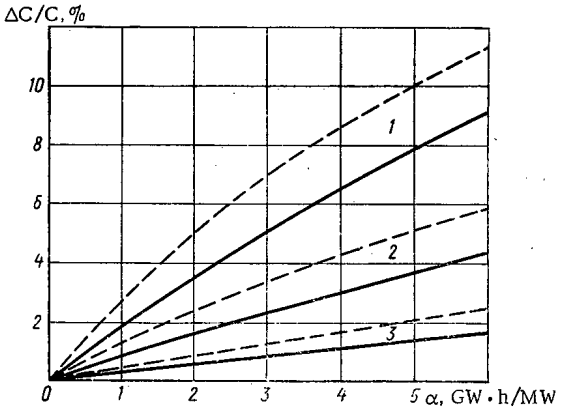

Fig. 3

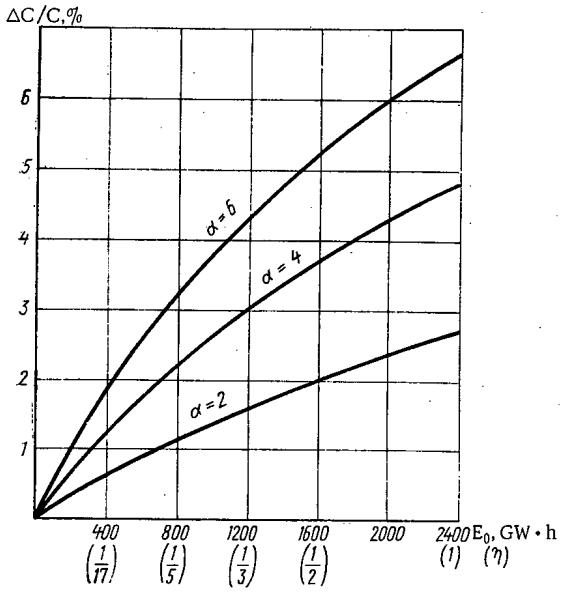

Fig. 4

Fig. 3. Relative reduction in the net cost of electrical energy on operating on atomic-power station with the optimum reduction in power before recharging for the first (– – –) and second (———) cases, with N_0 = 200 MW, E_0 = 1200 GW·h: 1) $C_T = 2C_p$; 2) $C_T = C_p$; 3) $C_T = 0.5C_p$.

Fig. 4. Relative fall in the net cost of electrical energy on operating an atomic-power station at a lower power before recharging (second case) in relation to the development of energy between the rechargings, with N_0 = 200 MW, $C_T = C_p$ (for corresponding proportions of recharged channels) and α equal to 6, 4, and 2GW·h/MW.

$$\bar{N} = \frac{E_0'}{\frac{E_0' - \Delta E}{N_0} + \frac{2\Delta E}{2N_0 - \Delta N}} = \frac{E_0 + \frac{2\Delta N \alpha \eta}{E_0(1+\eta)}}{\frac{E_0 - \Delta E \frac{1-\eta}{1+\eta}}{N_0} + \frac{2\Delta N \alpha}{2N_0 - \Delta N}},$$

and the increase in the constant component will be

$$\Delta C_p = \frac{1}{2N_0 - \Delta N} \cdot \frac{C_p \alpha \Delta N^2 (1+\eta)}{E_0(1+\eta) + 2\Delta N \alpha \eta}.$$

Thus in this case the reduction in the total net cost of electrical power will be:

$$\Delta C = \Delta C_T - \Delta C_p = \frac{\Delta N \alpha}{E_0(1+\eta) + 2\Delta N \alpha \eta}\left[2C_T\eta - \frac{C_p \Delta N (1+\eta)}{2N_0 - \Delta N}\right]. \quad (2)$$

It follows from formulas (1) and (2) that the reduction in the net cost of the electrical energy depends on the power coefficient of reactivity, the ratio of the constant and fuel components, and the production of electrical energy between the rechargings. It follows moreover from both formulas that, on operating atomic-power stations at a reduced power, there is a certain optimum value ΔN_{opt} for which the reduction in the net cost of the electrical energy reaches a maximum (Fig. 2). For the second case the condition $d\Delta C/d\Delta N = 0$ readily yields an equation for determining ΔN_{opt}:

$$\Delta N_{opt}^2 \{[2C_T\eta + C_p(1+\eta)]E_0 - 4N_0 C_p \alpha \eta\} - \Delta N_{opt} 4N_0 E_0 [2C_T\eta + C_p(1+\eta)] + 8N_0^2 E_0 C_T \eta = 0. \quad (3)$$

In order to obtain quantitative results, we considered a reactor with characteristics similar to those of the Novo-Voronezh and "Yankee Atomic" power-station reactors. The change in the net cost of electrical energy on operating the reactor at reduced power before recharging was studied in relation to the power coefficient of reactivity and the ratio of the constant and fuel components of the net cost of electrical energy. The results of the calculations are presented in Table 1 and Fig. 3. It follows from Table 1 and Fig. 3 that the operation of the atomic-power station with a reduced power before recharging enables us to reduce the net cost of electrical energy by an average of several percent. It should be noted that the economical effect will be somewhat smaller if we use, not the net cost of the electrical energy, but the reduced-expenditure index, now widely employed in economic calculations [5] as an economic index. This is due to the fact

that, on increasing the extent of burn-up, the fuel component of the reduced expenditure will fall more slowly than the fuel component of the net cost, since the run time of the fuel channels will increase with increasing burn-up, and hence so will the charges for the nuclear fuel.

Of the two cases considered, the former is the more advantageous. This is evidently due to the fact that, in the first case, the proportion of recharged channels is slightly smaller than in the second, which leads to a greater reduction in the fuel component.

On operating atomic-power stations with a reduced power before recharging, the reserve of reactivity for burn-up between rechargings diminishes, slightly more so in the first case than in the second.

Thus, on operating atomic-power stations with a reduced power before recharging, the unproductive losses of neutrons in the absorbing control rods diminish, i.e., the advantages of this mode are due to the same causal factors as the advantages of the operating mode with partial rechargings of the fuel. Thus if the mode under consideration is advantageous for regular partial rechargings it will also be advantageous during the transient stage, as well as on operating the atomic-power stations with repeated use of the fuel channels.

Hence the reduction in the net cost of the electrical energy on operating atomic-power stations at a reduced power before recharging will be the greater, the greater the development of electrical energy between the rechargings, i.e., the greater the proportion of channels recharged. This conclusion is illustrated by the computed data presented in Fig. 4.

The operation of atomic-power stations at a reduced power before fuel recharging is most expedient for light-water reactors of the vessel type, with relatively large power coefficients of reactivity; the proportion of the recharged fuel channels is much greater in these than in channel reactors, being approximately equal to 1/3. In this case the increase in the burn-up of the discharged fuel becomes very substantial (Table 1); the question as to the permissibility of such an increase in burn-up accordingly assumes a new importance.

In conclusion, the author wishes to thank V. K. Vikulov, A. D. Zhirnov, V. S. Smirnov, and V. M. Shuvalov for interest in the work and useful comments, and L. G. Khristoforova for carrying out the calculations.

LITERATURE CITED

1. F. Ya. Ovchinnikov, L. M. Voronin, and L. I. Golubev, At. Énerg., 27, 274 (1969).
2. A. Weckesser, Atomwirtschaft, 13, 190 (1968).
3. E. I. Grishanin, B. G. Ivanov, and V. N. Sharapov, At. Énerg., 10, 565 (1961).
4. A. Ya. Kramerov et al., At. Énerg., 17, 427 (1964).
5. V. V. Batov and Yu. I. Koryakin, Economics of Nuclear Power [in Russian], Atomizdat, Moscow (1960).

DESIGN AND OPTIMIZATION OF ION EXCHANGE FOR DEMINERALIZATION OF WATER FOR NUCLEAR REACTORS

I. V. Komarova, V. A. Nikashina,
R. N. Rubinshtein, and M. M. Senyavin

UDC 541.183+621.039

Ion exchange is of well-established importance in the processing of water for thermal and atomic electric power stations [1-3]. The large requirements of power stations for purified water, the stringent demineralization requirements, and the tendency to reduce consumption of materials, reagents, and labor to the economic limit all make it necessary to optimize the process of demineralization by ion exchange. For water of given composition and a plant of given output, it is necessary to solve the problems of choosing the ion-exchange resin, its amount and granularity, and the optimum water feed rate.

It is natural that optimization of such a complex group of parameters in multicomponent nonequilibrial ion-exchange systems cannot be solved by direct experiment, but requires computational data. The dynamics of ion-exchange sorption of multicomponent mixtures is represented, in the usual notation, by the following well-known system of differential equations:

$$-v\frac{\partial c_i}{\partial x}+\varkappa D\frac{\partial^2 c_i}{\partial x^2}=\frac{\partial a_i}{\partial t}+\varkappa\frac{\partial c_i}{\partial t}$$ is the balance equation; (1)

$$\frac{\partial a_i}{\partial t}=\varphi(c_1, c_2, \ldots, c_i; a_1, a_2, \ldots, a_i; v, r)$$ is the equation of kinetics; (2)

$$a_i=f(c_1, c_2, \ldots, c_i)$$ is the equation of the ion-exchange isotherm (3)

Equations (1)-(3) are solved for given initial conditions, $a_i(x, 0)=\psi(x)$, and given boundary conditions, $c_i(0, t)=\xi(t)$. However, so far this system of equations has not been solved in general form for exchange of mixtures of ions, owing to the mathematical difficulties.

In this article we describe possible approaches to the problem of ion-exchange demineralization of water in separate beds of ion-exchange resin, and the design analysis and optimization of this process. We discuss optimization of the process for a sorption cycle with a completely regenerated column. This problem, in particular, arises in the nuclear industry, in which the resin is used only once in production owing to its poor stability. Anyway, this problem is the first stage in any process of ion-exchange demineralization.

The method of calculation for sorption of mixtures which we shall describe and discuss in this article is based on a law established as a result of layer-by-layer calculations for many systems [4]. The law is that sorption of the least-sorbed ion in the parallel-transfer stage does not depend on the nature and concentration ratio of the other components in the mixture, but depends only on their total concentration. Thus the problem of sorption of a mixture of ions on an ion-exchange column can be reduced to the problem of sorption of the one least-sorbed ion of the mixture. Previously [5] we have suggested a direct method of calculating the dynamics of sorption of one-component systems, characterized by any exchange constant, in the region of external-diffusion kinetics.

Our results were plotted as a family of yield curves in dimensionless coordinates:

$$\left.\begin{aligned} u-T\ \left(u=\frac{c}{c_0}\right),\\ q-X\ \left(q=\frac{a}{a_0}\right)\end{aligned}\right\} \quad (4)$$

for various values of the exchange constant k_{ij}.

Translated from Atomnaya Énergiya, Vol. 30, No. 4, pp. 343-347, April, 1971. Original article submitted May 11, 1970; revision submitted October 26, 1970.

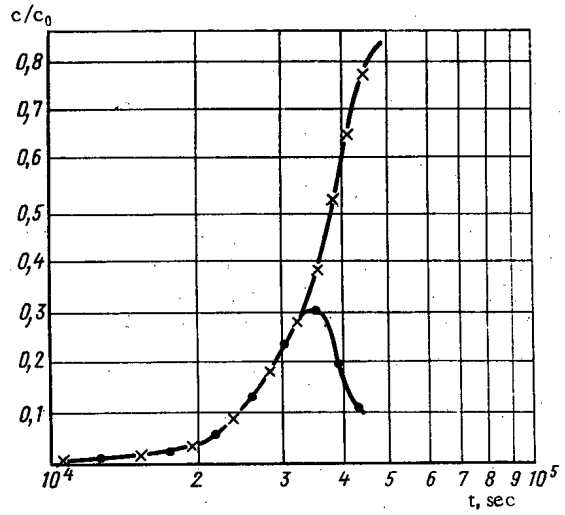

Fig. 1

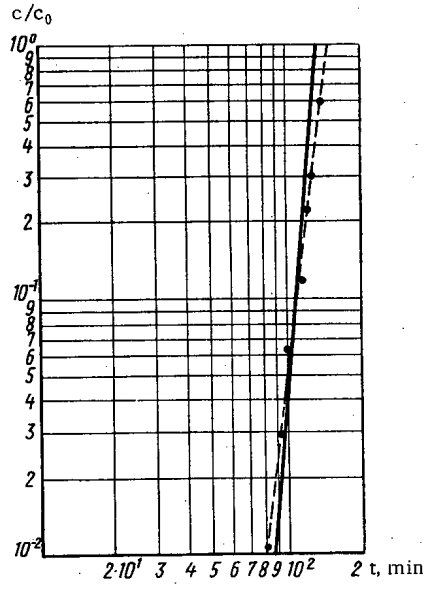

Fig. 2

Fig. 1. Theoretical (×) and experimental (•) yield curves of sodium for cation exchange of water.

Fig. 2. Theoretical (——) and experimental (– – –) yield curves of chloride during anion exchange of water.

In water processing we are dealing with dilute solutions; therefore, as we have shown, the kinetics of ion-exchange demineralization of water will also be governed by external diffusion. Therefore to analyze the sorption of the least-sorbed ion we used a method described in [5] for a one-component system. The initial data for solving this problem are the exchange constant of the least-sorbed ion (or its sorption isotherm) and its kinetic coefficient.

Let us successively consider two stages of demineralization – cation exchange and anion exchange – taking as an example the purification of chloride–sulfate water. In this case, in cation exchange the least-sorbed ion is sodium. As we have shown [6], sorption of sodium on the hydrogen form of KU-2 cation exchanger follows the Langmuir isotherm with an exchange constant of 1.25 [4]. The kinetic coefficient β which depends on the flow rate v and the granularity d is given by

$$\beta = 0.009\omega \frac{v^{0.5}}{d^{1.5}}. \qquad (5)$$

For sodium $\omega = 1$. With the aid of dimensionless graphs, for k = 1.25, by the above-described method [5] we obtained the theoretical yield curve of sodium, which is plotted in Fig. 1. For comparison the same graph shows the experimental yield curve of sodium from the mixture. We see that the experimental and theoretical curves agree up to $c/c_0 = 0.3$. The maximum on the experimental yield curve is due to mutual displacement during exchange of a mixture of ions.

In the anion-exchange stage the least-sorbed ion is the chloride ion. Let us consider the shape of the exchange isotherm of the chloride ion on an anion exchanger in the OH form in the presence of hydrogen ions, i.e., in the case of exchange accompanied by neutralization.

The exchange isotherm of chloride in dimensionless variables is

$$q = \frac{\frac{Kuc_0}{c_{OH}}}{1 + \frac{Kc_0u}{c_{OH}}}. \qquad (6)$$

Here the right-hand side can be transformed in conformity with the condition of electrical neutrality, $c_{OH} + c_{Cl} = c_H$; thus $c_{OH} = c_H - c_{Cl}$. Clearly, $c_{Cl} \to 0$ in the first stage of sorption (initial section of the isotherm), therefore $c_{OH} = c_H$ and c_{OH} can be found from the equation $c_{OH} = c_H = \sqrt{K_w}$ or $c_{OH} = \sqrt{K_w}$; then the

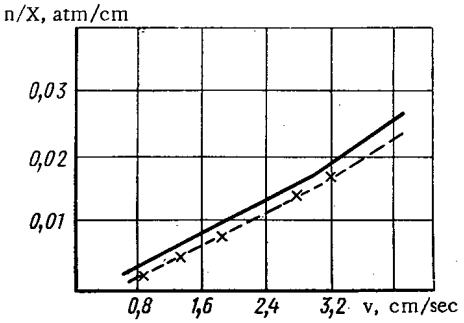

Fig. 3. Hydraulic resistance versus flow rate (bed depth 50 cm, grain diameter 0.04 cm).

isotherm takes the form

$$q = \frac{\frac{Kc_0}{\sqrt{K_w}}u}{1+\frac{Kc_0}{\sqrt{K_w}}u}. \quad (7)$$

Let us define a coefficient $K_{eff} = Kc_0/\sqrt{K_w}$. Then

$$q = \frac{K_{eff}\,u}{1+K_{eff}\,u}, \quad (8)$$

where K_{eff} is the gradient of the initial section of the isotherm of q versus u. It is known that if sorption follows the Langmuir isotherm, then when $K_{eff} \geq 10$ the isotherm practically merges with the axis of ordinates, i.e., the sorption process is represented by a nearly rectangular isotherm. Since $K_{eff} = Kc_0/\sqrt{K_w}$, therefore $K_{eff} \geq 10$ if $c_0 \geq 5 \cdot 10^{-7}$ N. We are considering $c_0 = 5 \cdot 10^{-5}$–$5 \cdot 10^{-6}$ N; the kinetic coefficient of the chloride ion was calculated from Eq. (5), which gave $\omega_{Cl} = 1.1$.

Figure 2 shows the theoretical and experimental yield curves for sorption of the chloride ion on AV-17 anion exchanger in the OH form; the curves show good agreement. The above mathematical model was here supplemented by the equation giving the hydraulic resistance h of the ion-exchanger bed in terms of the experimental parameters. This equation, according to Bennet and Mayers [7], takes the form

$$h = \frac{(150/Re + 1.75)\,xv^2(1-\varkappa)\,j}{d\varkappa^3}, \quad (9)$$

for any granular material; here j is the density of the solution in kg/cm^3, and $\varkappa$ is the porosity of the sorbent.

To verify this approximate dependence of the hydraulic resistance on the flow rate, we performed an experiment with a fairly wide range of velocities (0.8-4.0 cm/sec) for a bed of KU-2 cation exchanger, 50 cm in height, with a mean grain diameter of 0.04 cm (Fig. 3).

All the results so obtained confirm the adequacy of the mathematical model adopted, and we can thus use it to find the optimal conditions.

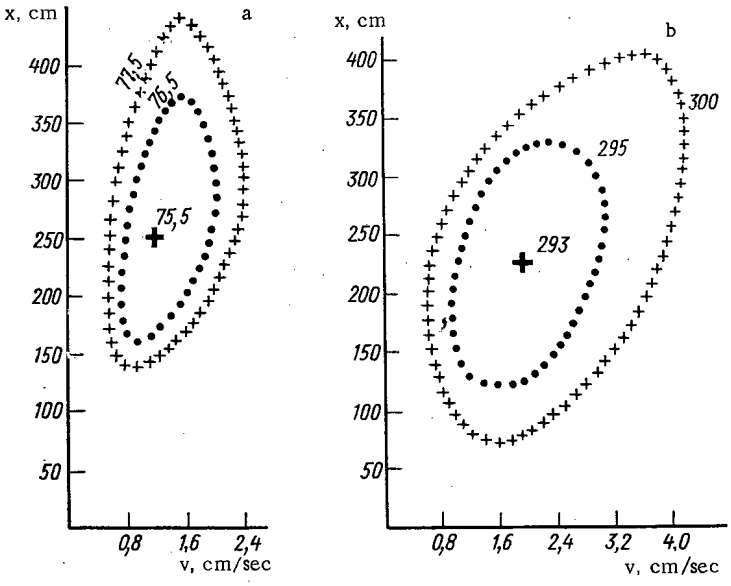

Fig. 4. Contour lines of optimization criterion Y for varying flow rate and bed depth ($c_0 = 5 \cdot 10^{-5}$ N, $c/c_0 = 0.01$, output 200 m^3/h, d = 0.05 cm). a) Cation exchange; b) anion exchange.

TABLE 1. Optimum Sorption Conditions, with Ion Exchanger Replaced after Each Cycle, for Various Types of Water and Various Degrees of Purification (Output 200 m^3/h)

	Cation exchanger			Anion exchanger		
c_0, N	$5 \cdot 10^{-5}$	$5 \cdot 10^{-6}$	$5 \cdot 10^{-5}$	$5 \cdot 10^{-5}$	$5 \cdot 10^{-6}$	$5 \cdot 10^{-5}$
c, N	$5 \cdot 10^{-7}$	$5 \cdot 10^{-7}$	$5 \cdot 10^{-6}$	$5 \cdot 10^{-7}$	$5 \cdot 10^{-7}$	$5 \cdot 10^{-6}$
c/c_0	0,01	0,1	0,1	0,01	0,1	0,1
v, cm/sec	1,2	2,0	1,2	2,0	2,0	2,0
x, cm	250	50	175	225	75	125
Y, thousand rubles	75,5	9,85	71,4	293	30,58	285,9

We calculated the optimal conditions with the aid of a computer, by the above scheme, with the optimization criterion [8]:

$$Y = E_C\lambda + E_M + E_a + E_{el}, \qquad (10)$$

where E_C is the capital cost in thousands of rubles, $E_C = f(v, x)$; λ is the normative cost recovery time; E_M is the cost of materials (replacement of ion exchanger after each cycle of water purification) in thousands of rubles, $E_M = f_1(v, x)/t_{fc}(v, x, d)$; E_a is the depreciation cost in thousands of rubles, $E_a = f_2(E_C)$; and E_{el} is the cost of electrical energy in thousands of rubles, $E_{el} = f_3(v, x, d)$.

The process of sorption on a fully regenerated column is characterized by three input variables: the flow rate v, the ion-exchange resin grain diameter d, and the bed depth x. We looked for the optimum in the following ranges of these variables: $0.4 \le v \le 6$ cm/sec; $0.05 \le d \le 0.1$ cm; and $25 \le x \le 300$ cm.

We found that the optimum grain diameter was the lower limiting value. This is because as the grain size decreases, the cost of materials E_M, which depends on the filtration cycle duration t_{fc}, decreases more rapidly than the rise in the cost of electrical energy E_{el}, which is governed by the pressure drop. Thus we needed to seek the optimum only in the two variables v and x. Figure 4 plots contour lines of the optimization criterion Y with varying v and x for a plant of output 200 m^3/h with d = 0.05 cm, $c_0 = 5 \cdot 10^{-5}$ N, $c/c_0 = 0.01$. In this case for cation columns the optimal conditions are v = 1.2 cm/sec, x = 250 cm; for anion columns they are v = 2.0 cm/sec, x = 225 cm. From these data we can assess also the gradient of the optimization criterion.

We also calculated the optimum conditions for purification processes characterized by various initial salt contents and degrees of purification. The results are listed in Table 1.

From Table 1 the following results follow.

a) If the degree of demineralization is constant (c/c_0 = const), as the salt content of the original water is reduced, it is advisable to increase the flow rate and reduce the bed depth, i.e., the operating conditions of the column should be changed at each stage in multistage demineralization.

In addition, this change of the parameters involves a marked change in the absolute value of the optimization criterion.

b) For a given output water quality (c = const), as the original salt content decreases, the optimum velocity increases and the bed depth decreases.

c) For a given original salt content (c_0 = const), as the required degree of water purification increases, the bed depth must be increased and the linear velocity decreased.

d) Comparison between the operating conditions of anion-exchange and cation-exchange columns shows that the optimum conditions for anion exchangers are displaced towards higher velocities and shallower columns in comparison with cation exchangers with the same water and degree of purification.

As the output increases, the position of the optimum point shifts towards lower velocities and higher bed depths. The optimization criterion increases with increasing output according to a nearly linear law (to within a few percent).

LITERATURE CITED

1. F. G. Prokhorov and M. S. Shkrob, Water Preparation and Water Conditions of Steam-Turbine Power Stations [in Russian], Gosénergoizdat, Moscow–Leningrad (1951).
2. A. A. Kastal'skii, Projected Plants for Chemical Desalting of Water [in Russian], Stroiizdat, Moscow (1964).
3. A. A. Kot, Water Preparation and Water Conditions of Atomic Power Stations [in Russian], Atomizdat, Moscow (1964).
4. N. K. Galkina and M. M. Senyavin, Zh. Fiz. Khim., 43, 1783 (1969).

5. V. A. Nikashina, R. N. Rubinshtein, and M. M. Senyavin, Abstracts of Reports to All-Union Conference: Inorganic Ion-Exchange Materials [in Russian], Leningrad (1970), p. 8.
6. V. A. Nikashina and B. I. Volkov, The Theory of Ion Exchange and Chromatography [in Russian], Nauka, Moscow (1968), p. 166.
7. K. O. Bennet and J. E. Mayers, Hydrodynamics, Heat Exchange, and Mass Exchange [Russian translation], Nedra, Moscow (1966).
8. I. V. Komarova, R. N. Rubinshtein, and M. M. Senyavin, Proceedings of Scientific-Technical Conference on Water Purification [in Russian], Izd-vo Voronezh. Gos. Un-ta, Voronezh (1961), p. 6.

PURIFICATION OF CIRCULATING WATER BY DISTILLATION

V. F. Bagretsov and S. I. Zakharov

UDC 621.15:621.039.714

Water in the primary circuits of the reactors and cooling ponds at the NIIAR Institute is purified by distillation in VN evaporation apparatus [1]. The steam is purified by a separation plant consisting of two wash plates and one equalizing plate. The first results of operation of the evaporation plant were published in [2]. In this article we give data describing how the quantity of distillate obtained is affected by the level of the evaporated solution, the throughput of the apparatus, the quantity of reflux, the concentrations of salts in the evaporated solution, and the pressure of the secondary steam. Before the investigation certain changes were made in the plant design. 1) In the reflux overflow tubes we installed water seals 250 mm high (eliminating the possibility of steam leaking from the evaporator into the separator except via the washing plates). 2) Initial solution was fed into the lower part of the circulation tube. 3) A salt-meter with sensor was installed following the condenser to permit continuous monitoring of the quality of the distillate. Auxiliary devices were installed on the control board.

The chemical and radiochemical compositions of the initial solutions were the same as before [2]. The results of the experiments are listed in Tables 1-4.

The volume of the separator between the liquid being concentrated and the washing plate was large (4.8 m^3), and it might have appeared that a slight change in this volume (5-7.5%), due to changes in the level of the liquid being concentrated, would not have much effect on purification of the steam. However, from Table 1 we see that when the level of the liquid being concentrated varied by 300-450 mm, the radioactive-element content of the steam changed by a factor of three. Thus in our apparatus the optimal "cold" level must be taken as that lying 300-400 mm below the square junction flange between the heating chamber and the separator. The results of this experiment give grounds to affirm that changes in the volume of the vapor space of the separator are inadvisable.

From Table 2 we see that increasing the reflux flow rate above 5.0% (for each plate) has little influence on the degree of decontamination of the steam. Other conditions being constant, increase in the pressure of the secondary steam leads to improvement in purification of the steam, because the linear velocity of the steam then decreases. A washing plant of irregular type permits the output of the plant to be increased by a factor of 1.5 if necessary. In this case the degree of purification of the steam is not appreciably reduced. This is yet another advantage of having washing plates before the glass fiber.

TABLE 1. Influence of "Cold" Level of Evaporated Liquid on Quality of Distillate

Level of liquid in evaporator, mm	Specific activity, Ci/liter		
	distillate	reflux from middle plate	reflux from upper plate
—180	$3 \cdot 10^{-9}$	$9{,}4 \cdot 10^{-8}$	$6 \cdot 10^{-8}$
—100	$2{,}6 \cdot 10^{-9}$	$1{,}6 \cdot 10^{-7}$	$4{,}2 \cdot 10^{-8}$
—50	$3{,}1 \cdot 10^{-9}$	$1{,}1 \cdot 10^{-7}$	$3{,}2 \cdot 10^{-8}$
+100	$8{,}7 \cdot 10^{-9}$	$2{,}8 \cdot 10^{-7}$	$8{,}8 \cdot 10^{-8}$
+250	$9{,}6 \cdot 10^{-9}$	$1{,}2 \cdot 10^{-6}$	$1{,}5 \cdot 10^{-7}$

Note: Output 5 tons/h; reflux flow rate 500 kg/h; pressure of secondary steam 0.2 kg/cm^2. Zero position of "cold" level of liquid in evaporator was 250 mm below square junction flange between heating chamber and separator.

To free steam from very small particles of liquid, Kasatkin et al. [3] have successfully used glass fiber; its advantage over other separating structures is that it does not require washing liquid (economy of steam heating). A drawback of glass fiber is that if the steam flow rate is raised above 0.4-0.5 m/sec it gets "flooded" (the liquid does not drain away from the glass fiber) so that the steam is not freed from drops of liquid, and hence is not freed from the impurities.

An important technological index of the operation of an evaporating plant is the decontamination factor K_{de} for purification of the steam from radioactive elements. To get distillate of

Translated from Atomnaya Énergiya, Vol. 30, No. 4, pp. 347-350, April, 1971. Original article submitted July 8, 1969.

TABLE 2. Dependence of Distillate Quality on Throughput of Apparatus, Pressure of Secondary Steam, and Reflux Flow Rate

Throughput of apparatus, tons/h	Pressure of secondary steam, kg /cm²	Reflux flow rate, kg/h	Distillate: specific activity, Ci /liter	Distillate: salt content, mg/liter	Reflux from middle plate: specific activity, Ci /liter	Reflux from middle plate: salt content, mg/liter	Reflux from top plate: specific activity, Ci /liter	Reflux from top plate: salt content, mg/liter
5,0	0,2	250	$4,3\cdot10^{-9}$	$\leqslant 1,0$	$1,3\cdot10^{-6}$	3,5	$4,5\cdot10^{-7}$	3,2
		500	$3,4\cdot10^{-9}$	$\leqslant 1,0$	$6,0\cdot10^{-7}$	3,0	$2,5\cdot10^{-7}$	1,2
		750	$5,0\cdot10^{-9}$	$\leqslant 1,0$	$3,8\cdot10^{-7}$	2,5	$1,2\cdot10^{-7}$	1,8
		1000	$6,0\cdot10^{-9}$	$\leqslant 1,0$	$3,1\cdot10^{-7}$	$\leqslant 1,0$	$6,7\cdot10^{-8}$	1,6
5,0	0,4	250	$1,2\cdot10^{-8}$	$\leqslant 1,0$	$9,0\cdot10^{-7}$	$\leqslant 1,0$	$3,5\cdot10^{-7}$	$\leqslant 1,0$
		500	$9,0\cdot10^{-9}$	$\leqslant 1,0$	$5,0\cdot10^{-7}$	2,2	$1,7\cdot10^{-7}$	1,4
		750	$8,0\cdot10^{-9}$	$\leqslant 1,0$	$2,6\cdot10^{-7}$	1,2	$8,8\cdot10^{-8}$	$\leqslant 1,0$
		1000	$6,0\cdot10^{-9}$	$\leqslant 1,0$	$3,0\cdot10^{-7}$	$\leqslant 1,0$	$6,2\cdot10^{-8}$	$\leqslant 1,0$
7,5	0,2	250	$2\cdot10^{-8}$	$\leqslant 1,0$	$4,3\cdot10^{-6}$	1,2	$5,7\cdot10^{-6}$	1,3
		500	$2,3\cdot10^{-8}$	$\leqslant 1,0$	$7,3\cdot10^{-6}$	2,0	$4,3\cdot10^{-6}$	1,6
		750	$1,0\cdot10^{-8}$	$\leqslant 1,0$	$4,2\cdot10^{-6}$	$\leqslant 1,0$	$1,7\cdot10^{-6}$	$\leqslant 1,0$
		1500	$1,3\cdot10^{-8}$	$\leqslant 1,0$	$6,2\cdot10^{-6}$	1,4	$1,2\cdot10^{-6}$	$\leqslant 1,0$
	0,4	375	$8\cdot10^{-9}$	$\leqslant 1,0$	$4,4\cdot10^{-6}$	$\leqslant 1,0$	$2,0\cdot10^{-6}$	$\leqslant 1,0$
		750	$9\cdot10^{-9}$	$\leqslant 1,0$	$2,4\cdot10^{-6}$	$\leqslant 1,0$	$8,1\cdot10^{-7}$	$\leqslant 1,0$
		1125	$8\cdot10^{-9}$	$\leqslant 1,0$	$1,4\cdot10^{-6}$	1,1	$3,0\cdot10^{-7}$	$\leqslant 1,0$
		1500	$1\cdot10^{-8}$	$\leqslant 1,0$	$2,5\cdot10^{-6}$	$\leqslant 1,0$	$5,0\cdot10^{-7}$	$\leqslant 1,0$

Note: Salt content in still concentrate ~1.0 g/liter.

TABLE 3. Quality of Distillate for Washing of Steam on One Plate

Distillate: pH	Distillate: specific activity, Ci /liter	Distillate: salt content, mg/liter	Reflux from middle plate: pH	Reflux from middle plate: specific activity, Ci /liter	Reflux from middle plate: salt content, mg/liter	Reflux from top plate: pH	Reflux from top plate: specific activity, Ci /liter	Reflux from top plate: salt content, mg/liter
6,1	$1,3\times10^{-8}$	$\leqslant 1,0$	6,3	$2,5\times10^{-6}$	3,0	—	—	—
7,1	$9\cdot10^{-9}$	$\leqslant 1,0$	—	—	—	6,6	$2,3\times10^{-6}$	4,1

Note: Output 7.5 tons/h; pressure of secondary steam, 0.25-0.28 kg/cm²; reflux flow rate, 750 kg/h.

given purity, according to the radiochemical composition and factor K_{de} of the radioactive elements, it is necessary to maintain a certain degree of concentration in the evaporator. In general, the higher K_{de}, the greater will be the degree of evaporation concentration which can be maintained in the plant, i.e., the lower will be the cost of treatment of the solutions.

Martynova et al. [4] propose calculating the concentration of radioactive elements in the steam by means of a nomogram for the apparent distribution coefficients K_i^{app} of "isotope compounds." They consider that "contamination" of saturated water vapor during boiling of water takes two routes, as follows.

1) By mechanical entrainment of water drops (here the contamination of the steam is governed by the wetness of the steam and the impurity concentration in the water).

2) By true solution of impurities in the steam. In this case the distribution coefficient K_{di} is governed by the chemical nature of the compound, its state in solution, and the pressure:

$$K_{di} = \frac{C_{si}}{C_{wi}},$$

where C_{si} and C_{wi} are the concentrations of the i-th component in the steam and water respectively. In the opinion of Martynova et al., at given pressure, the concentration of the i-th isotope in the steam is governed by its concentration in the water and by the coefficient of entrainment K_i^e. By "the coefficient of entrainment of the i-th component" we mean the ratio of its total concentration in the steam to the total concentration in the water.

Whereas, with certain stipulations, these considerations apply to systems with impurities in macroconcentrations, the laws are not at all observed in systems with impurities in microconcentrations. The apparent coefficient of isotope distribution K_i^{app} varies for constant pressure and wetness of the steam. The same authors [4] show that K_i^{app} will vary with the concentration of suspended particles in the water. It is known that radioactive elements are sorbed on the surface of metals, precipitated carbonates and phosphates, compounds of silicon, and hydroxides of metals; the degree of sorption strongly depends on the pH

TABLE 4. Effect of Salt Concentration in Evaporator on Decontamination Factor of Steam

No. of solution sample	Specific activity, Ci/liter			Salt content, mg/liter		Decontamination factor
	original solution	distillate	still residues	original solution	still residues	
1	$1 \cdot 10^{-3}$	$2 \cdot 10^{-8}$	—	9,0	—	—
2	$1 \cdot 10^{-3}$	$1 \cdot 10^{-5}$	$8 \cdot 10^{-1}$	10,5	—	$8 \cdot 10^{-4}$
3	$1{,}6 \cdot 10^{-2}$	$3 \cdot 10^{-6}$	—	27,0	—	—
4	$3{,}1 \cdot 10^{-3}$	$1 \cdot 10^{-6}$	—	19,0	—	—
5	$1 \cdot 10^{-5}$	$3 \cdot 10^{-8}$	$5{,}4 \cdot 10^{-2}$	—	3 930	$1{,}8 \cdot 10^{6}$
6	$5{,}7 \cdot 10^{-4}$	$3 \cdot 10^{-8}$	$1{,}7 \cdot 10^{-3}$	—	790 *	$5{,}7 \cdot 10^{4}$
7	$4{,}6 \cdot 10^{-4}$	$1 \cdot 10^{-8}$	$1{,}6 \cdot 10^{-1}$	—	14 870	$1{,}6 \cdot 10^{7}$
8	$4{,}7 \cdot 10^{-4}$	$4 \cdot 10^{-8}$	$1 \cdot 10^{-2}$	2,8	3 450 *	$2{,}5 \cdot 10^{5}$
9	$1{,}1 \cdot 10^{-4}$	$4 \cdot 10^{-8}$	$6 \cdot 10^{-4}$	—	136 *	$1{,}5 \cdot 10^{4}$
10	$6{,}9 \cdot 10^{-5}$	$3 \cdot 10^{-9}$	$1 \cdot 10^{-3}$	10,3	380	$3{,}3 \cdot 10^{5}$
11	—	$5 \cdot 10^{-9}$	$9 \cdot 10^{-4}$	—	330	$1{,}8 \cdot 10^{5}$

Note: Output 5 tons/h; reflux flow rate, 250 kg/h; pressure of secondary steam, 0.1-0.2 kg/cm^2; salt content of distillate, not more than 1 mg/liter.

* Part of solution from evaporator was removed.

of the medium. Part of these deposits will be found either as suspensions or as films on metal, i.e., the content of the i-th radioactive element in the water may change appreciably even for slight changes in the pH of the medium (sorption and desorption on surfaces of films).

Thus the values of K_i^{app} found experimentally depend very markedly on the conditions of the determination. Furthermore, it has long been known [5] that radioactive elements sorbed on precipitates lose their specific properties, i.e., in the system (steam–water + suspension) we must consider the distribution between water and steam, not of a given radioactive element, but of the precipitate. Finally, in neutral and alkaline media, many radioactive elements of Groups Three through Eight go into solution in the form of radiocolloids or pseudocolloids. As far as we are aware, the behavior of radiocolloids in aqueous systems at high temperatures has not yet been studied.

On the basis of the above considerations, we can expect that in many cases the discrepancies in the values of K_i^{app} for the i-th radioactive element may be 1000 or more. The data in [4, Tables 3, 4, Fig. 2] support this conclusion: for two similar reactors with the same parameters, the distribution coefficients for $Co^{58,60}$ were found to be $5 \cdot 10^{-2}$ and $3.3 \cdot 10^{-4}$, and for Fe^{59}, 0.11 and 10^{-3}. The data in our Table 4 also support the conclusion: for the same operating parameters of the evaporating plant, K_{de} depends markedly on the salt content of the solution, i.e., the more precipitates forming in the liquid phase, the greater is K_{de}.

Thus our data show that when evaporating apparatus of type VN is used to purify radioactive solutions with low salt contents, the optimum operating conditions must be chosen experimentally, and only one washing plate is necessary for washing the steam. The distribution coefficients of radioactive elements between the still residues and the vapor are not constant, but depend on many factors. Therefore the method, suggested by certain authors, for calculating the distribution of radioactive elements between the vapor and solution on the basis of the equation of mass balance is practically useless, since many laws of behavior of individual radioactive elements in vapor–solution and vapor–solid systems at high temperatures and pressures have not yet been studied.

LITERATURE CITED

1. G. A. Kolich and D. V. Radun, Evaporation Plant [in Russian], Mashgiz, Moscow (1963).
2. V. F. Bagretsov et al., Practices in the Treatment of Low- and Intermediate-Level Radioactive Wastes, IAEA, Vienna (1966), p. 339.
3. A. G. Kasatkin, Yu. I. Dytnerskii, and S. I. Umarev, Khimicheskaya Promyshlennost', No. 3, 38 (1958).
4. O. I. Martynova et al., At. Énerg., 23, 305 (1967).
5. A. K. Lavrukhina, T. V. Malysheva, and F. I. Pavlotskaya, Radiochemical Analysis [in Russian], Izd-vo AN SSSR, Moscow (1963), p. 14.

SOME QUESTIONS RELATING TO THE HYDRODYNAMICS OF A BOILING VESSEL-TYPE REACTOR

A. P. Sarygin, I. N. Sokolov,
V. I. Kondrat'ev, E. V. Kulikov,
I. S. Dubrovskii, and E. V. Kozin

UDC 621.039.576

The release of heat from a reactor by way of the natural convection of boiling water largely depends on the hydrodynamic characteristics of the circulation circuit. A study of the circulation circuit of the VK-50 reactor enabled us to refine the numerical values of certain parameters basic to the construction of the reactor, to develop methods of ensuring reliable operation, and to obtain experimental data required for the design of reactors of higher powers.

Circulation Circuit

The VK-50 reactor was fully described in earlier papers [1, 2]. The natural-circulation circuit of the reactor consists of a system of parallel steam-generating cassettes in the active zone, a "draft" or "pulling" section, and two parallel descending channels. The outer ("cold") descending channel, together with the central group of cassettes of the active zone, and the inner ("hot") descending channel together with the peripheral cassettes form two branches of the circuit, having a common draft section (Fig. 1).

The central group of the first-loading cassettes of the small active zone contains 42 working cassettes and 19 cassettes constituting the control-rod system; the remaining 30 working cassettes form the peripheral part of the active zone. The draft section of the circuit, in which the water–steam mixture issuing from the cassettes of the active zone creates the principal motive pressure, constitutes a shell of internal diameter 2.94 and height 2.8 m. The cassettes of the control-rod system have individual draft sections of varying height.

At the level of phase separation, steam bubbles emerge into the steam space of the reactor; the water is directed into the descent channels through 16 overflow windows (total cross section 3.2 m^2). Water is taken off from the cold descent section by means of pumps and passes into the circulation loops of the steam generators; supply water may be passed both to the hot and to the cold descent sections. The feeding systems ensure the uniform distribution of the water over the cross section of the descent channels; this ensures the effective condensation of the steam carried along by the flow of water into these channels.

Measuring System

The reactor is furnished with control and measuring devices giving information relating to the operational reliability and also data relating to the hydrodynamical parameters of the circulation circuit. The pressure, the flow of heat carrier, and the temperature at various points of the reactor installation are determined by means of standard measuring devices. The situation of the sensors providing the measurements inside the vessel are shown in Fig. 1. The velocity sensors situated in the working and compensating cassettes give the magnitude and direction of the circulation velocity of the heat carrier, the relative error in the measurement of this being ±13%. By measuring the pressure drops at various parts of the circulation circuit, the hydraulic resistances (impedances) and the effective (useful) pressure heads of the circuit were determined to a relative accuracy of 5-10%. In order to prevent the water from boiling over, the surge pipes were cooled with supply water. The majority of the sensors used for the internal measurements were placed uniformly around the perimeter of the descending and draft parts; the flow sensors

Translated from Atomnaya Énergiya, Vol. 30, No. 4, pp. 350-353, April, 1971. Original article submitted February 5, 1970; revision submitted April 21, 1970.

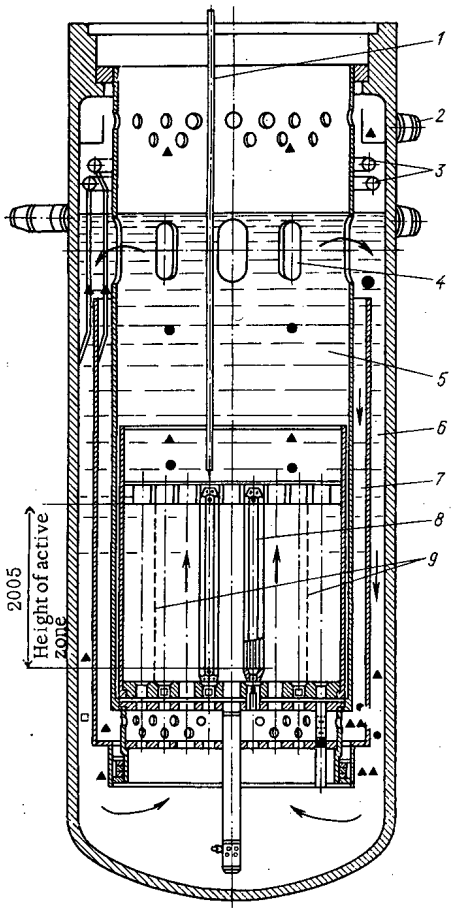

Fig. 1. Arrangement of the sensors for measurements inside the vessel: 1) channel for measuring the field of energy evolution; 2) steam take-off pipe; 3) supply collectors; 4) medium-level line; 5) draft section; 6) cold discharge; 7) hot discharge; 8) working cassette; 9) boundary of small active zone; □) velocity sensors; ▲) temperature sensors; •) static pressure sensors.

were calibrated in a test apparatus before installation in the reactor, together with sets of secondary devices.

RESULTS

The investigations were principally conducted at pressures of 35 and 70 bar and at powers between the initial and nominal (rated) values. The working conditions of the installation may be divided into two classifications: operating conditions in which steam was only developed in the reactor, and operating conditions in which steam was developed simultaneously in the steam generators and in the reactor.

Flow of the Heat Carrier. The variation in the total flow of water passing through the active zone and the velocity of the water in one of the working cassettes is illustrated in Fig. 2. The velocity of the water increases up to steam-delivery values of 1.0-1.2 m^3/sec, then remains almost constant. The quantitative and qualitative character of the relationship changes very little for different positions of the control-rod cassettes and different underheatings of the heat carrier relative to the saturation temperature. Over a wide range of powers, the flow of water has an extremely flat maximum; this may be explained as being due to equilibrium between the increasing resistance of the circulation circuit (as the steam loading increases) and the greater motive force (pressure) of the draft section. It is found that the existence of a common draft section ensures a constant water velocity over the radius of the active zone as the radial coefficient of nonuniformity of the energy evolution varies between 1.2 and 1.4. As a result of the individual draft sections situated above each of the fuel sections of the control-rod cassettes, the volumetric steam content of the latter is relatively high. The velocity of the heat-carrier circulation through the cassettes accordingly rises to approximately twice the value characterizing the working cassettes.

For a steam delivery of 60-80 tons/h or over in the reactor, the upper part of the common draft section, situated above the individual draft sections of the control-rod cassettes, contains a sufficiently large proportion of steam to ensure a reliable circulation through these cassettes, even when the fuel part of the control-rod cassettes is completely withdrawn from the active zone. This makes for extra convenience in using the reactor, since there is no longer any need to reduce the power on introducing several control-rod cassettes into the active zone.

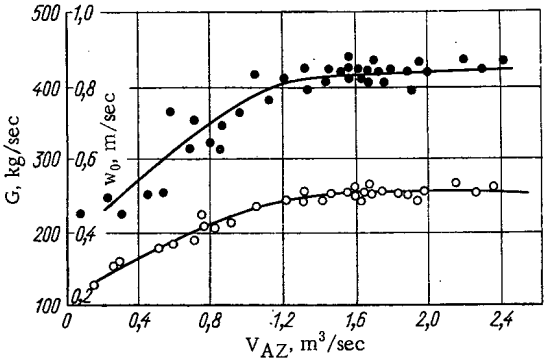

Fig. 2

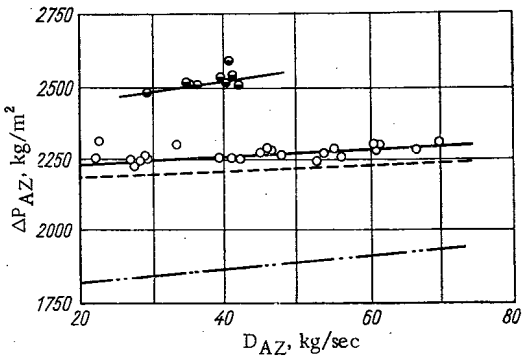

Fig. 3

Fig. 2. Flow of heat carrier around the circuit G (●) and velocity at the entrance into the working cassettes w_0 (○) as functions of the volumetric rate of steam production of the active zone V_{AZ} at P = 30-70 bar.

Fig. 3. Pressure drop in the active zone ΔP as a function of the steam delivery of the active zone D_{AZ}. Experimental values: ○) for P = 70 bar; ◒) for P = 30 bar. Calculated values: – – –) for P = 30 bar; – · · – · · –) for P = 70 bar.

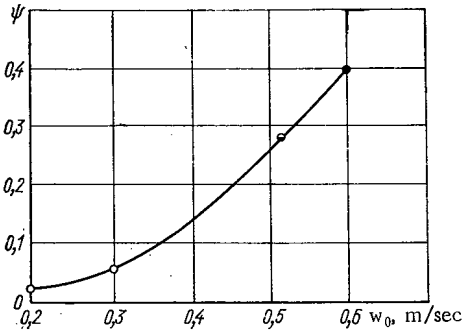

Fig. 4. Comparison of experimental data relating to the trapping of steam for various boiling reactors of the vessel type: ○) VK-50; ◒) EBWR; ●) "Humboldt Bay."

Comparison of the velocities of the water in the VK-50 reactor with the velocities in the EBWR and "Humbolt Bay" reactors shows that the heat-carrier flows are twice as great in the two latter. This is due to the difference in the construction of the draft sections of these reactors and the increased hydraulic resistance of the first-loading working cassettes in the VK-50 reactor.

Pressure Drop in the Active Zone. The calculated and measured relationships between the power and pressure drop are shown in Fig. 3. With increasing steam loading, there is an increase in the pressure drop, this being a consequence of the reduction in the weight of the column of water–steam mixture and the increase in resistance. The calculated dependences of the frictional resistance, the weight of the column, and the local resistances on the volumetric steam content are taken from earlier papers [3, 4]. It follows from Fig. 3 that the calculating formulas reduce the resistance of the circulation tract by some 20% as compared with the experimental results.

For this reason, before accumulating a large amount of experimental data, it is recommended that, in calculating the natural circulation circuit, a correction factor approximately equal to ~1.20 should be applied to the computed resistance of the tract.

Drawing of Steam into the Descending Channels. The drawing of steam into the descent channels of the circulation circuit (the "trapping" of the steam) was studied with and without the incorporation of steam generators in the system.

When the reactor operated without steam generators, the supply water was fed separately and simultaneously to the hot and cold parts of the descent channels. It was found that the steam trapping coefficient ψ, constituting the ratio of the amount of steam trapped in the descent channels to the steam delivery of the active zone, increased with increasing power. The relation between the steam trapping coefficient and the velocity of the heat carrier in the descent channels is of a threshold character; steam drag sets in when the velocity of the heat carrier in these channels equals 0.35 m/sec (Fig. 4).

When the reactor operates without the feeding of supply water into the hot or cold parts of the descent channels, there is hardly any reduction in the motive force (pressure head) at the velocities indicated. This suggests that steam bubbles may remain suspended in the initial section of the descent channel. These

results are in fair agreement with earlier experimental results [4, 5] as to the limiting velocities corresponding to the surfacing of the steam bubbles. It is important to note that an increase in the velocity of the heat carrier in the descent channels leads to an almost linear dependence of the amount of trapped steam on the flow of boiler water.

On connecting one or two steam generators into the system, the steam trapping coefficient increases to 0.35 and 0.45 respectively; this is due to the fact that the overflow windows lie close to the pipes taking the boiler water to the steam generators. Thus the greater velocities occurring in the region of the take-off pipes increase the trapping of steam in the descent channels.

The foregoing discussions lead to the following conclusions.

1. Natural circulation constitutes a simple and compact means of heat elimination for boiling reactors of the vessel type.

2. The constancy of the flow over a wide range of pressure and power changes implies the reliability of the reactor under stationary (steady-state), transitional (transient), and emergency operating conditions; this also means that for reduced levels of power (60-70%) an additional reserve of reactivity is freed, owing to the reduction in the average volumetric steam content of the active zone.

3. The possibility of feeding different amounts of supply water to the hot and cold descent sections of the reactor releases additional reactivity and increases the operating time of the fuel between rechargings.

4. The common draft section ensures a constant flow in all the cassettes of the active zone, the size of the latter not depending on the energy evolution in individual cassettes.

5. For the first fuel charging of the reactor, the effective pressure head of the draft section was relatively low, owing to the lack of agreement between the dimensions of the active zone and the geometrical dimensions of the draft section ($D_{AZ}/D_{DS} = 0.61$), and the hydraulic resistance of the working cassettes was too high.

These factors were responsible for the high values of the average volumetric steam contents (up to 35-45%) and the low circulation velocities ($w_0 \sim 0.5$ m/sec).

LITERATURE CITED

1. I. N. Sokolov et al., Contribution No. 306 presented by the Soviet Union to the Third International Conference on the Peaceful Use of Atomic Energy [in Russian], Geneva (1964).
2. I. N. Sokolov et al., Teploénergetika, No. 5, 62 (1968).
3. N. V. Tarasova, "Hydraulic resistance in the flow of water and a water–steam mixture through heated pipes and annular channels," in: Transactions of the Central Boiler Institute [in Russian], Vol. 59, Leningrad (1965), p. 47.
4. A. Ya. Kramerov and Ya. V. Shevelev, Engineering Calculations of Nuclear Reactors [in Russian], Atomizdat, Moscow (1964).
5. D. A. Labuntsov et al., Teploénergetika, No. 4, 62 (1968).

TEMPERATURE EFFECT IN THE RANGE FROM 20 TO 250°C IN THE CASE OF SOME STRICTLY REGULAR HETEROGENEOUS U – H_2O CRITICAL ASSEMBLIES

G. A. Bat', V. N. Gulimov,
Yu. V. Zarubin, V. K. Obukhov,
and Yu. V. Ushakov

UDC 621.039.516.25

Temperature effects constitute the touchstone for any reactor calculations scheme. In fact, a method describing the dependence of the critical mass N_{cr} on the pitch of the lattice comprising a cold reactor, with acceptable accuracy, can lead in some cases to errors even in the sign of the temperature effect, particularly in the region of optimum water–uranium ratios, where this effect is not very large. In any case, an excellent description of the dependence $N_{cr}(T)$ is a fairly reliable indicator of the adequacy of the computational method in question, and of the plausibility of the simplifying assumptions entertained in the method.

Unfortunately, the available information on experimentally investigated temperature effects of reactivity in reactors of simple structure is somewhat meagre. Aside from one sole exponential experiment [1] performed in the case of a strictly homogeneous critical assembly at temperatures up to ~200°C, all measurements with uranium lattices have been carried out either at atmospheric pressure in the temperature range T ≈ 20 to 90°C, or else over a wide range of temperatures but with real reactors and a complicated and inhomogeneous lattice, control rods and equipment, multilayer reflector, and other complicating structures, etc. Experiments of this type do not lend themselves to working out useful computational techniques. For this reason, the accuracy of the theoretically predicted temperature effect of reactivity, ~20%, is usually taken as reasonable, and few attempts are ventured at greater accuracy.

In the light of these problems, work on the study of the temperature effect has been directed to unperturbed and maximally uniform heterogeneous uranium–water systems, of simple configuration, over a wide range of U^{235} concentrations ($\rho_H/\rho_5 \approx 50$-600) and over a wide range of temperature (T ≈ 20-250°C)

Stress was laid on accuracy of measurements and simplicity in the interpretation of the results, in preparing and carrying out the experiments. Of course, some penalty had to be exacted in order to meet these requirements: the experiments were quite laborious, and took some time to complete. Actually, one experiment conducted in a high-pressure vessel usually yields the entire dependence $\rho(T)$ for a reactor kept in the critical state by its control rods. In the case of "clean" experiments, i.e., when criticality is achieved in the case of unperturbed and uniform assemblies, each experiment yields only one point on the $N_{cr}(T)$ curve, and at most two points in some isolated instances. The reason for this is that only one type of fuel element was studied exhaustively in the experiments.

The integrated character of the critical experiments provides only minimal information (N_{cr}, δ the effective reflector savings, shape of the power production field) on each specific assembly. However, a fairly extensive array of experiments of this type, carried out with different fuel elements and over a broad range of lattice pitch values and temperatures, could amply supplement the data on the microscopic parameters, and go a long way in replacing such parameters.

Fuel Elements and Test Beds

Four types of fuel elements [2], differing solely in the concentration of uranium, were employed in the experiments, and only one of them was investigated in the temperature range above 90°C (the fuel element

Translated from Atomnaya Énergiya, Vol. 30, No. 4, pp. 354-358, April, 1971. Original article submitted September 15, 1969; revision submitted September 30, 1970.

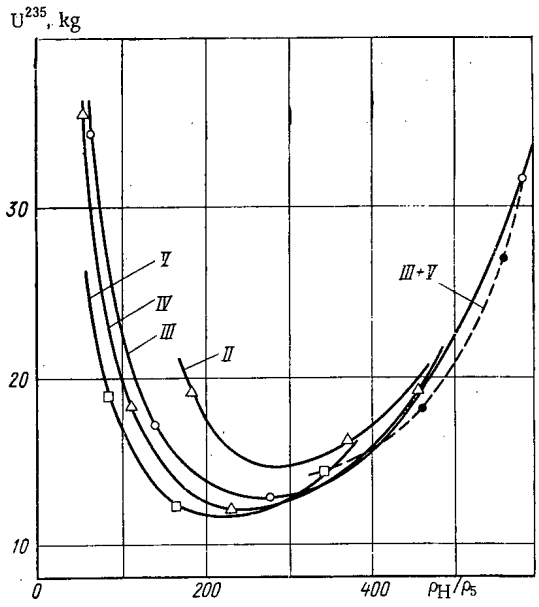

Fig. 1. Dependence of the critical mass of U^{235} on the ρ_H/ρ_5 ratio, at different ρ_5 values (plotted for different types of fuel elements, II to V).

TABLE 1. Fuel Composition (wt. %)

Type of fuel element	U^{235}	U^{238}	O_2	Al	Fe*	λ, g/cm³
III	24.70	6.174	4.532	63.30	0.969	3.50†
IV	28.78	7.20	5.280	57.560	0.880	3.745†

* Included in the aluminum as impurities.
† Indicated density slightly below real value: zirconium bottoms of cladding arbitrarily transferred to side wall of cladding.

with 40.5 g U^{235} content). Each fuel element could be disassembled, and consisted of 16 zirconium-clad slugs enclosed in an overall steel casing. The clad diameter was 10 mm, the cladding thickness was 0.5 mm, and the composition: 99% Zr + 1% Nb. The casing diameter was 13 mm, its thickness 1.2 mm, and its composition: 73% Fe + 18% Cr + 9% Ni. The total length of the slugs, 976 mm, was far shorter than the distance between the perforated plates of the test bed. The slugs (fuel diameter 7 mm, length 60 mm) contained 80% enriched uranium dioxide diluted with aluminum powder such that the amount of uranium present in each successive modification of the fuel elements would be roughly 30% greater than in the preceding modification. The minimum U^{235} content in the fuel was 0.50 g/cm³, the maximum U^{235} content was ~1.5 g/cm³; we distinguished fuel elements of types I, II, III, IV, and V according to the U^{235} content (but type I fuel elements with 0.5 g/cm³ U^{235} were not used in these experiments). Table 1 lists the calculated concentrations of fuel mixture components for types III and IV.

The design and equipment of the open critical test stand for "low temperature" experiments do not differ basically from the design and equipment of other test stands of the type, with the setup of the core properly the only specific feature of this one. The holes for fuel elements in the spacing plates formed an annular lattice, rather than the usual hexagonal or square lattice. In each successive annular row the number of holes is six greater than in the preceding row. The radii at which the axes of the fuel elements were placed were selected such that the annular lattice would correspond, in cell area, to a hexagonal lattice with pitch a equal to 1.57, 1.89, 2.36, and 3.15 cm (the values of a will be used in the sequel to characterize the lattices used).

All of the rods in the control and protection system were introduced directly into the water between the fuel elements. For experiments conducted at temperatures above 100°C, the assembly was enclosed in a thick-walled vessel with packless control rod drives on the top to displace the "wet" absorbing rods.

Because of the absence of lines on the control rods, the assembly remained homogeneous when all the absorber rods were retracted.

EXPERIMENTAL METHOD

By adding peripheral fuel rods to the water-filled tank ($T \approx 20°C$), we were able to bring the assembly up to a near-critical state, and determine N_{cr} by the supercritical completion method (the dependence of the excess reactivity on the number of fuel elements present is extrapolated to zero). The assembly was then heated another 10°C, the temperature stabilized, and the supercritical completion experiment was repeated. For instance, the assembly was brought up to a temperature ~80°C in steps of 10°C each. While being heated to the stabilized temperature, the assembly was kept critical by using a control rod and by varying the number of fuel elements. Of course, the supercritical completion was carried out with the rod completely withdrawn. At $T \approx 20°C$ and at $T \approx 80°C$, the neutron flux rose to a level sufficient for activation of the fuel elements. Measurements of the γ-activity of the fuel elements make it possible to find the radial power production field and to determine δ. This procedure was used in the open test stand experiments.

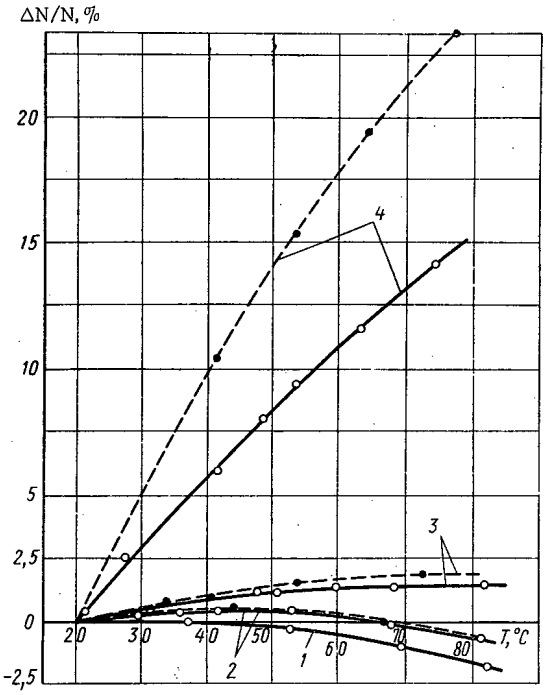

Fig. 2

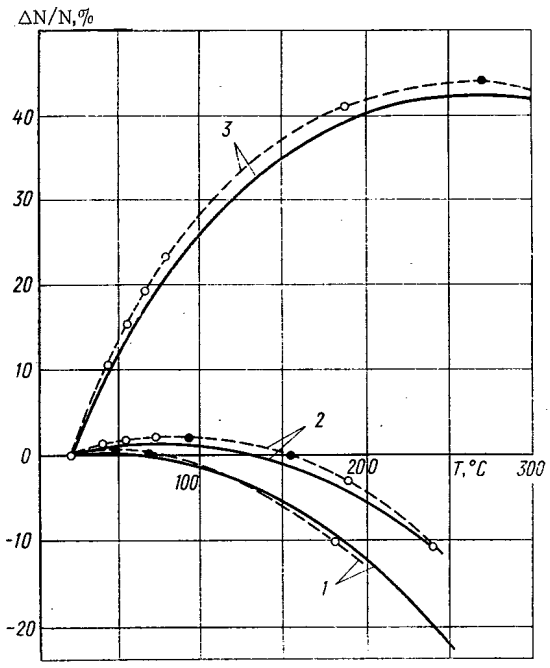

Fig. 3

Fig. 2. Dependence of the relative change in the critical mass N_{cr} on the temperature in the 20-80°C range, for fuel elements of type III (•) and type IV (○): $\Delta N/N = (N_{cr}(20°C) - N_{cr}(T))/N_{cr}(20°C)$; 1) a = 1.57 cm; 2) 1.89 cm; 3) 2.36 cm; 4) 3.15 cm.

Fig. 3. Dependence of the relative change in the critical mass N_{cr} on the temperature in the 20-285°C range for fuel elements of type III: • and ○) experiment [•) points for $\Delta N/N|_{max}$ and $\Delta N/N = 0$]; ———) predicted data; 1) a = 1.89 cm; 2) a = 2.36 cm; 3) a = 3.15 cm.

Assemblies with the number of fuel elements corresponding to the rated value of N_{cr} at the higher temperature were placed in the "hot" test stand. When the expected temperature effect was positive, the assembly was subcritical at 20°C; but if negative, the excess reactivity of the assembly was suppressed by a multiple-rod compensating device which was completely removed during the heating process.

To achieve coordination with the experiments conducted on the open test stand, the variation in reactivity brought about by a rise in pressure from 1 to 120 atm was determined before the heating was commenced. This was then compared to the contribution made by the peripheral fuel element to the reactivity, which was known beforehand and taken into account as a correction to the earlier dependences $N_{cr}(T)$ in the temperature range below 80°C. This correction turned out to be small (roughly one or two fuel elements) in all instances, and added no difficulties to interpretation of the results. The next step was to begin increasing the temperature (by pumping water heated by an external heat source through the assembly). At higher values of a, when the still unheated assembly was subcritical, the critical temperature was determined by three methods: a) by constructing a reciprocal count vs. temperature curve for the region $T \leq T_{cr}$; b) by extrapolating the $\rho(T)$ dependence to zero at $T \geq T_{cr}$; c) from the position of the current maximum of the galvanometer (I) on the combined graph of I and T as functions of the time, during the cooldown.

All three methods yielded results converging within ±0.5°C (about the same accuracy as thermocouples).

At low a values, the assembly was critical during the heating, and was kept critical by displacing the multiple-rod compensating device. When this device was removed from the top reflector, T_{cr} was determined by methods b) and c), with method c) being used during the heating process.

Each heating cycle terminated in a rise in the power needed to irradiate the fuel elements.

RESULTS

Figure 1 shows results, already published in a slightly different format [2], of critical-mass measurements* at room temperature. The change in the scales proved convenient for demonstrating the weak

*Reference [2] also contains predicted data, but these were left off the graph here so as not to overload it.

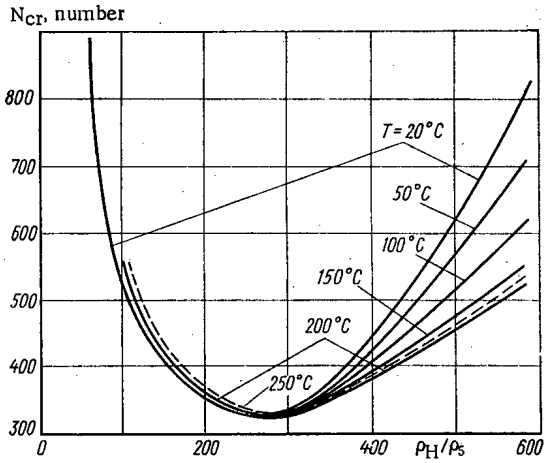

Fig. 4

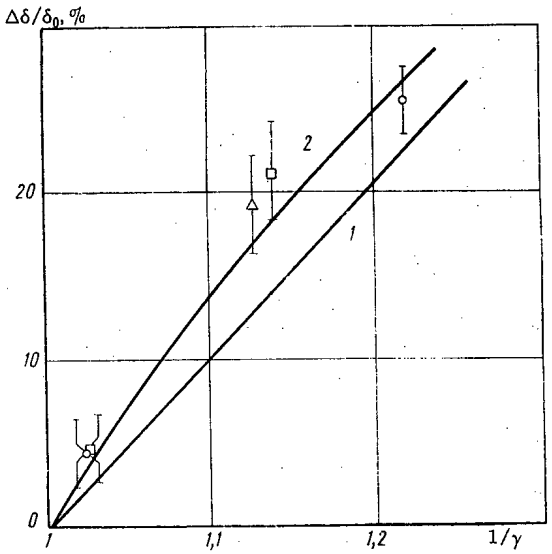

Fig. 5

Fig. 4. Dependence of N_{cr} on ρ_H ρ_5 at different temperatures.

Fig. 5. Variation in effective reflector savings δ during heating: data points are experimental values; Δ) a = 1.89 cm; ○) a = 2.36 cm; □) a = 3.15 cm; 1) calculations with $\delta \sim 1/\gamma$ assumed; 2) one-dimensional diffusion calculations for reactor in four-group model.

dependence of the U^{235} critical load on the uranium concentration in the fuel elements, particularly at values of the ρ_H/ρ_5 ratio twice as large, or larger still, as the optimum values. It could be expected that the temperature effect of reactivity in this region (stemming above all from changes in the leakage and utilization factor of thermal neutrons) will also be stable if the lattices with the same ρ_H/ρ_5 ratios are compared with variations occurring in the amount of U^{235} present in the fuel elements. This "equivalence principle," despite its approximate character and restricted range of application, nevertheless remains convenient for estimates, and obviates the need to perform temperature experiments with all sets of existing types of fuel elements.

Similar arguments can be expressed relative to the region $\rho_H/\rho_5 \lesssim (\rho_H/\rho_5)_{opt}/2$, with this difference, that in this instance the curves are roughly equidistant, and the temperature effects for different types of fuel elements have to be estimated with the initial shift taken into account.

The results of temperature experiments conducted on an open test stand (T ≈ 20-80°C) are plotted in Fig. 2. These results encompass the range of temperature coefficients of reactivity $d\rho/dT|_{T=20°C}$ from zero to extremely high values (roughly $3 \cdot 10^{-4} °C^{-1}$). The absence of negative values of $d\rho/dT|_{T=20°C}$ even in the case of the compact lattice with the pitch a = 1.57 cm ($\rho_H/\rho_5 \approx 50$), corresponding to the very steep portion of the left branch of the U^{235} (ρ_H/ρ_5) curve, is quite striking. The underlying reason is that the density effect, which is not manifested at room temperature, is basic in compact lattices. The role of hardening of the thermal neutron spectrum in response to heating of large-pitch lattices is strikingly enhanced against the background of the slight effect of changes in water density. The last factor also accounts for the separation of the paired curves corresponding to different U^{235} concentrations in the fuel elements as the pitch of the lattice is increased.

The procedure described above for performing "clean" high-temperature experiments in the case of uniform heterogeneous uranium–water systems proved convenient (the number of experiments conducted in a high-pressure vessel for each lattice pitch need not be greater than one or two) and at the same time sufficiently accurate ($\Delta T_{cr} \leq \pm 2°C$).

The basic results are presented in Fig. 3. The graph of the temperature dependence of the relative change in critical mass $N_{cr}(T)$ covers the 20-285°C temperature range, the range ρ_H/ρ_5 = 85-585, so that several inferences can be drawn.

We begin by noting the entirely satisfactory accuracy of the calculations, particularly when we deal with the general shape of the curves and the quantitative effect in heating to 200°C and above.

The appreciable relative errors in the calculations are not so serious when the quantitative effect is fairly small, and can be eliminated successfully by using a program of higher class than the PRYaNIK-1 ("CAKE-1") program [3] which we used, a program which implies homogenization of the lattice in the four-group approximation, with the universal constants of the slowing-down region, and treatment of thermalization in the improved hydrogen-gas approximation.

The change in the relationship between the density effects of reactivity and the purely temperature effects of reactivity, in the transition from large lattice spacings to small ones, is also striking. When a = 3.15 cm, the initial portion of the curve is due primarily to purely temperature effects, while the final portion of the curve corresponds to a practically total balance of the reactivity effects in the variation of T and γ. When a = 1.89 cm, all the reactivity effects in the 20-80°C range almost balance out completely, while the predominating effect in the range of higher temperatures is that exerted by the water density, and $\Delta N/N \approx 1/\gamma$ quite rigorously.

Figure 4 analyzes deformation of the experimental $N_{cr}(\rho_H/\rho_5)$ curve for the fuel elements investigated when lattices with different pitch are investigated. The criticality of lattices with large ρ_H/ρ_5 depends weakly on the composition of the fuel elements (see Fig. 1), but turns out to be quite sensitive to the temperature (the variation in critical mass is roughly 30% in response to heating to 200°C). Conversely, the criticality of compact lattices depends essentially on the composition of the fuel elements, but is highly stable to heating. On the whole the minimum on the $N_{cr}(\rho_H/\rho_5)_{T=const}$ curve broadens slightly with increase in temperature.

Results of calculations and measurements of the radial power production profile were in excellent mutual agreement, which predetermined agreement between the "measured" and calculated values of the effective reflector savings δ. The value of δ at 20°C is determined, to within an error ~2-3 mm, by the approximate formula $\delta = 4.3(1 + 0.4/V_{H_2O}/V_{cell})$. However, the temperature dependence of δ (Fig. 5) is a more complicated one than the one dealt with when the factor $1/\gamma$ is introduced into that formula, as is sometimes done. The relative change in δ in the first approximation is independent of the value of δ at γ = 1 (i.e., independent on the lattice pitch).

LITERATURE CITED

1. R. Hellens and G. Price, Reactor Technology, Selected Review, BNL (1969).
2. G. A. Bat', V. N. Gulimov, and V. K. Obukhov, At. Énerg., 26, 7 (1969).
3. G. A. Bat', N. M. Trukhachev, and M. V. Fedulov, in: Physics of Nuclear Reactors [in Russian], Vol. 1, Atomizdat, Moscow (1966), p. 129.

KINETICS OF FISSION YIELD FROM CERAMIC FUEL

B. V. Samsonov and A. K. Frei

UDC 621.039.542.34.548.343

It has been shown recently [1, 2] that the escape of gaseous fission fragments from uranium dioxide is more complex than would follow from the equivalent-spheres model [3, 4]. The gradual decrease of the diffusion coefficient observed in UO_2 specimens irradiated with various integral doses is explained by the presence of a certain porosity in the crystalline lattice [1, 2].

It is reasonable to assume that the change in the diffusion coefficient of fission fragments in the crystalline lattice (as long as the latter is not damaged by radiation) is negligible. Thus, the diffusion coefficient that varies as a result of porosity should be regarded as an apparent diffusion coefficient.

A study of the yield of gaseous fission products in an SM-2 reactor made possible a comparison of the apparent diffusion coefficients of various kinds of ceramic fuel and in particular of UC and UC_2 whose properties are less well known [5, 6] than those of the thoroughly investigated UO_2 [1, 4, 7].

EXPERIMENTAL METHOD

A 300-500 mg specimen of the studied material was poured into a stainless steel tube and covered by nickel gauze. The tube could be moved along the active portion of the channel so that the desired irradiation conditions could be selected or the sample could be moved out to a low-temperature region. A helium stream of 1-2 liter/min (Fig. 1) flowing through the specimen traps the fission fragments and carries them to the measuring setup in about 0.5 to 1 min. The gas stream passes through γ-, β-, and n-counters, a trap for short-lived fragments (FT), and a system of filters. The trap is an electrostatic precipitator of atoms that undergo in it β-decay; this makes it possible to find the amount of the precursor isotope that passed through it [8]. For sample collection, a vacuumized sampler is attached to valve 3 (see Fig. 1). Valve 2 is then closed and the flow of helium stops for a given time. By opening valves 1 and 5 the entire gas in suspension is collected in the vessel. The volume of this vessel is twice the channel volume so that the gaseous fission fragments from the entire channel are collected in it. The samples are analyzed with a single-crystal γ-spectrometer, the isotope content in the sample being measured to within 20-25%.

It has been found that iodine isotopes leaving the sample are completely adsorbed in the channel parts [1]. This made it possible to find the apparent diffusion coefficient of iodine isotopes. By determining the amount of Xe^{133} and Xe^{135} isotopes in the extracted sample it is possible to determine the amount of I^{133} and I^{135} isotopes, and with the aid of the short-lived-fragments trap also to find the number of Xe^{138} atoms. The characteristics of the studied specimens are listed in Table 1. The equivalent-sphere radius was determined by the well-known techniques [3, 9].

The specimen temperature was calculated to within ±100°C by measuring the yoke temperature with a thermocouple. The accuracy of determination of relative temperatures of different specimens was considerably higher as all specimens were held in absolutely identical conditions.

The following notation is employed in the expressions used to process the experimental results: a is the radius of equivalent sphere, cm; D is the diffusion coefficient, cm^2/sec; D' is the reduced diffusion coefficient, $D' = D/a^2$, sec^{-1}; G is the flow rate of helium through the channel, liter/sec; λ_i is the disintegration constant of the i-th isotope, sec^{-1} (adopted from [10, 11]. For Xe^{135} $\lambda_{tot} = \lambda + 2.7 \cdot 10^6 \cdot 10^{-24}$ F [10]); ν_i is the leakage constant of the i-th isotope, sec^{-1}; N_U is the number of U^{235} atoms in the specimen; N_{Xe}^{sam} is the number of xenon atoms in the given sample; $R_{Xe}(t)$ is the yield of xenon atoms from the

Translated from Atomnaya Énergiya, Vol. 30, No. 4, pp. 358-362, April, 1971. Original article submitted January 16, 1970; revision submitted April 16, 1970.

TABLE 1. Characteristics of Studied Samples

Type of fuel, index	Preparation and treatment	Density, g/cm³	Radius of equivalent sphere, μ
UO_2-I	Electrolysis of molten NaCl – KCl – UO_2Cl_2	10.5	45
UO_2-II	Ammonium; molded at 1.5 ton /cm², sintered, crushed, and dispersed into fractions	10.2 ± 0.1	30
UC-I UC-II	Reduction of UO_2 by carbon at 2000°C with subsequent hot molding, crushing, and dispersion into fractions	13.0-13.1	30
UC_2-I UC_2-II	Hot molding of dicarbide briquettes in vacuum of at least 10^{-1} torr at 2000°C, crushing, and dispersion into fractions	11.3 ± 0.1	30

TABLE 2. Variation of Apparent Diffusion Coefficient in the Course of Irradiation at 1400°K

Specimen	Isotope	Irradiation dose, dis /cm³	D', cm²/sec	
			beginning of irradiation	end of irradiation
UO_2-I	Xe^{133}	$\sim 8\cdot10^{18}$	$3{,}5\cdot10^{-12}$	$5\cdot10^{-17}$
	Xe^{135}		$1{,}2\cdot10^{-13}$	$6\cdot10^{-16}$
	Xe^{138}		10^{-12}	$6\cdot10^{-14}$
UO_2-II	Xe^{133}	$\sim 10^{19}$	10^{-12}	10^{-17}
	Xe^{135}		10^{-14}	$5\cdot10^{-17}$
	Xe^{138}		$5\cdot10^{-13}$	$9\cdot10^{-14}$
UC-I	Xe^{133}	$\sim 5\cdot10^{18}$	10^{-11}	10^{-16}
	Xe^{135}		—	$2\cdot10^{-15}$
	Xe^{138}		10^{-14}	$2\cdot10^{-15}$
UC-II	Xe^{133}	$\sim 5\cdot10^{18}$	10^{-11}	$3\cdot10^{-16}$
	Xe^{138}		$4\cdot10^{-14}$	10^{-14}
UC-I	Xe^{133}	$\sim 5\cdot10^{18}$	10^{-12}	10^{-16}
	Xe^{135}		$2\cdot10^{-13}$	10^{-15}
	Xe^{138}		$2\cdot10^{-13}$	$5\cdot10^{-14}$
UC_2	Xe^{133}	$\sim 7\cdot10^{18}$	$5\cdot10^{-12}$	$1{,}3\cdot10^{-16}$
	Xe^{135}		10^{-12}	$5\cdot10^{-16}$
	Xe^{138}		$1{,}2\cdot10^{-15}$	$3\cdot10^{-16}$

specimen at the given instant, atoms/sec; $R_I^{ch}(t)$ is the number of iodine atoms in the channel at the given instant; σ is the fission cross section of U^{235} (taken as 450 b with all corrections); t denotes time in sec; τ is the channel shut off time, sec; y_i is the fission yield of the i-th isotope, %; (adopted from [10]); Φ is the neutron flux intensity, $n/cm^2 \cdot sec$; and v is the channel volume, liter.

The fission yield is (according to the equivalent-spheres model) given by the expression

$$\frac{v}{3(\lambda+v)} = \sqrt{\frac{D'}{\lambda}}\,\mathrm{cth}\sqrt{\frac{\lambda}{D'}} - \frac{D'}{\lambda} - 2e^{-\lambda t}\sum_{1}^{\infty}\frac{e^{-n^2\pi^2 D' t}}{n^2\pi^2 + \frac{\lambda}{D'}}. \quad (1)$$

The leakage constant of iodine and xenon isotopes was found from

$$R_I^{ch}(t) = \frac{\nu_I \sigma \Phi N_{U^{235}}}{\lambda_I + \nu_I}\left[\frac{1-e^{-\lambda t}}{\lambda_I} - \frac{1-e^{-\nu_I t}}{\nu_I}e^{-\lambda_I t}\right]; \quad (2)$$

$$R_{Xe}(t) = \frac{\nu_{Xe}\sigma\Phi N_{U^{235}Xe}}{(\lambda_I+\nu_I)(\lambda_{Xe}+\nu_{Xe})(\lambda_{Xe}+\nu_{Xe}-\lambda_I-\nu_I)}[(\lambda_{Xe}$$

$$+\nu_{Xe}-\lambda_I-\nu_I)-(\lambda_{Xe}-\nu_{Xe})e^{-(\lambda_I+\nu_I)t}+(\lambda_I+\nu_I)e^{-(\lambda_{Xe}+\nu_{Xe})t}]. \quad (3)$$

$R_{Xe}(t)$ and $R_I^{ch}(t)$ were calculated from experimental data using the expressions

$$N_{Xe}^{sam} = [R_{Xe}(t) + \lambda_I R_I^{ch}(t)]\left(\tau + \frac{v}{G}\right) \quad (4)$$

(specimen in the core), and

$$N_{Xe}^{sam} = \lambda_I R_I^{ch}(t)\left(\tau + \frac{v}{G}\right) \quad (5)$$

(specimen extracted from core).

Xe^{138} samples were counted using the technique described in [8].

RESULTS

The obtained results were plotted as a dependence of the reduced apparent diffusion coefficient D' on the irradiation dose (Figs. 2 and 3). Since D' varies in approximately the same manner for all specimens it is sufficient to cite only the steady-state values of D' at the beginning and end of the experiment (Table 2).

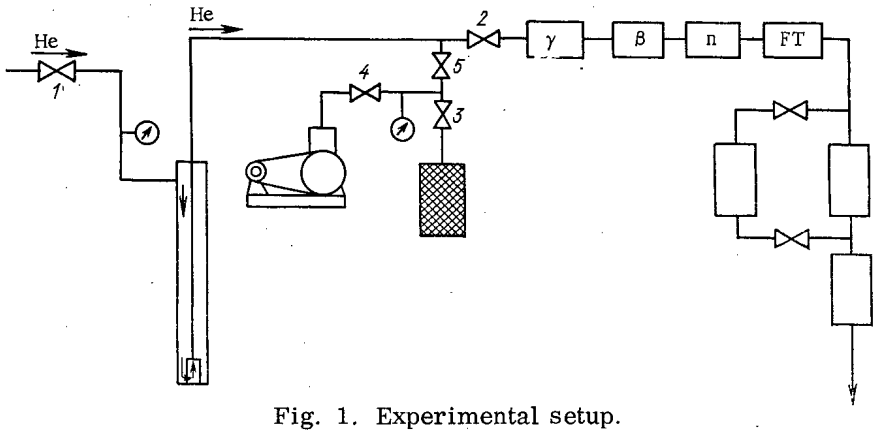

Fig. 1. Experimental setup.

TABLE 3. Comparison of Experimental and Calculated Specimen Temperatures

Specimen	D_0, cm^2/sec	E, cal/mole	Specimen temperature, °K	
			experimental	calculated
UO_2	$1,5 \cdot 10^{-6}$	70 000	1400	1340
UC	10^{-2}	75 000	1400	1600
UC_2	$4,6 \cdot 10^{-6}$	68 000	1400	1370

DISCUSSION

An analysis of the results shown in Figs. 2 and 3 and in Table 2 leads to the conclusion that beginning with an irradiation dose of $\sim 2 \cdot 10^{16}$ dis/cm^3 the diffusion of gaseous fission fragments decreases with increasing doses and stabilizes at $5 \cdot 10^{18}$ to $5 \cdot 10^{19}$ dis/cm^3. In the accepted system of counting this decrease in diffusion manifests itself as an apparent reduction of diffusion coefficients. This reduction is different for the different xenon isotopes: it is highest for Xe^{133} (by a factor of 10^4 to 10^6), less for Xe^{135} (10^2 to 10^3 times), and the lowest for Xe^{138} (5 to 20 times). This reduction can only be explained by assuming that the fragments are trapped in internal pores that are formed during irradiation of ceramic materials. Assumption of a decrease of the surface of "equivalent" grains would lead to an equal reduction of the yield for all isotopes and to a much less pronounced effect.

However, the experimental values of D' at the beginning of irradiation are very high. It is hardly reasonable to assume that xenon atoms, which are of a relatively great size, can diffuse so easily in the dense crystalline lattice of the investigated materials [9]. The processes taking place can be given the following qualitative interpretation. It is known [12] that the presence of point defects in irradiated materials facilitates diffusion. It can be thus assumed that the initial (at an irradiation dose of 10^{16} dis/cm^3) high value of the apparent diffusion coefficient of xenon isotopes depends on easy "transport" of the isotopes through point defects that tend to accumulate at grain boundaries in the crystalline lattice which still does not contain a great number of traps. At the same time, since the half-life of Xe^{133} is very long, of Xe^{135} shorter, and of Xe^{138} the shortest, point defects transport Xe^{133} atoms from very deep layers of the grain and in an amount much greater than follows from the equivalent-spheres model. Correspondingly, the effect of point defects should be less for Xe^{135}, and the least for Xe^{138}. The lowest (at a dose of 10^{19} dis/cm^3) steady-state values of apparent diffusion coefficients for xenon isotopes are also different; the least for Xe^{133}, higher for Xe^{135}, and the highest for Xe^{138}. This can also be explained by their different half-lives. Coming from the deepest grain layers, Xe^{133} meets on its path the highest number of traps and thus becomes most "sensitive" to them. Similarly, the effect of traps is less on Xe^{135}, and the least on Xe^{138}.

The generally accepted (at present) diffusion parameters D_0 and E for ceramic fuel [3, 6] are listed in Table 3. The specimen temperatures also listed in Table 3 were calculated from these parameters and from the experimental values of the final steady-state diffusion coefficients of Xe^{133}.

Good agreement between the calculated and experimental temperature has been observed for both UO_2 and UC_2. The difference observed in the case of monocarbide is somewhat higher than the experimental error. For this value of D an activation energy of 65,000 cal/mole corresponds to a temperature of ~1400°K. It has been reported [6] that for carbides the activation energy is 55,000 cal/mole. The average value of energy between the maximum of 75,000 cal/mole and the minimum of 55,000 cal/mole agrees with the suggested value of 65,000 cal/mole.

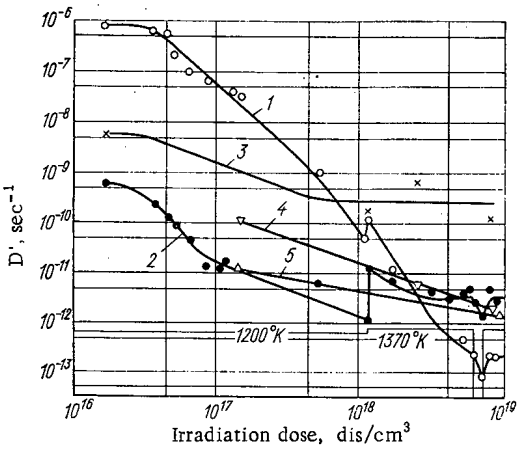

Fig. 2. Reduced apparent diffusion coefficient D' of UO_2-I specimens as a function of if-irradiation dose: 1) Xe^{133}; 2) Xe^{135}; 3) Xe^{138}; 4) I^{133}; 5) I^{135}.

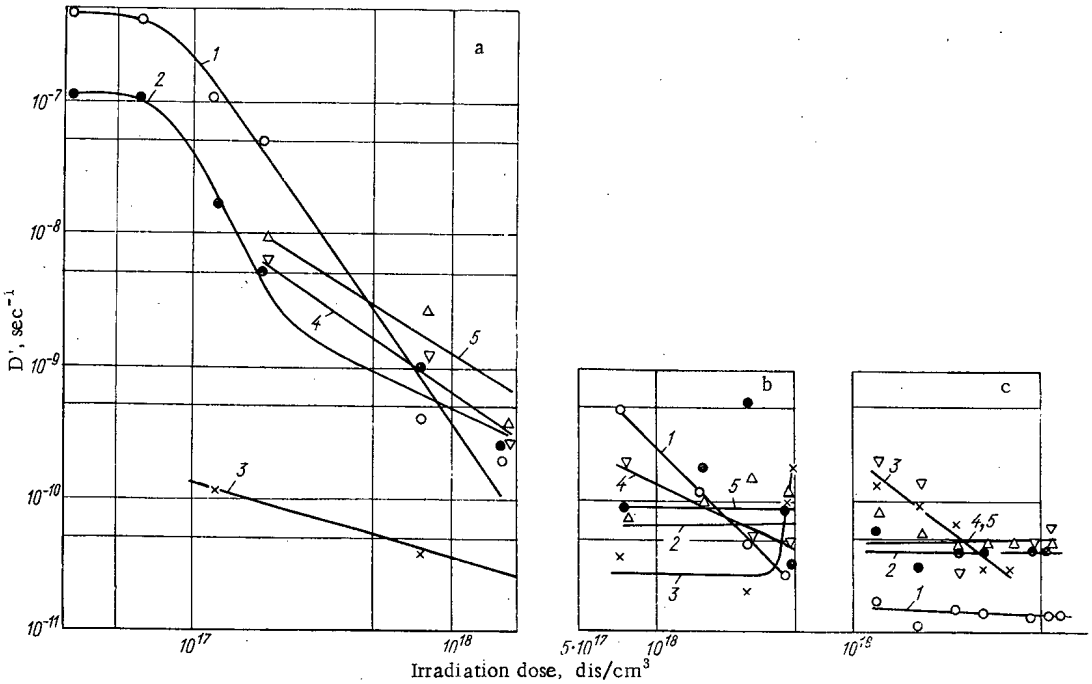

Fig. 3. Reduced apparent diffusion coefficient D' of UC_2-II specimen as a function of irradiation dose: 1) Xe^{133}; 2) Xe^{135}; 3) Xe^{138}; 4) I^{133}; 5) I^{135}. The curves b and c show data obtained for intermittent irradiation.

A noteworthy fact is the intense diffusion of iodine isotopes. At the end of the experiments the number of atoms of Xe^{133} and X^{135} produced by iodine atoms escaping from the specimens and precipitating in the channel was 3 to 5 times the number of atoms directly escaping from the specimens.

The results indicate that the yield of gaseous fission fragments from ceramic fuel decreases noticeably in the course of irradiation. This effect can be explained by the appearance as a result of irradiation of internal porosities that act as traps capturing gaseous fission fragments and hindering their escape from the specimen.

The authors thank S. T. Konobeevskii, N. V. Krasnoyarov, V. A. Tsykanov, and V. N. Raetskii for their advice and help, and A. I. Kashtanov for preparing the specimens.

LITERATURE CITED

1. R. Carroll and P. Reagan, Nucl. Sci. and Engng., 21, 141 (1965).
2. F. Felix et al., Report P/427, by the FRG Delegation to the Third Intern. Conf. on Peaceful Uses of Atomic Energy, Geneva (1964).

3. B. Lastman, Radiation Effects in Uranium Dioxide [in Russian], Atomizdat, Moscow (1964).
4. V. I. Polikarpov et al., Testing the Airtightness of Fuel Elements [in Russian], Atomizdat, Moscow (1964).
5. L. Zumwalt et al., Nucl. Sci. and Engng., 21, 1 (1965).
6. I. Wiliams, AECR, T1D-7546, 2 (1958).
7. I. MacEwan and W. Stevens, J. Nucl. Materials, 11, 77 (1964).
8. C. Townley et al., Nucl. Sci. and Engng., 10, 346 (1961).
9. S. T. Konobeevskii, The Effect of Radiation on Materials [in Russian], Atomizdat, Moscow (1967).
10. Yu. A. Zysin, A. A. Lbov, and L. I. Sel'chenkov, Fission Yield and Its Mass Distribution [in Russian], Gosatomizdat, Moscow (1963).
11. I. V. Gordeev, D. A. Kardashev, and A. V. Malyshev, Nuclear Physics Constants [in Russian], Gosatomizdat, Moscow (1963).
12. A. C. Damask and G. J. Dienes, Point Defects in Metals, Gordon and Beach (1964).

MEASUREMENT OF THE RATIO OF THE CROSS SECTIONS FOR RADIATIVE CAPTURE AND FISSION (α) FOR Pu^{239} IN THE NEUTRON ENERGY RANGE 0.1-30 keV

M. A. Kurov, Yu. V. Ryabov, So Tong Hsik,
N. Chikov, V. N. Kononov,
E. D. Poletaev, Yu. S. Prokopets,
and Yu. Ya. Stavisskii

UDC 539.172.4

The value of α for Pu^{239} is one of the fundamental constants that determines the technical and economic basis of modern nuclear power. This constant largely determines the value of the reproduction coefficient of nuclear fuel and detailed information about α is, therefore, of fundamental importance for the choice of the optimal design of industrial fast-neutron reactors. The experimental accuracy in the determination of α for Pu^{239} required for the design of large reactors has been analyzed in several investigations. In Table 1 we give the results of the analysis of Gribler et al. [1]. The table also contains an estimate of the accuracy of all the experimental data published prior to 1968.

In view of the unsatisfactory state of the experimental data on $\alpha(E)$, especially in the neutron energy range 0.1-30 keV, we measured the values of $\alpha(E)$ for Pu^{239} in this energy range in the present investigation.

EXPERIMENTAL METHOD

Apparatus. The cross section $\alpha(E) = \sigma_{n\gamma}(E)/\sigma_f(E)$ was measured by the time-of-flight method with a base line of 250 m and a resolution equal to ~220 and ~15 nsec/m. The source of resonance neutrons in the first case was a pulsed fast reactor of the Joint Institute of Nuclear Research and in the second case a pulsed fast reactor with an electron microtron-injector [2].

The experimental method consisted of comparing the number of counts of an ionization fission chamber containing "thin" Pu^{239} layers and a large liquid scintillation detector that measured the radiative capture and fission γ-rays from a "thick" Pu^{239} sample as a function of the neutron time of flight.

In the experiments we employed a high-efficiency ionization fission chamber [3] containing 120 mg of Pu^{239}. Approximately 70% of the fission events in the chamber were detected. An increase in the efficiency of detection of the fission fragments despite the presence of a large background of α-particles ($3.2 \cdot 10^8$ α-particles/sec) was achieved by an appreciable increase in the speed of response of the ionization chamber. The duration of the pulses from the chamber at the output of the amplifier, which determined the background of the multiple superpositions of α-particles, was $\lesssim$ 20 nsec. An appreciable increase in the speed of response of the chamber was achieved by making direct use of the current pulses that arose in the chamber, these pulses being subsequently amplified and discriminated by means of wide-band current devices.

The capture and fission γ-rays were detected by a large 500 liter scintillation tank. The detector contained a central channel through which the neutron beam passed. The sample was placed in this channel, the geometry being almost 4π. To decrease the background due to the radioactivity of the sample and cosmic rays the detector was split into two halves, these being connected for coincidence. Boron was introduced into the scintillator to decrease the background due to the detection of neutrons scattered by the sample. A special experiment showed that not more than 0.3% of the neutrons scattered by the sample

Translated from Atomnaya Énergiya, Vol. 30, No. 4, pp. 362-369, April, 1971. Original article submitted June 1, 1970.

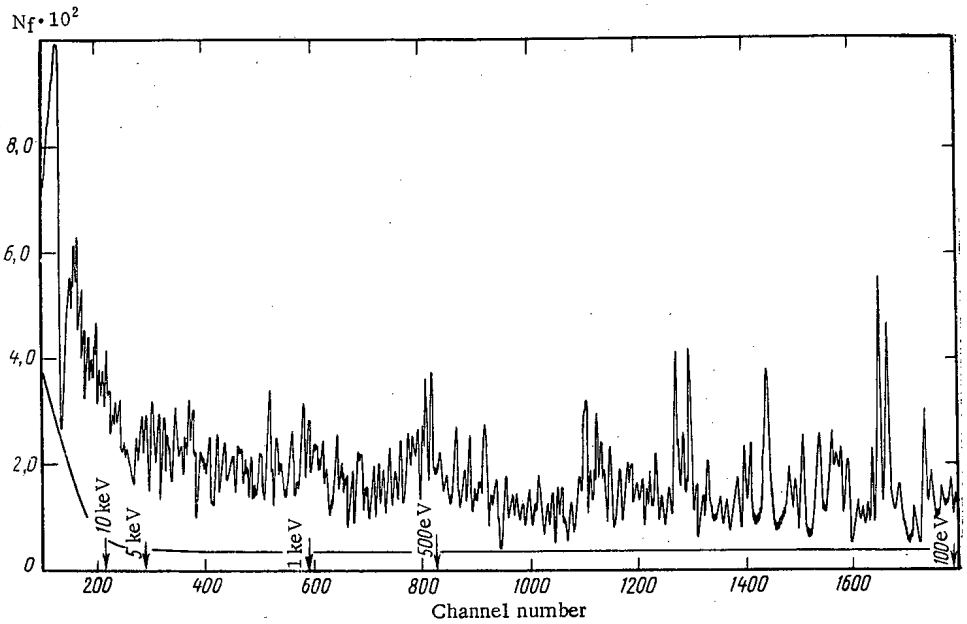

Fig. 1. Time-delay spectrum of pulses from the fission chamber (resolution 15 nsec/m).

TABLE 1. Accuracy in the Determination of α(E) for Pu^{239}

Neutron energy, keV	0,1	1	10	100	1000	10 000
Required accuracy	←5%	→←3%	→←5%	→←10%		
Existing accuracy	←—100—150%	→←15—20%	—→			

were detected. The effective detection threshold of γ-rays for both halves of the detector was ~0.8 MeV. The capture detection efficiency was thus ~20%. The use of coincidences between the two halves of the detector (which made it possible to reduce greatly the background) led to an appreciable decrease in the efficiency of detection of events accompanied by the emission of only a single γ-ray. However, since there was little change in the spectrum of the radiative capture γ-rays, this did not have a serious effect on the energy dependence of the efficiency [4].

In Figs. 1-4, we give the spectrograms obtained by means of the fission chamber and the scintillation detector for two conditions of measurements. These figures also include the background level, which was determined experimentally by means of absorbing resonance filters (Na 2.85 keV, Mn 0.337 keV, Co 0.132 keV, Ag 5.2 eV), these eliminating neutrons with the given energy from the beam. Unfortunately, this method of measuring the background could only be carried out reliably up to neutron energies of ~5 keV. At higher neutron energies suitable filters for measuring the background are not available and the background was therefore extrapolated with allowance for the dip in the spectra at E_0 = 35 keV connected with the filtration of neutrons in the aluminum stoppers of the neutron guide. However, the energy resolution in our experiments was clearly inadequate to make a reliable determination of the background level from the resonance in aluminum at 35 keV.

Evaluation of Experimental Data. The number of counts of the fission chamber and the γ-ray detector in an individual time-delay channel of the analyzer after elimination of the background can be represented in the form

$$N_f = n_f^0 \varepsilon_f;$$
$$N_\gamma = n_{n\gamma}\varepsilon_{n\gamma} + n_f\varepsilon_{\gamma f},$$

where n_f^0 and n_f are the number of fission events in the chamber and the sample; $n_{n\gamma}$ is the number of radiative capture events in the sample; ε_f, $\varepsilon_{\gamma f}$, and $\varepsilon_{n\gamma}$ are, respectively, the efficiencies of detection of fission events in the chamber and fission and radiative capture events in the sample. These relations yield an expression for α:

$$\alpha = A\frac{N_\gamma}{N_f} - B,$$

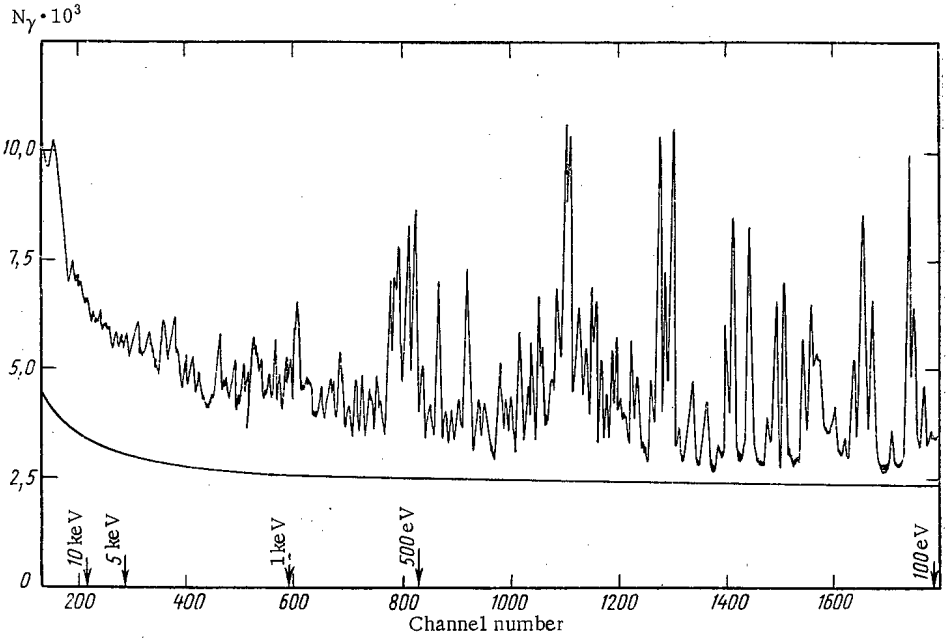

Fig. 2. Time-delay spectrum of pulses from the detector of the radiative capture and fission γ-rays in a Pu^{239} sample (resolution 15 nsec/m).

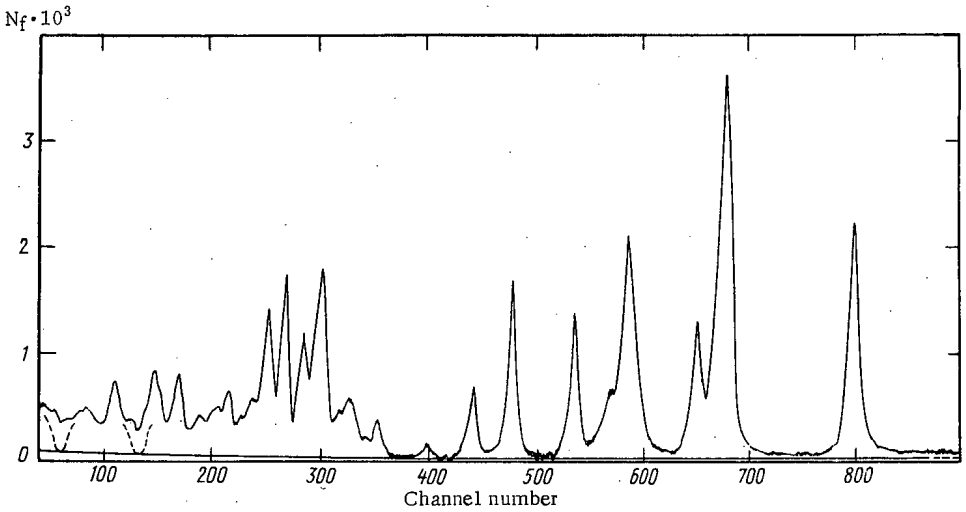

Fig. 3. Time-delay spectrum of pulses from the fission chamber (resolution 220 nsec/m).

where $A = (m^0/m)(\varepsilon_f/\varepsilon_{n\gamma})$, $B = \varepsilon_{\gamma f}/\varepsilon_{n\gamma}$ are constants which are obviously independent of the neutron energy under the assumption that $\varepsilon_{n\gamma}$ is only slightly sensitive to possible changes in the spectrum of the radiative capture γ-rays (m and m^0 are the amounts of Pu^{239} in the sample and chamber, respectively).

To determine A and B we used values of α_0 for well-resolved resonances. Calibration in series with the best resolution was carried out for 12 well-resolved resonances and in series with poor resolution for seven resonances. Allowance was made for the sample thickness (by means of the known resonance parameters [5, 6]) in the calibration.

Apart from α we also obtained the fission cross sections for Pu^{239} up to neutron energies of 30 keV With an absolute normalization of the fission cross sections we used the expression

$$\sigma_f(E) = \frac{kN_f(E)\,E^q}{\Delta E},$$

where ΔE is the energy width of the time-delay channel; E^{-q} is the relative dependence of the neutron flux

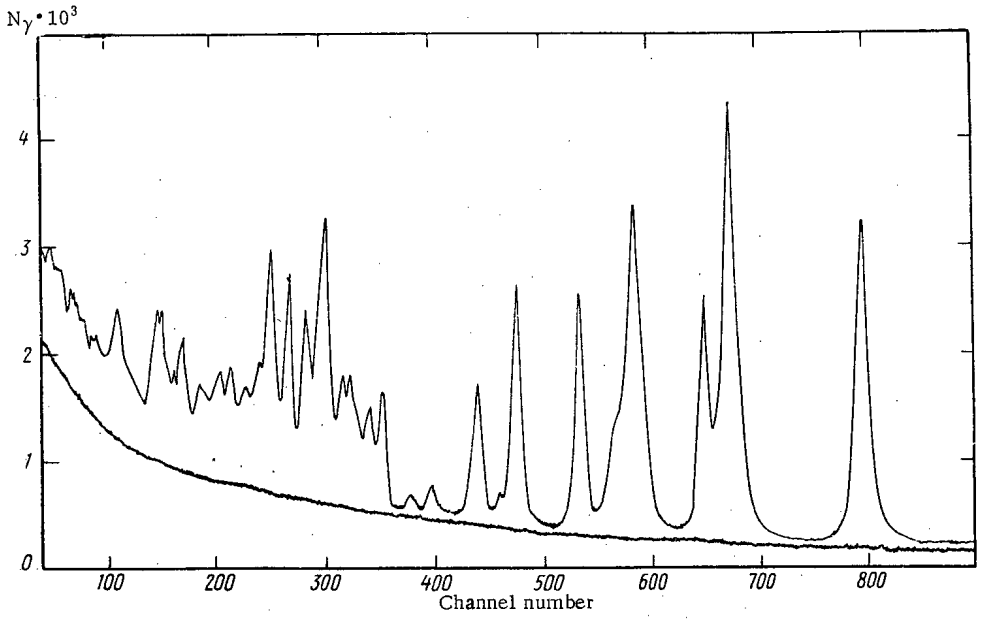

Fig. 4. Time-delay spectrum of pulses from the detector of the radiative capture and fission γ-rays in a Pu^{239} sample (resolution 220 nsec/m).

TABLE 2. Average Cross Sections $\langle \sigma_f(E) \rangle$ of Pu^{239} Obtained in Measurements with a Resolution of 15 nsec/m

E, keV	$\langle \sigma_f(E) \rangle \pm 15\%$,* b	$\langle \sigma_f(E) \rangle$,† b	E, keV	$\langle \sigma_f(E) \rangle \pm 15\%$,* b	$\langle \sigma_f(E) \rangle$,† b
20—29,6	2,05	1,57	1—2	5,56	3,85
10,1—20	2,09	1,71	0,9—1	10,93	
9,1—10,1	2,22	2,06	0,8—0,9	7,03	
8—9,1	2,32	2,25	0,7—0,8	6,57	
7—8	2,55	2,14	0,6—0,7	7,34	
6—7	2,13	2,19	0,5—0,6	18,33	
5—6	2,36	2,50	0,4—0,5	12,30	
4—5	2,65	2,45	0,3—0,4	7,30	
3—4	3,65	2,95	0,2—0,3	18,78	
2—3	3,61	3,07	0,1—0,2	21,63	

* Data of our investigation.

† Data of [8].

TABLE 3. Errors in the Determination of $\alpha(E)$

Value of α	Error associated with the calibration, %
0,2	35
0,5	14,8
1	7,4
1,5	4,9

measured by means of a BF_3 proportional counter; k is the constant of the cross section normalization deduced from the known values of $(\pi/2)\sigma_0\Gamma_f$ of several isolated resonances.

In the present investigation we made three series of measurements with the samples, one series with the fission chamber under microtron conditions, and one series with the chamber and the sample under reactor conditions. All the experimental data were evaluated with a computer.

DISCUSSION OF RESULTS

Fission Cross Section. To normalize the fission cross section we used the values of $\sigma_0\Gamma_f$ given in [5-7]. The accuracy with which this parameter is known for the low-lying resonances is 2% but the indeterminacy in the fission cross sections obtained in our experiment was due primarily to the statistical error, which amounts to 5-15% within the limits of the averaging interval. The fission cross sections obtained are given in Table 2. Agreement is observed within the experimental errors with the average fission cross sections recommended by James and Patrick [8] but the cross sections obtained in our investigation are systematically higher in the whole energy range by 5-20%.

Results for $\alpha(E)$. For the normalization of α we used the values of α_0 for 12 well-resolved resonances taken from [5, 6, 9]. The error in α_0 for the individual resonances was 10-40%. Therefore, to obtain normalized values of A and B by the method of least squares we used all the known data for α_0 with allowance for their weight, which was adopted in accordance with the error specified by the authors.

TABLE 4. Values of α_0 of the Resolved Resonances Used for Calibration

E_0, eV	Laboratory							
	Saclay [5]	ANL [9]	BNL [7]	Harwell [10]	ORNL [10]	RPI [10]	LNF [6]	JINR [6]
7,83	0,85±0,09	0,98±0,10	1,04±0,09	1,0±0,1	0,85±0,02	0,84±0,04	0,87±0,07	0,85±0,02
10,97	0,38±0,08	0,22±0,10	0,32±0,08	0,36±0,08	0,27±0,05	0,24±0,03	0,27±0,04	0,35±0,08
11,91	1,75±0,25	1,86±0,35	1,86±0,20	1,56±0,20	1,56±0,10	1,52±0,10	1,38±0,21	1,54±0,16
14,36	0,51±0,14	0,66±0,16	1,82±0,20	0,67±0,13	0,55±0,02	0,58±0,04	0,67±0,10	—
14,75	1,25±0,07	1,21±0,18	1,32±0,25	1,31±0,13	1,13±0,05	1,11±0,08	1,25±0,14	—
17,69	1,15±0,04	0,84±0,21	1,0±0,2	1,15±0,10	1,14±0,05	—	0,92±0,13	1,04±0,08
22,33	0,71±0,07	0,46±0,24	0,59±0,14	0,76±0,07	0,64±0,01	—	0,71±0,06	0,80±0,08
26,31	0,84±0,17	1,07±0,21	1,22±0,26	1,21±0,15	0,91±0,03	0,91±0,05	0,68±0,21	0,82±0,09
44,6	9,28±0,40	9,61±0,91	7,3±1,7	8,5±0,5	9,52±1,00	9,38±0,30	4,6±2,5	—
47,92	0,31±0,10	0,13±0,05	0,16±0,07	0,36±0,08	0,32±0,06	—	0,11±0,06	—
50,18	3,5±0,4	1,20±0,33	1,27±0,23	2,08±0,30	—	2,45±0,10	1,51±0,43	—
52,8	5,25±0,20	4,40±0,66	4,6±1,2	4,99±0,49	—	5,22±0,20	4,1±0,9	—

TABLE 5. Averaged Value $<\alpha>$ for Pu^{239} Obtained in the Measurements with the Resolutions 15 and 220 nsec/m

Averaging interval, keV	Resolution	
	15 nsec/m	220 nsec/m
10,1—29.5	0.48±0,10	0,36±0,08
9,1—10.1	0,43±0.06	0,46±0,09
8—9.1	0.49±0,06	0.43±0,08
7—8	0,46±0,07	0.44±0,08
6—7	0,97±0,08	0,59±0,10
5—6	0,90±0,05	0,65±0,09
4—5	0,95±0,08	0.71±0,08
3—4	0,67±0,08	0,77±0,11
2—3	0.89±0,14	0.83±0.14
1—2	0.65±0,14	0,78±0,13
0,9—1	0,48±0,11	0,65±0,15
0,8—0,9	0,68±0,14	0,63±0.14
0,7—0,9	1.03±0,07	0,70±0,16
0,6—0,7	0.75±0,13	0,92±0,21
0,6—0,6	0.68±0,10	0,70±0,10
0,4—0,5	0.48±0,16	0,60±0,12
0,3—0,4	1,71±0,28	0.82±0,23
0.2—0,3	1,31±0,23	0,72±0,16
0,1—0.2	0.71±0.07	0.73±0,05

For 10 resonances chosen for the calibration the value of α_0 lay in the interval 0.22-1.66. This range of values is of the most interest since the values of $\alpha(E)$ for the range of neutron energies 1-30 keV correspond to precisely this interval. However, two resonances with a large value of α have the greatest weight in the determination of the slope of the calibration straight line. Unfortunately, the value of α_0 is less well known for just these resonances.

In Table 3 we give the error in the values of $\alpha(E)$ due to the calibration, the errors in the data given in Table 4, and also to the application of the method of least squares to calculate the coefficients A and B.

The values of α obtained in the present investigation are given in Table 5. In the experiments we used a Pu^{239} sample of thickness $0.7 \cdot 10^{21}$ nuclei/cm^2. The results for the microtron conditions were obtained by averaging over three series of measurements and the specified errors characterize the root-mean-square spread of the data of these series. The indeterminacy in the value of α due to the statistical error in the measurements of the ratio N_γ/N_f and also allowance for the background of each series amounts to 20-50%. The final data for the microtron conditions were obtained by averaging the fission and radiative capture cross sections over the intervals 0.1, 1, 20 keV. For the reactor conditions an estimate of the accuracy of the results of the measurements based on allowance for the statistical errors in the ratio N_γ/N_f, the statistical error in the determination of the background level, and the errors associated with the calibration lead to an indeterminacy in the value of α that ranges from ±15 to ±20%.

Comparison of our results with those already published (Fig. 5) reveals satisfactory agreement with the data of [10] and discrepancies (that exceed the limits of the errors) with the results of [11] in the energy range 2-5 keV and [12] in the energy range 2-30 keV. Note the good agreement of our data in the whole energy range with the recent measurements made at Dubna with a resolution of 60 nsec/m [14]. Note also that in the cases when the energy resolution of the spectrometers was sufficiently high (the energy range below 1 keV) the structure in the energy dependence of $\alpha(E)$ due to the fluctuations of the fission widths is well reproduced.

It is clear that the considerable discrepancy between the results of measurements of $\alpha(E)$ in different laboratories in the neutron energy range 1-30 keV cannot be explained solely by the inadequate accuracy of the values of the resonance parameters used for the calibration. The cause of these discrepancies is most probably to be found in an inadequate procedure for measuring the background level by the method of resonance filters. This applies particularly to experiments with linear accelerators, for which the shortest base lengths are used (25-35 m) since the variable component of the background associated with neutrons scattered in the measuring section may be appreciable for times of flight less than 200 μsec. Therefore, to obtain more reliable data on α in the neutron energy range 1-30 keV it is best to use spectrometers

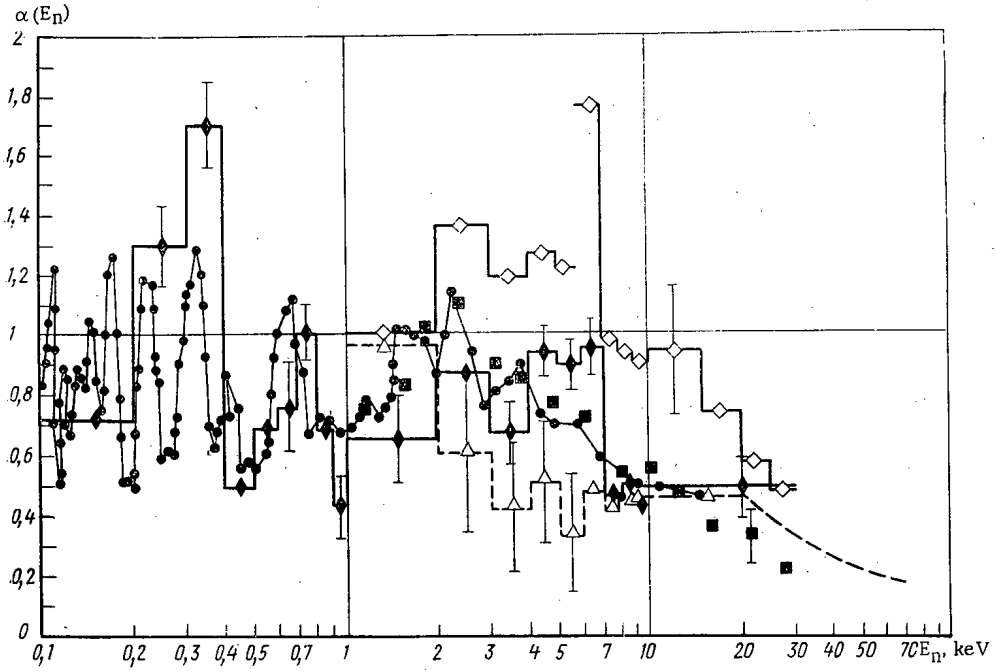

Fig. 5. Results of measurements of α in the range 0.1-100 keV: –●–) present investigation, resolution 220 nsec/m; –◆–) present investigation, resolution 15 nsec/m (sample with $0.7 \cdot 10^{21}$ nuclei/cm^2); ■) data of [9]; – – –Δ– – –) [11]; –◇–) [12] (the mean result for several series of measurements is given); – – –) [13].

with long base lines. A promising development would be to make experiments with pulsed van der Graaf accelerators in the range of lower neutron energies.

The authors would like to express their sincere gratitude to A. I. Leipunskii, F. L. Shapiro, and L. N. Usachev for their constant interest in the investigation; to L. B. Pikel'ner for making it possible to carry out the measurements with the scintillation (n, γ) detector; and to L. N. Sedlakova, Ts. Panteleev, and Yu. Kolgin for assistance in evaluating the results with a computer and for helping with the measurements.

LITERATURE CITED

1. P. Gribler et al., Nucl. Applic., No. 5, 297 (1968).
2. V. L. Anan'ev et al., At. Énerg., 20, 106 (1966).
3. V. N. Kononov et al., Prib. Tekh. Éksp., No. 6, 51 (1969).
4. Yu. A. Aleksandrov, Yu. V. Ryabov, and G. S. Samosvat, Preprint JINR R-2014 [in Russian], Dubna (1965).
5. H. Darrien et al., Nucl. Data for Reactors, Vol. 11, IAEA, Vienna (1967), p. 195.
6. Yu. V. Ryabov et al., Yad. Fiz., 5, 925 (1967).
7. BNL-325, Suppl. 2 (1965).
8. G. James and B. Patrick, AERE-M2068 (1968).
9. L. M. Bollinger et al., Proceedings of the Second United Nations International Conference on the Peaceful Uses of Atomic Energy, Geneva, 1958, Published by the United Nations, Geneva (1958).
10. Proceedings of the Conference of Experts of the International Atomic Energy Agency on α (Pu-239), Winfrith (England) (1969).
11. Yu. V. Ryabov et al., At. Énerg., 4, 351 (1968).
12. M. Sowerby et al., Fast Reactor Phys., Vol. 1, IAEA, Vienna (1968), p. 289.
13. G. de Saussure et al., Nucl. Data for Reactors, Vol. 11, IAEA, Vienna (1967), p. 233.
14. M. A. Kurov et al., Preprint JINR R3-5002 [in Russian], Dubna (1970).

CROSS SECTION OF THE $Am^{241}(n, \gamma)Am^{242}$ REACTION FOR A NEUTRON SPECTRUM SIMILAR TO THE FISSION SPECTRUM

N. I. Ivanova, A. N. Kobzev,
N. G. Krylov, A. A. Lbov,
N. P. Martynov, A. E. Trikanov,
and A. I. Shelamkov

UDC 539.172.4

This investigation is concerned with the use of the activation method for measuring the cross section of the $Am^{241}(n, \gamma)Am^{242}$ reaction ($T_{1/2}$ = 16.01 h) for neutrons having a spectrum similar to the fission spectrum.* Existing data [1] relating to the cross sections of the (n, γ) reaction of Am^{241} only refer to thermal neutrons. There are no such data for fast neutrons.

EXPERIMENTAL METHOD

The use of the activation method for measuring the cross section of the $Am^{241}(n, \gamma)Am^{242}$ reaction encounters serious difficulties associated with the necessity of recording the β-activity of the developing Am^{242} on the much greater background of the intrinsic α- and γ-activity of the irradiated Am^{241} and the fission fragments formed.

For the 1 mg samples of Am^{241} here studied, the α-activity equalled $\sim 7.2 \cdot 10^9$ decays/min, and the γ-activity, which was almost entirely determined by a line with an energy of 59.57 keV (quantum yield 0.37 [2]) was equal to $\simeq 2.7 \cdot 10^9$ quanta/min. An estimate of the expected β-activity of the Am^{242}, based on an integrated flux of $2 \cdot 10^{15}$ neutrons/cm^2 at the sample and a possible cross section of the (n, γ) reactions of $\sim$0.3 b, amounted to $\sim 0.9 \cdot 10^6$ decays/min at the end of the irradiation period. Here it was assumed that 83.6% and (16.4 $\pm$ 0.3)% of the total were associated with β-decay and electron capture respectively [2].

Taking account of the time (some 20 h) needed to separate the americium chemically and purify it from fission products, the β-activity of Am^{242} at the target may be equated to $(3\text{–}4) \cdot 10^5$ decays/min.

In order to measure the β-activity of the Am^{242}, we used a sensor containing a plastic scintillator 53 × 1 mm in size and an FÉU-11B photomultiplier. The pulses from the sensor fell on a single-channel amplitude analyzer, operating in the integrated mode of recording.

In order to eliminate the influence of the background α-activity of the sample when making the measurements, an aluminum absorber was employed; the contribution of the γ-activity and x-radiation was reduced by pulse discrimination in the recording system. An aluminum absorber 100 μ thick was placed between the sample and the the crystal; the measurements were made with differing registration thresholds, corresponding to $E_\beta \approx$ 150–300 keV. For the preliminary calibration of the apparatus with respect to efficiency, we used the following isotopes: Sr^{90} (E_β = 0.54 MeV), Tl^{204} (E_β = 0.765 MeV), and Au^{198} (E_β = 0.963 MeV). The choice of these isotopes for the calibration was determined by the fact that the Am^{242} had E_β = 0.667 MeV (40%) and E_β = 0.625 MeV (60%) [2]. The recording efficiency for Am^{242} under the measuring conditions chosen was 13.7 and 11%, depending on the value of the threshold. In order to eliminate the influence of the activity arising from the fragments, radiochemical purification was incorporated.

*The neutron spectrum is characterized by the following energy distribution: 0–0.1 MeV 3.8%; 0.1–0.4 MeV 19.3%; 0.4–0.9 MeV 26.9%; 0.9–1.4 MeV 15.0%; 1.4–3.0 MeV 23.8%; over 3.0 MeV 11.2%.

Translated from Atomnaya Énergiya, Vol. 30, No. 4, pp. 369–372, April, 1971. Original article submitted October 15, 1970.

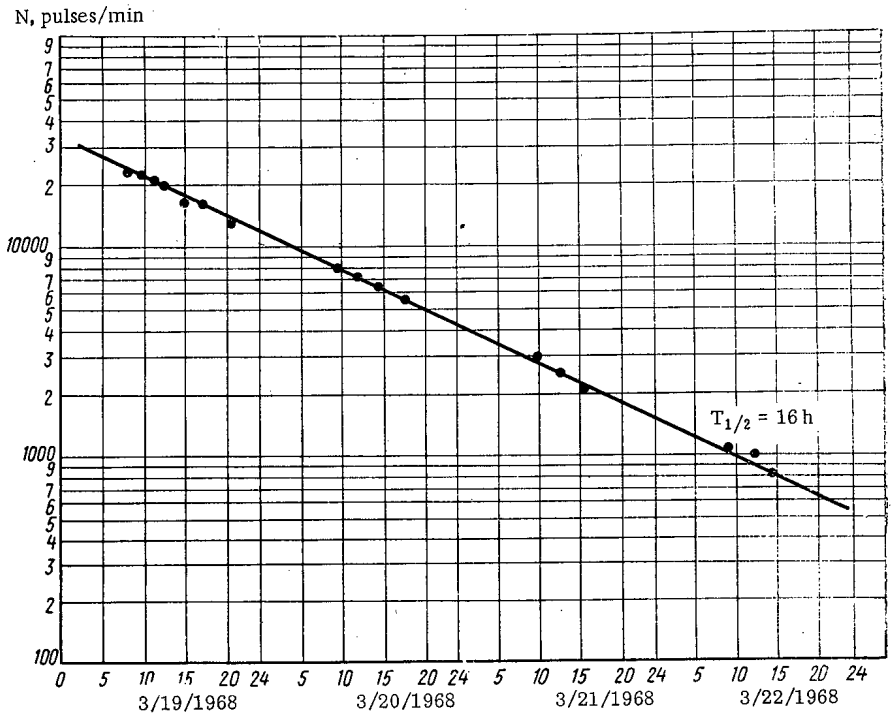

Fig. 1. Decay curve of Am^{242} (sample No. 3).

Before the irradiation, the original material, taken in the form of americium chloride, was subjected to chemical processing in order to remove fission products and other possible impurities. After evaporation to dryness in quartz cassettes, the americium chloride was irradiated. The amount of material in each cassette was about 1 mg. In order to eliminate the influence of the thermal-neutron background, the quartz cassettes were placed in cadmium sheaths with a wall thickness of 0.5 mm; at the bottom of each cadmium-shielded cassette was an Au^{197} foil approximately 2 mg in weight (for monitoring the neutron flux).

Three neutron irradiations were carried out. In each experiment two Am^{241} cassettes were irradiated. The integrated neutron flux, measured by means of the fission chambers, approximately equalled $2 \cdot 10^5$ neutrons/cm^2.

The active sample containing the americium and its fission products was subjected to chemical purification immediately after irradiation. In view of the comparatively short half life of the Am^{242} formed ($T_{1/2}$ = 16.01 h), the principal requirement laid upon the method of chemical purification was that of maximum speed, with a reasonably high coefficient of purification from the fission products.

After irradiation, the americium was leached from the quartz cassette with concentrated hydrochloric acid, and the solution was passed through Dowex 2X8 resin, which retained many of the transition elements and also elements constituting fission products (operation 1).

After passing through the column, the solution was evaporated to dryness, the residue was dissolved in concentrated hydrochloric acid, and operation 1 was then repeated (operation 2).

The separation of the americium from the rare-earth and alkaline-earth elements and also from various other fission products was effected in Dowex 2X8 resin in the thiocyanate form. We used columns 0.2 mm × 11 cm in size. For filling the column we used resin in the chloride form, the rate of deposition of the particles in the water being 0.2-0.4 cm/min. The anion exchanger was converted into the thiocyanate form by prolonged washing with a solution characterized by a strength index of 5 M with respect to NH_4CNS and 0.1 M with respect to HCl. After operation 2, the eluate was evaporated to dryness, and the residue was dissolved in two or three drops of a similar solution. The resultant solution was transferred to the thiocyanate column for the sorption of the americium and the fission products. The fission products were washed from this column with a solution characterized by a strength index of 1 M with respect to NH_4CNS and 0.01 M with respect to HCl, containing 40% of ethyl alcohol. Then the americium was washed from the column with 0.1 M HCl (2-2.5 free volumes of the column). The eluate was collected on a platinum substrate and dried under an infrared heater in order to remove the solvents and a small amount of ammonium thiocyanate.

TABLE 1. Principal Experimental Results

Serial No. of irradiation	Serial No. of sample	Integrated neutron flux, neutrons/cm^2	Amount of Am^{241} in the target, atoms	Absolute activity of the Am^{242}, decays/min	Measured cross sections, mb	Average cross section, mb
I	1	$1,96 \cdot 10^{15}$	$2,32 \cdot 10^{18}$	$7,4 \cdot 10^5$	228	240 ± 30
	2	$1,96 \cdot 10^{15}$	$1,23 \cdot 10^{18}$	$4,0 \cdot 10^5$	232	
II	3	$1,97 \cdot 10^{15}$	$2,06 \cdot 10^{18}$	$6,8 \cdot 10^5$	233	
	4	$1,97 \cdot 10^{15}$	$4,9 \cdot 40^{17}$	$1,9 \cdot 10^5$	273	
III	5	$2,0 \cdot 10^{15}$	$1,89 \cdot 10^{18}$	$6,4 \cdot 10^5$	235	
	6	$2,0 \cdot 10^{15}$	$4,22 \cdot 10^{17}$	$1,5 \cdot 10^5$	248	

The foregoing chemical method of separating the americium yielded a coefficient of purification from the fission products of about 10^5 (some 15-20 h after irradiation had ended); the chemical yield of americium equalled 80-90%. The period required for the separation was 15-20 h. However, the actual chemical yield was not over-important, since the calculation of the cross section was based on measurements of the α- and β-activity arising from the same sample.

RESULTS

The fall in the β-activity of the samples with time was measured for a period equal to four or five Am^{242} half lives. After this time the sensor recorded only the constant background activity of the target, principally that due to the γ-radiation of the Am^{241}, with an energy of 59.57 keV. After subtracting the constant background activity, the β-activity due to the Am^{242} was readily distinguished (Fig. 1).

The amount of Am^{241} in the target was determined from the total α-activity measured in the integrating ionization chamber.

The cross section was calculated from the well-known relation

$$\sigma(n, \gamma) = \frac{AT_{1/2}}{n_0 Q \cdot 0.693},$$

where A is the absolute activity of the Am^{242} in the target at the instant at which the irradiation ended (allowing for the recording efficiency, corrections for decays taking place during the irradiation period, corrections for inaccuracies in the decay scheme); $T_{1/2}$ is the half life of the Am^{242}; n_0 is the number of Am^{241} atoms in the target; Q is the neutron flux of a spectrum closely resembling the fission spectrum.

We obtained the cross section corresponding to the radiative capture of neutrons in Am^{241} for six samples (Table 1). The results of the individual measurements had no appreciable scatter over and above that of the experimental errors. The average cross section of the $Am^{241}(n, \gamma)Am^{242}$ reaction was equal to $\sigma(n, \gamma)Am^{241} = (240 \pm 30) \cdot 10^{-27}$ cm^2.*

The errors committed in the cross-section measurements comprise inaccuracies in determining the activity of the samples (2-4%), the half life of the Am^{242} (2%), the neutron flux (7%), and the amount of material in the target (4%), and also errors introduced when determining the efficiency of the sensor (3%); the total measuring error is 10-12%.

In order to check for the presence of possible systematic errors in the measuring method, an Au^{197} sample was irradiated at the same time as the Am^{241}.

The cross section for the $Au^{197}(n, \gamma)Au^{198}$ reaction measured with the plastic scintillator equalled $\sigma(n, \gamma)Au^{197} = (140 \pm 15) \cdot 10^{-27}$ cm^2, in excellent agreement with the earlier value of $\sigma(n, \gamma)Au^{197} = 150 \cdot 10^{-27}$ cm^2 [3]; this verified the applicability of the method in question for measuring the capture cross section of fast neutrons in Am^{241}.

LITERATURE CITED

1. J. Stehr et al., Neutron Cross Sections, BNL-325 (1966).
2. V. M. Gorbachev et al., Fundamental Characteristics of the Isotopes of Heavy Elements [in Russian], Atomizdat, Moscow (1970).
3. I. V. Gordeev et al., Nuclear-Physics Constants [in Russian], Atomizdat, Moscow (1963), p. 316.

*That is, the cross section only leading to the formation of Am^{242} with $T_{1/2} = 16.01$ h.

CHEMICAL AND PHASE TRANSFORMATIONS IN URANIUM HEXAFLUORIDE AT HIGH TEMPERATURES

N. P. Galkin and Yu. N. Tumanov

UDC 546.791:546.16

Uranium hexafluoride is a thermally stable compound. This is evidenced, in particular, by the fact that during the production of uranium hexafluoride in the fluorination of the tetrafluoride with elementary fluorine, temperatures exceeding 1400°K are developed in the flame reactor [1].

In the work of Kudrin [2] it is indicated that in the temperature interval $5 \cdot 10^3$–$3 \cdot 10^4$°K, the basic components of the plasma, produced from the initial gas uranium hexafluoride, are U, F_2, F, and F'. The equilibrium constants of the reaction [3]

$$(UF_6)_{gas} \rightarrow (UF_4)_{gas} + 2(F)_{gas}$$

were also calculated.

To resolve certain practical questions it is necessary to know the thermodynamic and kinetic characteristics of the process of gas phase decomposition of uranium hexafluoride, heated to a temperature of $\sim 3 \cdot 10^3$°K. Uranium tetrafluoride can be isolated under these conditions. In this work an attempt was made to determine the indicated characteristics.

Mechanism of the Decomposition of UF_6

The mechanism of the decomposition of uranium hexafluoride to the tetrafluoride can evidently be represented by the following scheme of potentially possible reactions:

$$(UF_6)_{gas} \rightarrow (UF_5)_{gas} + (F)_{gas}, \quad \Delta H^0_{293} = 80\,720 \text{ cal}; \tag{1}$$

$$(UF_5)_{gas} \rightarrow (UF_4)_{gas} + (F)_{gas}, \quad \Delta H^0_{298} = 93\,200 \text{ cal}; \tag{2}$$

$$2(F)_{gas} \rightarrow (F_2)_{gas}, \quad \Delta H^0_{298} = -38\,000 \text{ cal}; \tag{3}$$

$$(UF_6)_{gas} + (F)_{gas} \rightarrow (UF_5)_{gas} + (F_2)_{gas}, \quad \Delta H^0_{293} = -42\,720 \text{ cal}; \tag{4}$$

$$(UF_5)_{gas} + (F)_{gas} \rightarrow (UF_4)_{gas} + (F_2)_{gas}, \quad \Delta H^0_{298} = -55\,200 \text{ cal}. \tag{5}$$

Reactions (1) and (2) have a positive entropy change; reactions (3)–(5) have a negative entropy change. Since reactions (1), (2), (4), and (5) are endothermic, we should consider only reactions (1), (2), and the exothermic reaction (3) at high temperatures.

Thermodynamics of the Decomposition of UF_6

To find the equilibrium partial pressures in the mixture obtained when uranium hexafluoride is heated, it is necessary to solve a system of five equations:

$$K_{p_1} = \frac{p_{UF_5} p_F}{p_{UF_6}}; \tag{6}$$

$$K_{p_2} = \frac{p_{UF_4} p_F}{p_{UF_5}}; \tag{7}$$

$$K_{p_3} = \frac{p_{F_2}}{p_F^2}; \tag{8}$$

$$p_{UF_6} + p_{UF_5} + p_{UF_4} + p_{UF_2} + p_F = 1 \text{ abs. atm}; \tag{9}$$

$$\frac{p_{UF_6} + p_{UF_5} + p_{UF_4}}{6p_{UF_6} + 5p_{UF_5} + 4p_{UF_4} + 2p_{F_2} + p_F} = \frac{1}{6}. \tag{10}$$

Translated from Atomnaya Énergiya, Vol. 30, No. 4, pp. 372–376, April, 1971. Original article submitted February 13, 1970; revision submitted May 4, 1970.

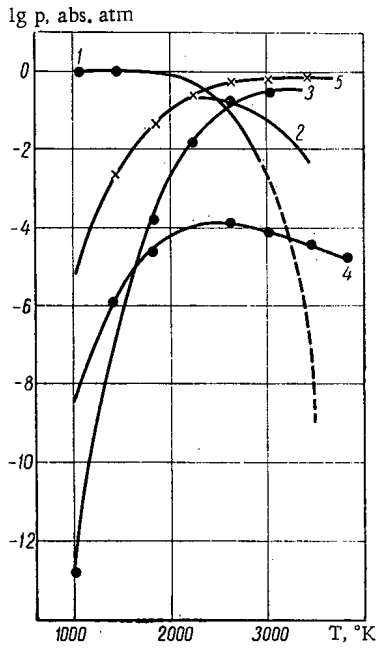

Fig. 1. Partial pressures of uranium fluorides as a function of the temperature: 1) p_{UF_6}; 2) p_{UF_5}; 3) p_{UF_4}; 4) p_{F_2}; 5) p_F.

TABLE 1. Values of the Reduced Thermodynamic Potential of Gaseous Uranium Fluorides (cal/mole · deg)

T, °K	UF_6	UF_5*		UF_4† (T_d)
		D_{3h}	C_{4v}	
1000	101,641	95,167	94,487	90,250
1400	112,396	104,005	103,355	97,590
1800	120,764	110,923	110,293	103,00
2200	127,610	116,608	115,998	107,558
2600	134,404	121,426	120,826	111,443
3000	139,424	125,610	125,020	114,810
3400	142,854	129,307	128,727	117,795
3800	146,817	132,618	131,048	120,459
4200	150,403	135,616	135,066	122,841

* The UF_5 molecule has one free electron, and its ground state is assumed to be doublet.

† A singlet state is assumed for the UF_4 molecule.

Here p_i represents the partial pressures of the components of the high-temperature gas mixture;

$$K_{e_i} = e^{1/R\left(\Delta\Phi^*_{T,i} - \frac{\Delta H^0_{0,i}}{T}\right)}, \qquad (11)$$

where K_{ei} are the equilibrium constants of reactions (1)-(3); $\Delta\Phi^*_{T,i}$ and $\Delta H^0_{0,i}$ are the changes in the reduced thermodynamic potential at the temperature T and the enthalpies of the reaction at absolute zero; R is the gas constant. The values of $\Phi^*_{F_2}$ and Φ^*_F are known [4]. The values of $\Phi^*_{UF_6}$ were calculated in the approximation of a rigid rotator – harmonic oscillator – according to the known values of the molecular constants, taken from [5]. The thermodynamic properties of gaseous uranium tetrafluoride were calculated according to the equivalent molecular constants T_d of the model of the UF_4 molecule [6].

The thermodynamic properties of uranium pentafluoride were calculated by the method outlined in [7], on the assumption that UF_5 molecules, just like other pentafluoride molecules [8], have the structure either of a trigonal bipyramid of the point group D_{3h} or a tetragonal pyramid of the point group C_{4v}.

Hoskins and Lord [9] have shown that pentafluoride molecules, for example, PF_5 and AsF_5, during the process of intramolecular exchange of fluorine atoms, exist with some probability both in the form of a trigonal bipyramid and in the form of a tetragonal pyramid. The frequency of exchange is determined by the expression

$$\nu(\text{sec}^{-1}) = \frac{kT}{h}\exp\left(-\frac{1000\Delta E^*}{RT}\right)\exp(\Delta S/R), \qquad (12)$$

where k and h are the Boltzmann and Planck constants, respectively; ΔS is the entropy difference of the D_{3h} and C_{4v} structures; R is the gas constant; ΔE^* is the difference of the potential energies of the D_{3h} and C_{4v} structures.

According to the estimate of Hoskins and Lord [9], $\exp(\Delta S/R)$ lies in the interval 1-10, but is closer to 1, while ΔS lies in the interval 0-4.53 cal/mole · deg. For heavy molecules the values of $(S^0_T)_{D_{3h}} - (S^0_T)_{C_{4v}}$ and $(\Phi^*_T)_{D_{3h}} - (\Phi^*_T)_{C_{4v}}$ are less than 1 cal/mole · deg [7]; therefore in the calculations we can use the thermodynamic properties of the D_{3h} and C_{4v} structures of UF_5.

The molecular constants according to which the thermodynamic properties of the three uranium fluorides in the ideal gas state were calculated, are cited in [4, 6, 7]. The values of the reduced thermodynamic potential of the three uranium fluorides are presented in Table 1. To calculate the equilibrium constants K_{e_1} and K_{e_2} we used the values of Φ^*_T of the D_{3h} model of the UF_5 molecules, which is an analog of the $MoCl_5$ and WCl_5 molecules, which have a trigonal bipyramid structure [10].

Figure 1 presents the calculated dependences of the partial pressures of fragments of the UF_6 molecule on the temperature at a total pressure equal to 1 atm. The partial pressure of the hexafluoride

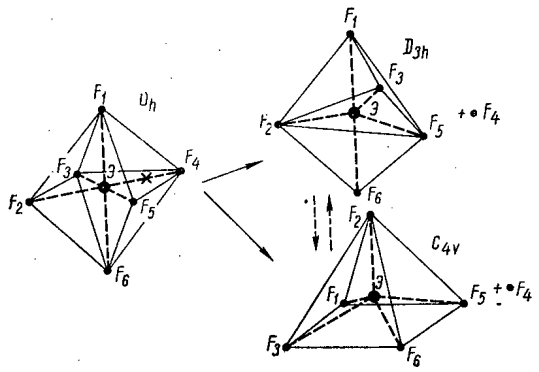

Fig. 2

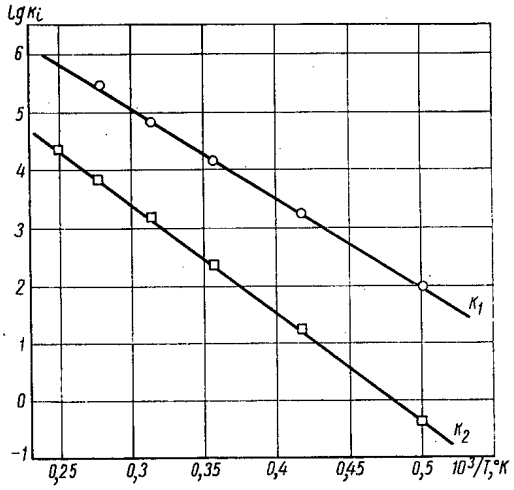

Fig. 3

Fig. 2. Structural changes during reaction (1).

Fig. 3. Dependence of the logarithms of the rate constants of reactions (1) and (2) on the reciprocals of the temperature.

decreases sharply after 2200°K; the uranium hexafluoride pressure has a maximum at T = $2.4 \cdot 10^3$°K; the pressure of the tetrafluoride has a maximum at T = $3.2 \cdot 10^3$°K. For complete conversion of uranium hexafluoride to the tetrafluoride and fluorine, it is necessary to heat the hexafluoride to 3200-3400°K.

Kinetics of the Decomposition of Uranium Fluorides

Complex polyatomic molecules with high energies of bond cleavage are characterized by a monomolecular mechanism of decomposition [11-13].

The rate constant of the monomolecular reaction can be estimated by the expression [14]

$$k_i = \lambda_{0,\,i} e^{-\varepsilon_i/kT} \frac{1}{(f-1)!} \left(\frac{\varepsilon_i}{kT}\right)^{f-1}, \qquad (13)$$

where $\lambda_{0,\,i}$ is the fraction of activated molecules reacting per unit time; ε_i is the activation energy; f is the number of oscillators; k is Boltzmann's constant; T is the absolute temperature.

Reactions (1) and (2) represent the elementary step of the decomposition of UF_6. It may be assumed that the electronic levels of the UF_6 and UF_5 molecules lie rather high, and the dissociation of these molecules occurs from the electronic ground state. In this case the activation energy of reactions (1) and (2) is equal to the cleavage energy of the bond. For reaction (1) ε_1 = 80,720 cal; for reaction (2) ε_2 = 93,200 cal. In both cases fkT < ε_i. The values of λ_{0i} can be estimated according to the following function [14]:

$$\lambda_{0,\,i} = 2nr_{1,2}^2 \left(\frac{4\pi kT}{m}\right)^{1/2} \approx \lambda_{-1,\,i}, \qquad (14)$$

where n is the concentration of particles at which the order of the reaction changes; $r_{1,2}$ is the sum of the radii of the colliding particles; m is the mass of the particle; $\lambda_{-1,\,i}$ is the fraction of active particles deactivated per unit time.

At low pressures, monomolecular reactions proceed according to second order, while at high pressures they proceed according to first order. The upper and lower limits of the pressures, within which the reaction order changes, were found according to the empirical dependence of the pressure of the transition on the number of excited oscillators in the molecule, constructed according to the literature data [14]. From this dependence it was found that in the pressure interval 0.3-150 mm Hg, for UF_6 and UF_5 molecules, second order changes to first. Above a pressure of 150 mm Hg, both reactions proceed according to first order.

The possible structural changes that occur during reaction (1) are presented in Fig. 2. The cross marks the bond to be broken in the octahedral UF_6 molecule. From the standpoint of the principle of least pressure [15], it makes no difference which bond in the UF_6 molecule is broken, since they are all equivalent.

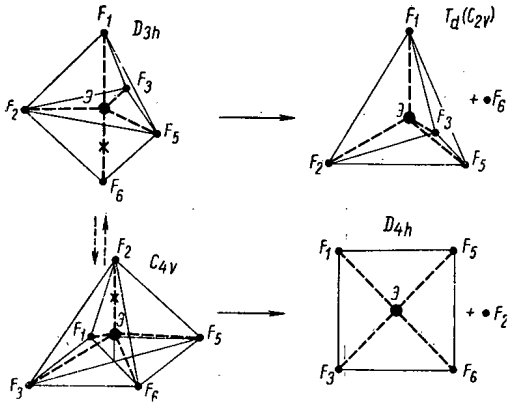

Fig. 4

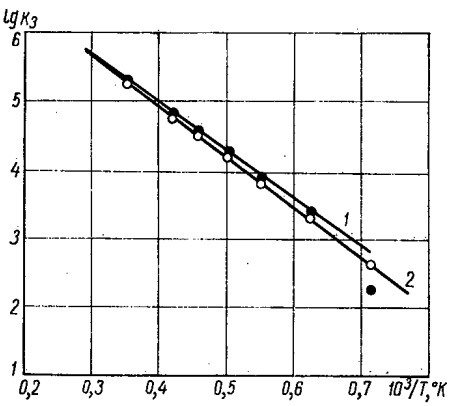

Fig. 5

Fig. 4. Structural changes during reaction (2).

Fig. 5. Dependence of the logarithms of the rate constants of reaction (3) on the values of $10^3/T$: 1) calculation; 2) experiment.

TABLE 2. Rate Constants of Recombination ($cm^3 \cdot sec^{-1}$) of Uranium Fluorides and Fluorine

T, °K	$UF_5 + F \rightarrow UF_6$	$UF_4 + F \rightarrow UF_5$	$F + F \rightarrow F_2$
	k_1^1	k_2^1	k_3^1
2000	$1{,}032 \cdot 10^{-18}$	$4{,}77 \cdot 10^{-20}$	$2{,}25 \cdot 10^{-17}$
2400	$5{,}77 \cdot 10^{-19}$	$4{,}06 \cdot 10^{-20}$	$9{,}67 \cdot 10^{-18}$
2800	$4{,}77 \cdot 10^{-19}$	$3{,}11 \cdot 10^{-20}$	$6{,}36 \cdot 10^{-18}$
3200	$3{,}41 \cdot 10^{-19}$	$2{,}79 \cdot 10^{-20}$	—

According to the same principle, both configurations of the UF_5 molecule (D_{3h} and C_{4v}) are equally probable. By analogy with the $MoCl_5$ and WCl_5 molecules, we might expect a greater probability for the D_{3h} model of the UF_5 molecule [10], but in the case of intramolecular movement, a transition $D_{3h} \rightleftharpoons C_{4v}$ is possible [9].

For reaction (1), $r_{1,2} = 2r_{U-F} + 2r_F = 5.274$ Å, $m_1 = 5.84 \cdot 10^{-22}$ g, $n = 5.31 \cdot 10^{18}\ 273/T\ cm^{-3}$, $f = 3$. The latter follows from the principle found by Leermakers [16], in accord with which the number of oscillators participating in a reaction is equal to three times the number of heavy atoms in the molecule. Moreover, the $UF_5 - F$ bond corresponds to approximately three oscillators. The calculation was performed beginning with temperature $T \geq 2000°K$. The dependence of the rate constant on the temperature is presented in semilogarithmic form in Fig. 3.

The structural changes that occur during reaction (2) are presented in Fig. 4. In the D_{3h} structure of the UF_5 molecule, cleavage at the $U(V) - F_1$ and $U(V) - F_6$ bonds is more probable; in the C_{4v} structure, cleavage at the $U(V) - F_2$ bond is more probable. From the standpoint of the principle of least movement, the transitions $D_{3h} \rightarrow C_{2v}(T_d)$; $C_{4v} \rightarrow D_{4h}$ are more probable. By analogy with pentafluorides, we can represent the interconversions

$$C_{2v} \rightleftharpoons T_d$$
$$\searrow \quad \swarrow$$
$$D_{4h}$$

The mass of the UF_5 molecule $m_2 = 5.526 \cdot 10^{-22}$ g, $r_{1,2} \approx 5.274$ Å, $f = 2$.

Reactions of Recombination

The temperature dependence of the rate constant of the reactions $F_2 + Ne \xrightarrow{k_{F_2}} 2F + Ne$ is described by an equation obtained experimentally by Diesen [17]:

$$k_{F_2} = 2.0 \cdot 10^{10} e^{-35\,000/RT} [M]^{-1} \text{ sec}^{-1}, \quad (15)$$

where [M] is the neon concentration, M. With some approximation we can assume [M] = const. Then

$$k_{F_2}[M] \approx k_3 \ (\text{sec}^{-1}). \quad (16)$$

The activation energy of the reaction is close to the energy of cleavage of the F–F bond, equal to 38,000 cal. The value of k_3 can also be calculated according to formula (13), on the assumption that $\varepsilon_3 = 38{,}000$ cal, $f = 2$, pressure of the transition 1 abs. atm, and the reaction mechanism is monomolecular. The results of calculation according to formulas (13) and (15) are in satisfactory agreement (Fig. 5).

The rate constants of recombination of the fluorine atoms k_3^1 were calculated in terms of the equilibrium constant of reaction (3), K_{e_3}, and the constant k_3, and are cited in Table 2. There also are cited the rate constants of the recombination of uranium flourides, calculated according to the formula

$$k_i^1 = k_i kT K_{e_i}^1, \tag{17}$$

where K_{pi}^1 is the equilibrium constant of the corresponding recombination reaction.

Kinetics of the Condensation of Uranium Tetrafluoride

In the case of abrupt cooling of high-temperature gas mixtures of uranium fluorides, the partial pressures of which are cited in Fig. 1, there is a condensation of uranium penta- and tetrafluoride. If the mixture has a temperature of ~3200°K, and if the cooling is performed sufficiently rapidly, uranium tetrafluoride may condense. For this the time of the elementary event of condensation must be less than the time of recombination processes.

The rates of condensation (in reciprocal seconds/molecule) can be estimated according to the Frenkel' equation [18]:

$$w_{\text{cond}} = e^{\frac{4\pi\sigma r_*^2}{3kT}} 2\pi r_*^2 \frac{p}{kT} \sqrt{\frac{\varphi_v - \varphi_c}{3m}} g^*, \tag{18}$$

where σ is the surface tension at the gas/condensed phase boundary; r_* is the critical value of the radius of the condensing particle; p is the pressure of the gas; k is Boltzmann's constant; m is the mass of the particle; φ_v and φ_c are the thermodynamic potentials of the vapor and condensed phases, related to one molecule; g* is the critical size of nuclei of the condensing substance.

The values of the surface tension of uranium tetrafluoride are unknown. Depending on the complexity of the molecule, the temperature, and the volatility, the surface tension may vary in the range from several erg/cm^2 to ~10^3 erg/cm^2. Let $r_* \approx 3 \cdot 10^{-8}$ sec, the temperature of the condensing surface $T = 3 \cdot 10^{2}$°K, $p_{UF_4} = 0.30$ atm, $\sigma \approx 4 \cdot 10$ erg·cm^2, $g^* \approx 10$, $m_{UF_4} = 5.85 \cdot 10^{-22}$ g, $\varphi_v - \varphi_c = 4 \cdot 10^{-12}$ erg. In this case the rate of condensation $w_{\text{cond}} = 1.6 \cdot 10^8$ sec^{-1}. The influence of the noncondensing gas (fluorine) is not considered here.

We should estimate what cooling of uranium tetrafluoride is provided by condensation. The rate of cooling of the tetrafluoride on account of condensation can be estimated according to the formula

$$\frac{dT}{dt} = -\frac{T_1 - T_2}{\tau_{\text{cond}}} \text{ (deg/sec)}, \tag{19}$$

where T_1 is the temperature of the gas; T_2 is the temperature of the condensing surface, τ_{cond} is the time of condensation. If $T_1 = 3.2 \cdot 10^{3}$°K, $T_2 = 3 \cdot 10^{2}$°K, $\tau_{\text{cond}} = 6.25 \cdot 10^{-9}$ sec, then $dT/dt \approx 4.7 \cdot 10^{11}$ deg/sec. The rate of cooling of the tetrafluoride obtained is several orders of magnitude greater than the required level, determined by the time of recombination processes.

LITERATURE CITED

1. N. P. Galkin et al., The Technology of Uranium [in Russian], Atomizdat, Moscow (1964), p. 310.
2. L. P. Kudrin, At. Energ., 22, 265 (1967).
3. Yu. N. Tumanov, Zh. Neorgan. Khim., 13, 1488 (1968).
4. V. P. Glushko (editor), Thermodynamic Properties of Inorganic Substances [in Russian], Izd-vo AN SSSR (1962).
5. B. Weinstock and G. Goodman, Advances Chem. Phys., 9, 169 (1965).
6. Yu. N. Tumanov and N. P. Galkin, Zh. Fiz. Khim., 43, 836 (1969).
7. N. P. Galkin, Yu. N. Tumanov, and Yu. P. Butylkin, Khim. Vys. Énerg., 4, 512 (1970).
8. K. Hakamoto, Infrared Spectra of Inorganic and Coordination Compounds [Russian translation], Mir, Moscow (1966), p. 162.
9. L. Hoskins and R. Lord, J. Chem. Phys., 46, 2406 (1967).
10. R. Bader, Kun Po Huang, J. Chem. Phys., 43, 3760 (1965).
11. F. B. Vurzel', L. S. Polak, and V. S. Shipachev, Kinetika i Kataliz, 7, No. 6 (1966).
12. V. N. Kondrat'ev, in: Chemical Kinetics and Catalysis [in Russian], V. N. Kondrat'ev (editor), Nauka, Moscow (1966), p. 165.
13. V. N. Kondrat'ev, The Kinetics of Chemical Gas Reactions [in Russian], Izd-vo AN SSSR, Moscow (1958), p. 263.

14. M. S. Zakhar'evskii, Kinetics and Catalysis [in Russian], Izd-vo LGU, Leningrad (1963), p. 81.
15. F. Rice and E. Teller, J. Chem. Phys., 6, 489 (1938).
16. J. Leermakers, J. Amer. Chem. Soc., 55, 3098 (1938).
17. R. Diesen, J. Phys. Chem., 72, 108 (1968).
18. Ya. I. Frenkel', Collection of Selected Works [in Russian], Vol. 3, Izd-vo AN SSSR, Moscow–Leningrad (1959), p. 358.

TUNGSTEN ISOTOPES IN FRESH RADIOACTIVE FALLOUT IN DECEMBER 1968

Yu. A. Izraél', A. A. Ter-Saakov,
S. G. Malakhov, V. M. Kurganskaya,
F. Ya. Rovinskii, E. D. Stukin,
S. B. Iokhel'son, V. N. Churkin,
and Z. S. Shulepko

UDC 551.510.7

Fresh radioactive isotopes were detected in the ground air and precipitates, against the background of global fallout, on the territory of the Soviet Union (European sector and Central Asia) in mid-December, 1968.

News of an underground nuclear explosion ("Schooner") carried out in the state of Nevada (USA) on December 8, 1968 appeared in the press at that time. The nuclear explosion, 35 kiloton power, touched off at a depth of 106 m, formed a crater 260 m in diameter and 60 m deep. The radioactive products ejected into the atmosphere were disseminated over considerable distances not only over the territories of the USA but also outside its boundaries [1].

The trajectories of the airborne particles at a height of 5 km constructed from the site of the nuclear explosion, showed that the air masses from the region of the explosion reached the territories of the Soviet Union on December 15 and moved over the USSR land mass over an approximate six-day period (Fig. 1).

Samples of air and fallout precipitation over some cities of the Soviet Union taken during December 1968 with filters and horizontal planchets were subjected to γ-ray spectrometric and radiochemical analyses in early January 1969. The volume of one sample of air pumped through a filter in one month was 10^5 to 10^6 m^3.

TABLE 1. Monthly Average Concentrations of Various Isotopes in the Ground Air over the Territory of the Soviet Union in December 1968 (10^{-15} Ci/m^3)

Sampling site	$Zr^{95}+Nb^{95}$	Cs^{137}	$Ce^{144}+Pr^{144}$	W^{181}	Sr^{89}	Sr^{90}
Moscow and environs	2.3	1.3	–	6.4	–	–
Eastern Arkhangel'sk region	–	–	–	0.55	–	–
Gor'kii	2.3	1.7	–	10.6	–	–
Kursk	2.6	2.2	4.8	11.4	0.033*	0.64*
Odessa	1.2	1.1	2.2	5.1		
Tbilisi	1.8	1.7	6.3	13.2		
Tashkent	2.6	1.9	4.6	19.2	–	–
Frunze	2.6	1.3	–	6.9	–	–
Novosibirsk	0.58	0.62	3.6	0.46	–	0.64
Chita	–	–	–	0	–	–
Vladivostok	–	–	–	0	–	–

* Average taken over three cities.

Translated from Atomnaya Énergiya, Vol. 30, No. 4, pp. 377-380, April, 1971. Original article submitted February 5, 1970.

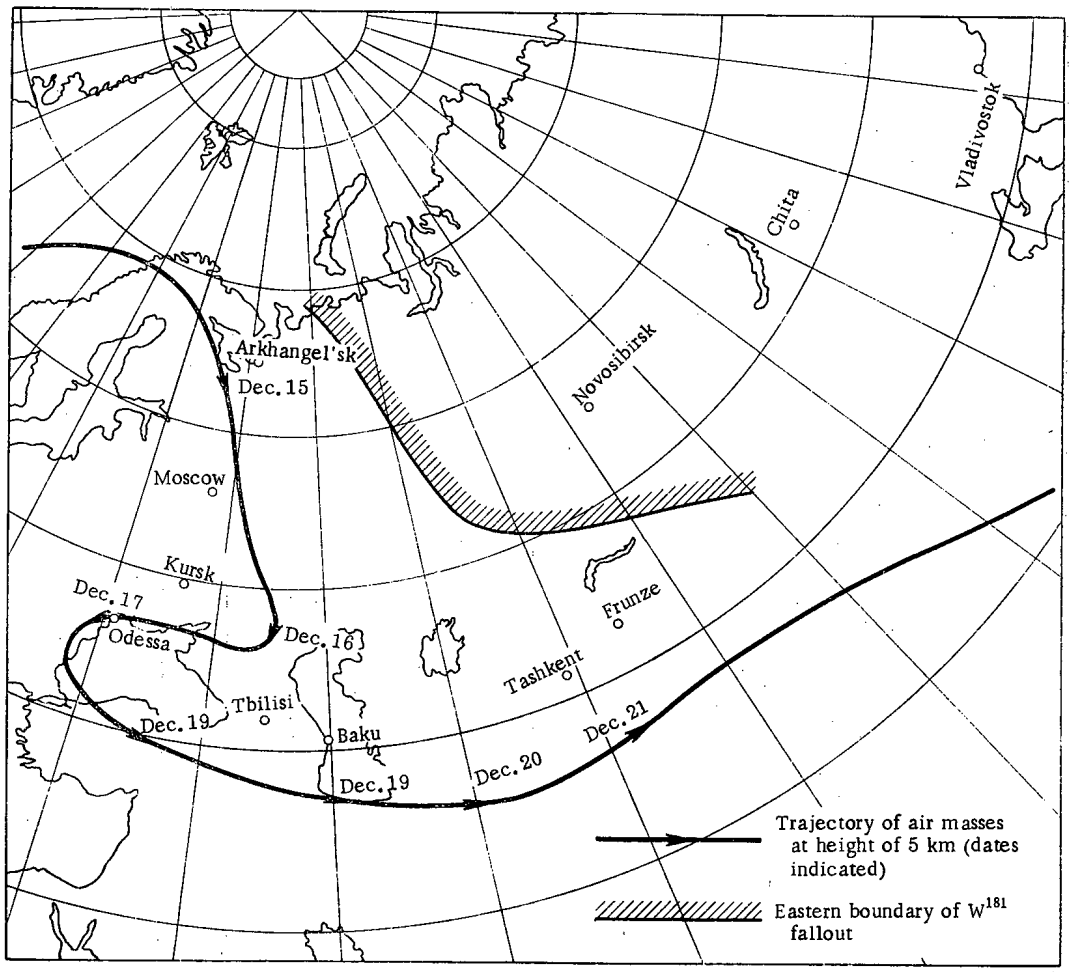

Fig. 1. Trajectory of airborne particles formed in the state of Nevada [USA] on December 8, 1968, at a height of 5 km above the territory of the Soviet Union and neighboring countries.

Figure 2 shows γ-ray spectra of radioactive air samples taken in the region around Moscow before the appearance of the radioactive products (curve 1) and during the December 13-21 period (curve 2). Comparison of these curves shows clearly that the 59 keV curve appeared in air samples taken after December 15. The half-life of the radioactive products in this sample, determined from the rates of decreases in the intensity of this curve, were found to be ~140 days. W^{181} was identified in the samples from these data.

The dynamics of the variation in W^{181} concentration at three points in the Moscow region are illustrated in Fig. 3. The onset of the appearance of W^{181} in the ground air (December 15), and the first and second waves of radioactivity enhancement (the second appearing after traveling completely around the globe), stand out clearly in the diagram.

The monthly average concentrations of diverse isotopes in the ground air samples taken at several cities in the Soviet Union are reproduced in Table 1. If we assume that the W^{181}-contaminated air masses traversed a given site over a six-day period, then the average W^{181} concentration during the traversal of any point can be found by multiplying by the five monthly-average values listed in Table 1.

Table 2 compares the average isotope composition in the fallout zone (in the form of the average ratio of number of nuclei to Zr^{95} nuclei) according to data obtained at several points, and similar values of global fallout from past tests measured in April-June, 1968 in the North Atlantic and over the territory of the USSR in September, 1968. The isotope composition was also compared to characteristic fallout values stemming from an underground nuclear explosion [2]. It is clear from Table 2 that Ba^{140} and Sr^{89}, which are characteristic of fallout deriving from underground explosions with radioactive products ejected into the atmosphere, are completely absent in the fresh fallout (December, 1968). The composition of the

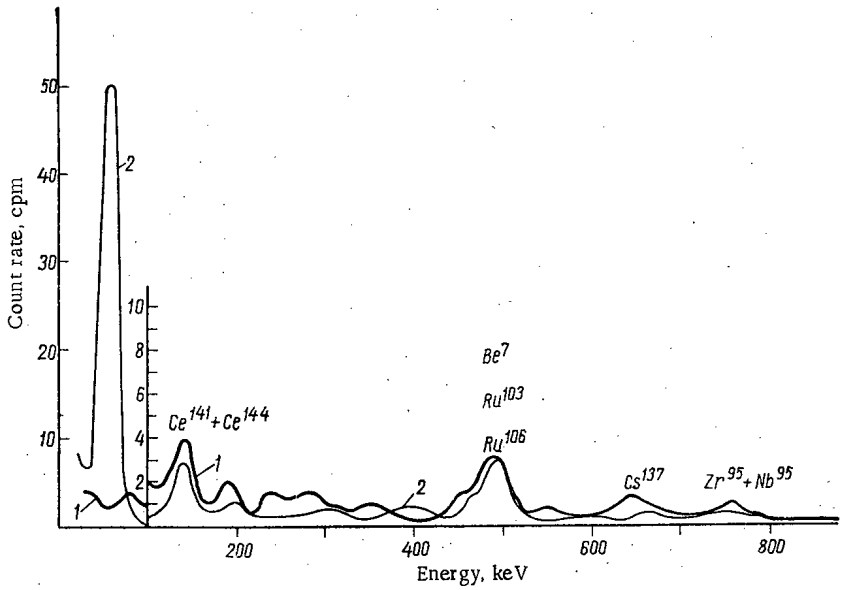

Fig. 2. Energy spectra of γ-ray emission from samples of radioactive fallout [curve 1) background sample; curve 2) sample of "fresh" fallout in December 1968].

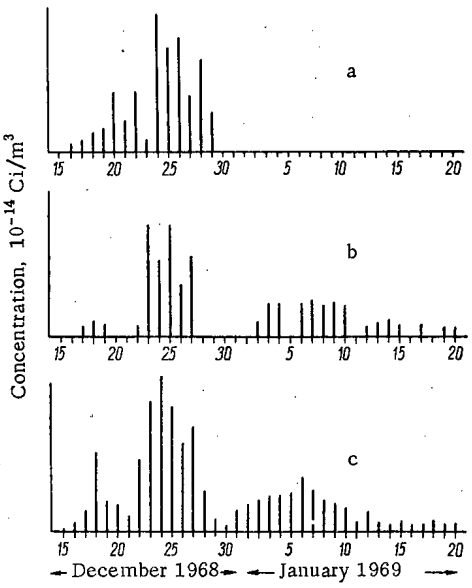

Fig. 3. Daily average W^{181} concentrations at three sites in the Moscow region.

TABLE 2. Average Ratio of Number of Nuclei of Diverse Isotopes to Zr^{95} in Ground Air Samples

Isotope	April-June 1968*	September 1968*	Underground nuclear explosion with ejectamenta†	December 1968
Sr^{89}	0,07	—	122	0,08
Ba^{140}	0	0	18	0
Sr^{90}	310	—	51	320
Cs^{137}	790	400	178	480
Ce^{144}	55	70	—	21

* Figures for December 1968.

† Ratio to Mo^{99}, the behavior of which is presumed similar to that of Zr^{95} (fractionation absent).

fission fragments in the December fallout is practically the same as the composition typical of global fallout. The distinguishing feature of the December fallout is the considerable amount of W^{181} which, apparently, is a product of activation in nuclear explosions. Hence, the daily-average W^{181} concentrations in the air in the Moscow region attained levels of $4.6 \cdot 10^{-14}$ Ci/m^3.

In the samples taken W^{185} was also identified, and the ratio of its activity to that of W^{181} at the time of the explosion ranged from 0.9 to 4.6, depending on the sample; the average was 2.7 ± 0.6.

Considerable amounts of W^{181} were observed precisely in the region traversed by airborne particles deriving from the explosion (see Fig. 1). In regions to the east of Arkhangel'sk, and at Novosibirsk, the amount of W^{181} was insignificant, and none was detected at Chita or Vladivostok. During the preceding months, no W^{181} at all had been observed over the territories of the Soviet Union.

The appearance of W^{181} and W^{185} over the territories of the Soviet Union in the period from December 15 through December 21, 1968 (at some sites still later), i.e., in the period during which the trajectory of air masses deriving from the state of Nevada traversed those territories, proves that the tungsten isotopes belong to the American underground nuclear explosion "Schooner" which was detonated on December 8, 1968.

The isotopes W^{181} and W^{185} are products of activation by the nuclear explosion neutrons, and were observed in fallout samples of earlier date that were associated with aerial nuclear weapons tests or American underground nuclear explosions [3-5].

The ratio of the activities of W^{185} and W^{181} at the time of the explosion, in calculations of induced activity based on the reaction (n, γ), was 70 in the thermal approximation; this ratio is roughly 7.0 in the case of neutron energies 10 to 100 eV, which corresponds to a temperature of 10^5 to 10^6°K.

The ratio found by theoretical calculations based on the reaction (n, 2n) is 2.06 for 14 MeV neutrons [4], and 3.7 when using the cross sections of the reaction [6]. The cross sections of the (n, 2n) reactions are slightly greater than the cross sections of (n, γ) reactions.

We now estimate the W^{181} activity in a cloud passing over the territory of the Soviet Union from December 15 through December 21, 1968. The average concentration of W^{181} in a cloud about 1500 km wide, according to data from 11 samples taken during that period,* was about 0.1 decay/min · m^3. When the explosion-derived cloud moved at a height of 5 km over the territory of the USSR over a six-day period, at an average speed of about 40 km/h, and extent of about 6000 km, the total W^{181} activity in the cloud amounted to $5 \cdot 10^{15}$ decays/min, or $2.3 \cdot 10^3$ Ci. If we assume that even as much as 10% of the total amount of W^{181} was retained in that cloud, that would mean that not less than $2.3 \cdot 10^4$ Ci W^{181} was formed in the nuclear explosion. As a result of activation in the soil in the 35-kiloton underground nuclear explosion, and with a 10^{-3}% weight ratio of tungsten in the rock material affected by the explosion, not more than $2.4 \cdot 10^2$ Ci W^{181} could have formed (taking into account resonance absorption of neutrons at high temperatures in the cavity scooped out by the nuclear explosion).

We may infer from the foregoing that the tungsten isotopes detected in radioactive fallout from the American underground nuclear explosion "Schooner" over the territories of the Soviet Union are products of activation by neutrons released in the explosion which originated in elements directly incorporated in the structure of the nuclear device.

LITERATURE CITED

1. Applied Atomics, No. 690, 7 (1968).
2. F. Cray and R. Fried, in: Radioactive Fallout from Nuclear Explosions, Yu. A. Izraél' (editor) [Russian translation], Mir, Moscow (1968).
3. Yu. A. Izraél' and E. D. Stukin, γ-Radiation of Radioactive Fallout [in Russian], Atomizdat, Moscow (1967).
4. B. V. Kurchatov et al., At. Énerg., 13, No. 6, 576 (1962).
5. E. Martell, J. Atoms. Sci., 25, No. 1, 113 (1968).
6. A. I. Aliev et al., Nuclear Physics Constants for Neutron Activation Analysis [in Russian], Atomizdat, Moscow (1969).

ABSTRACTS

REACTIVITY MEASUREMENTS BY ROD DROP METHOD WITH REAL MOVEMENT OF ABSORBER TAKEN INTO ACCOUNT

J. Bouzik, S. Chwaszczewski, and J. Jabloński

UDC 621.039.516.2

The real movement of absorber in the reactor must be taken into account when interpreting results of reactivity measurements by the rod drop method, particularly in measurements of high reactivity levels. Using the single-point equations of reactor kinetics as point of departure, we can derive a general formula which enables us to refine the results of reactivity measurements by the rod drop method (the formula is readily extended to the method of neutron source removal):

$$\rho_0 = \frac{\Theta(0)\,[\Lambda^* + \bar{\lambda}^{-1}]}{\int_0^\infty \rho'(t)\,\Theta(t)\,dt}. \qquad (1)$$

Here the time dependence of reactivity assumes the form

$$\rho(t) = -\rho_0 \rho'(t) \qquad (2)$$

when the following initial and asymptotic conditions are satisfied: $\rho' = 0$ when $t = 0$ and $\rho' = 1$ when $t = \infty$, while $\Theta(t)$ is the amplitude of the signal from the neutron detector placed inside the reactor. The remaining designations in formula (1) are conventional ones. The proposed reactivity measurement method was verified experimentally on the critical assembly "Anna." The absorber is introduced into the reactor, in the form of a cadmium cylinder, with the aid of a pneumatic device. The time required to get the absorber into the reactor ranged from 0.5 to 15 sec. The in-pile location of the absorber was recorded by measuring voltages on a potentiometer connected to the absorber, and also by the number of pulses generated as the absorber is moved. The conversion from the time dependence of the in-pile position of the absorber to reactivity was achieved either by means of additional calculations or additional measurements.

The basic reactivity measurements were taken by three methods. In the first, digital, method, absorber position pulses were compared to pulses from the neutron counter, using a 400-channel time distribution analyzer. In the second, analog-digital, method, the absorber position was placed synchronously, by means of an x–y dataplotting recorder, across the input of an analyzer which simultaneously records the time rate of change in the neutron detector count rate. The third, analog, method is based on the use of an analog computer connected to the setup. When the normalization of the input signal across the output is properly selected, the reciprocal reactivity is obtained accurate to within a known coefficient.

The results of the measurements confirm the validity of the proposed method for application to exact determinations of high reactivity levels. The results confirm the feasibility of utilizing an analog computer system in reactivity measurements.

Translated from Atomnaya Énergiya, Vol. 30, No. 4, p. 381, April, 1971. Original article submitted May 14, 1970; abstract submitted November 25, 1970.

NOTE ON THE STABILITY OF COUPLED NUCLEAR REACTORS

V. D. Goryachenko

UDC 621.039.515

The primary purpose of the article is to derive the sufficient stability conditions for the stationary mode of operation of a reactor consisting of two different coupled cores.

The kinetics of coupled reactor cores have been described [1, 2] in terms of a multipoint model:

$$\frac{dN_k}{dt}=\frac{\rho_k-\beta_k}{l_k}N_k+\sum_{i=1}^{m}\lambda_{ik}C_{ik}+\frac{\alpha_{kj}}{l_k}\int_0^\infty \varphi_{kj}(u)\,N_j(t-u)\,du;\quad \frac{dC_{ik}}{dt}=\frac{\beta_{ik}}{l_k}N_k-\lambda_{ik}C_{ik},\ i=1,\ldots,m;\ k=1,2;\ j=1,2;\ j\neq k, \tag{1}$$

where N_k and ρ_k are the neutron density and the reactivity in the k-th core; l_k is the neutron lifetime; C_{ik}, λ_{ik}, β_{ik} are respectively the concentration, decay constant, and fraction of the i-th group of emitters of delayed neutrons; $\beta_k=\sum_i \beta_{ik}$; α_{kj} are coupling coefficients; $\varphi_{kj}(t)$ is the distribution function (with respect to the time) of the probability of transition of neutrons from the j-th core to the k-th core. Clearly, we have

$$\varphi_{kj}(t)\geqslant 0,\quad \int_0^\infty \varphi_{kj}(t)\,dt=1. \tag{2}$$

Intercore coupling is assumed weak, i.e., we assume α_{kj} = const, with the reactivity ρ_k independent of the variables describing the j-th core ($j \neq k$).

For the purpose of investigating the stationary mode:

$$N_k=N_{k0},\ C_{ik}=C_{ik0},\ \rho_k=\rho_{k0},\ k=1,2;\ i=1,\ldots,m, \tag{3}$$

Eqs. (1) were linearized and supplemented with the linearized feedback equations for each core. The latter were presented in integral form:

$$\frac{\rho_k-\rho_{k0}}{l_k}=-\int_0^t f_k(t-\tau)\,\frac{N_k(\tau)-N_{k0}}{N_{k0}}\,d\tau, \tag{4}$$

and the form of the kernels f_k, dependent on the type of feedback equations, was not concretized. The characteristic equation of the linearized system was set up and its analysis made it possible to derive the following stability criterion.

The equilibrium state (3) is asymptotically stable at any positive coupling coefficients whenever

$$\operatorname{Re} w_1(p)>0 \text{ and } \operatorname{Re} w_2(p)>0 \text{ when } \operatorname{Re} p\geqslant 0, \tag{5}$$

where

$$w_k(p)=p+\frac{\beta_k}{l_k}+F_k(p)-\sum_i \frac{\beta_{ik}}{l_k}\,\frac{\lambda_{ik}}{p+\lambda_{ik}},\quad k=1,2, \tag{6}$$

$F_k(p)$ is the feedback transfer coefficient for the k-th core [i.e., the Laplace transform of the kernel $f_k(t)$].

The functions of the complex variable p which conform to the constraints (5) are positive real functions [3], while the constraints (5) are equivalent [3] to the conditions: 1) $\operatorname{Re} w_1(j\omega) > 0$, $\operatorname{Re} w_2(j\omega) > 0$ for all $\omega \geq 0$; 2) the functions w_1 and w_2 do not have poles to the right of the imaginary axis or on the imaginary axis itself (one exception is the case where there are only simple poles on the imaginary axis, and only poles with positive residues).

It is shown that the constraint

$$\operatorname{Re} w(p)=\operatorname{Re}\left[p+\frac{\beta}{l}+F(p)-\sum\frac{\beta_i}{l}\,\frac{\lambda_i}{p+\lambda_i}\right]>0 \text{ when } \operatorname{Re} p\geqslant 0, \tag{7}$$

Translated from Atomnaya Énergiya, Vol. 30, No. 4, pp. 381-382, April, 1971. Original article submitted May 11, 1970; abstract submitted October 26, 1970.

written for a noncoupled ("point") critical reactor, is a sufficient condition of asymptotic stability for the stationary mode of this reactor.

LITERATURE CITED

1. S. Gage et al., in: Neutron Dynamics and Control [Proceedings of the symposium on nuclear engineering held April 5-7, 1965, at the University of Arizona, Tucson] (1966).
2. H. Plaza and W. Köhler, Nucl. Sci. and Engng., 26, 419 (1966).
3. B. V. Bulgakov, Oscillations [in Russian], Gostekhizdat, Moscow (1954).

OPTIMUM SHUTDOWN OF A HIGH-FLUX REACTOR

T. S. Zaritskaya and A. P. Rudik

UDC 621.039.56

We consider the problem of finding the optimum reactor shutdown regime ensuring maximum energy release during the transient process. We choose the reactor power as the function to be varied – the control. We solve the problem by using the mathematical apparatus of the nonclassical calculus of variations in the form of the L. S. Pontryagin maximum principle from which it follows that only four kinds of control are possible: 1) maximum power; 2) complete reactor shutdown; 3) power varying with time in such a way that the xenon concentration has its maximum admissible value; 4) power determined by the classical calculus of variations.

By using L. S. Pontryagin's principle [1], which states that each portion of an optimum path is also an optimum path, the general form of the optimum path in the present problem can be found by a numerical comparison of various combinations of admissible kinds of control. It turns out that in the present case the optimum transient regime consists of the following three stages:

1) zero reactor power until the xenon concentration reaches its maximum admissible value.

2) power varying in such a way that the xenon concentration remains constant at its maximum admissible value;

3) maximum power at which the reactor operates up to the time of planned shutdown. Quantitative estimates are given of the gain in released energy during the optimum transient process.

LITERATURE CITED

1. L. S. Pontryagin et al., The Mathematical Theory of Optimum Processes [in Russian], Fizmatgiz, Moscow (1961).

Translated from Atomnaya Énergiya, Vol. 30, No. 4, p. 382, April, 1971. Original article submitted September 29, 1969; abstract submitted September 21, 1970.

SOME PHYSICOCHEMICAL PROPERTIES OF THE COMPOUND $XeF_2 \cdot UF_6$

V. K. Ezhov*

UDC 541.123

The possible existence of the compounds in the vapor phase has been investigated by either of two methods.

The first technique relies on study of the behavior of a vapor-phase equimolar mixture of uranium hexafluoride and xenon difluoride at different temperatures. The second technique involves investigating the possibility of selective isolation of uranium hexafluoride from the compound with xenon difluoride existing in a condensed state. The existence of the compound $XeF_2 \cdot UF_6$ in the vapor phase has not been detected successfully by either of these techniques.

Processing of experimental data on determinations of the dissociation pressure of the compound $XeF_2 \cdot UF_6$ as a function of the temperature has shown that the dependence described by the equation

$$\lg p_{mm} = 9.30 - \frac{2171}{T\,^\circ K}.$$

holds in the temperature range from 24-100°C.

The heat of dissociation of the complex $XeF_2 \cdot UF_6$ was calculated over that temperature range with due attention to the fact that the pressure in the system studied is made up of equal contributions by the partial pressures of uranium hexafluoride and xenon difluoride. It was found to be a constant, 18.6 ± 0.5 kcal/mole (77.9 ± 2.1 kJ/mole).

The heat of fusion of the compound $XeF_2 \cdot UF_6$ was determined thermographically from the area under the peak on the differential curve. The error allowed as a result of the approximations in those calculations was not greater than 0.3%.

The average heat of fusion of the compound $XeF_2 \cdot UF_6$ was 3.5 ± 0.3 kcal/mole (14.6 ± 1.3 kJ/mole).

THE INTERACTION OF BERYLLIUM WITH MOLTEN SODIUM FLUORIDE AND UF_4 – NaF SALT MIXTURES

G. P. Novoselov, I. N Kashcheev, and A. V. Zolotarev†

UDC 546.791.4

In [1] we investigated the possibility of reprocessing of irradiated uranium with molten fluorides of the alkali metals. It was shown that uranium, plutonium, and the rare earth elements interact under nonequilibrium conditions with the fluorides of the alkali metals, forming nonvolatile fluorides and liberating the alkali metal.

In this work we investigated the interaction of beryllium with molten sodium fluoride and UF_4–NaF salt mixtures. It was established that under nonequilibrium conditions, at the temperature 1000°C, metallic beryllium (0.2 g sample) interacts almost entirely with molten sodium fluoride within 30 min according to

*Translated from Atomnaya Énergiya, Vol. 30, No. 4, p. 383, April, 1971. Original article submitted March 30, 1970; abstract submitted October 21, 1970; revision submitted October 21, 1970.

†Translated from Atomnaya Énergiya, Vol. 30, No. 4, p. 383, April, 1971. Original article submitted March 20, 1970; revision submitted August 31, 1970.

the reaction

$$Be + 2NaF \longrightarrow BeF_2 + 2Na.$$

In this case the interaction proceeds similarly to that described earlier [1]; the main cause of the interaction is evaporation of metallic sodium from the reaction zone.

In the presence of an excess of sodium fluoride over the stoichiometrically necessary amount, the salt phase was obtained in the form of a finely divided powder. The powder was formed as a result of spontaneous pulverization of the low-temperature modification of sodium fluoberyllate [2] during cooling.

When salt mixtures UF_4–NaF were melted in the presence of metallic beryllium for 60 min, beryllium also interacted entirely with the salt melt, and the deposition of metallic sodium was observed. In the case of subsequent cooling of the salt solution to room temperature (rate of cooling 33 deg/min), the formation of two layers was observed. The lower layer represented a brown-colored melt and contained 96.5-98.7% by weight of the original amount of uranium. The upper layer was in the form of a white, readily separated powder.

LITERATURE CITED

1. G. P. Novoselov et al., At. Énerg., 28, 48 (1970).
2. E. Tilo and H. Shreder, in: Beryllium [Russian translation], Vol. 1, Izd-vo IL, Moscow (1953), p. 32.

APPROXIMATION OF PHOTOELECTRIC ABSORPTION CROSS SECTIONS

L. V. Popova and L. A. Sholokhova

UDC 539.122.173

The experimental values of the photoelectric absorption cross sections for hydrogen, carbon, aluminum, silicon, copper, tin, platinum, and water are approximated. The approximation functions have the

TABLE 1. Coefficients A, B, and C for Calculating Photoelectric Absorption Cross Sections by Eq. (1) (in units of 10^{-24} cm^2/atom)

Element, material	Energy range	A	B	C	Element, material	Energy range	A	B	C
Hydrogen	[0,01957; 0,02925] *	0	$4{,}310\cdot10^{-9}$	3,53	Tin	[0,1566; 1,1742)	$2{,}767\cdot10^{-2}$	$2{,}141\cdot10^{-1}$	3,042
						[1,1742; 1,957]	$1{,}520\cdot10^{-2}$	$2{,}273\cdot10^{-1}$	2,80
Carbon	[0,01957; 0,05871)	—0,0065	$8{,}435\cdot10^{-5}$	3,314		[0,01957; 0,05724)	—25	$2{,}775\cdot10^{-1}$	2,89
	[0,05871; 0,2935]	—0,0004	$7{,}026\cdot10^{-5}$	3,376		[0,05724; 0,1174]	—39	3,8433	2,7
Aluminum	[0,01957; 0,07828)	—1,789	$7{,}289\cdot10^{-3}$	3,048		(0,1174; 0,5871)	0,1775	2,6207	2,874
						[0,5871; 1,1742)	0,5267	2,3029	3,225
	[0,07828; 0,3914)	$2{,}667\cdot10^{-4}$	$4{,}032\cdot10^{-3}$	3,23		[1,1742; 2,935]	0,1345	2,5532	2,412
	[0,3914; 0,7828]	$5{,}4\cdot10^{-3}$	$1{,}712\cdot10^{-3}$	4,024	Platinum	[0,02722; 0,07828]	$-1{,}8791\cdot10^{2}$	2,5378	2,766
Silicon	[0,01957; 0,07828)	—2,725	$1{,}088\cdot10^{-2}$	3,023		(0,07828; 0,1538)	4,885	1,345	3,00
	[0,07828; 0,3914)	$3{\cdot}33\cdot10^{-3}$	$5{,}569\cdot10^{-3}$	3,24		[0,1538; 1,1742)	2,7273	17,4068	2,728
						[1,1742; 2,935]	1,145	19,307	2,5
	[0,3914; 0,7828]	$5{,}010\cdot10^{-3}$	$7{,}307\cdot10^{-3}$	2,938	Water	[0,01957; 0,09785)	$-9{,}35\cdot10^{-2}$	$4{,}268\cdot10^{-4}$	3,24
Copper	[0,01957; 0,05871)	$-6{,}14325\cdot10$	$5{,}409\cdot10^{-1}$	2,718		[0,09785; 0,1957)	$4\cdot10^{-3}$	$2{,}55\cdot10^{-7}$	3,425
	[0,05871; 0,1566)	2,343	2,264	3,00		[0,1957; 0,3914]	$4{,}5\cdot10^{-3}$	$1{,}873\cdot10^{-4}$	3,6

* Square bracket denotes closed interval and parenthesis open interval. For example [0.01957; 0.02925) means $0.01957 \le \alpha < 0.02925$.

Translated from Atomnaya Énergiya, Vol. 30, No. 4, p. 384, 1971. Original article submitted May 25, 1970; abstract submitted July 3, 1070.

form

$$\sigma_b = A + B\alpha^{-C}, \quad (1)$$

where α is the γ-energy in units of m_0c^2 and the coefficients A, B, and C are listed in Table 1. The error in the approximation does not exceed 1% over the whole energy range except at isolated points where it reaches 3%.

γ-RADIATION FROM THE EARTH AND NEUTRINO EXPERIMENTS

V. I. Glotov

UDC 539.122.04:539.123

The most important sources of natural terrestrial γ-radiation constituting a basic component of the external background in electronic neutrino detectors, and in particular in the lithium-drifted electronic detector, are discussed. The discussion centers around the example of granite of average chemical composition containing $3.5 \cdot 10^{-6}$ g/g uranium, $1.8 \cdot 10^{-5}$ g/g of thorium, and $3.3 \cdot 10^{-2}$ g/g potassium. Yields of γ-photons generated through decay of uranium, thorium, and potassium, and in spontaneous fission of U^{238} in $(\alpha\gamma)$, $(\alpha,\alpha'\gamma)$, $(\alpha, n\gamma)$, $(\alpha, p\gamma)$, $(n\gamma)$, $(n, n'\gamma)$ reactions are estimated.

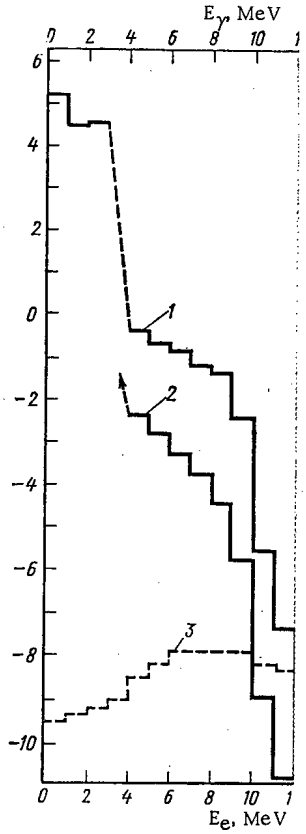

Fig. 1. Flux of unscattered γ-radiation from granite, and magnitude of electron background in lithium neutrino detector.

Translated from Atomnaya Energiya, Vol. 30, No. 4, pp. 384-385, April, 1971. Original article submitted May 14, 1970; abstract submitted July 13, 1970.

Experimental data on nuclear processes are borrowed from the literature in arriving at the estimates. In other instances, the result is arrived at on the basis of general theoretical concepts, while invoking assumptions simplifying the calculations. It is demonstrated that the decisive role in the formation of γ-photons of energy <3 MeV in granite is played by radioactive decay events, and that the decisive role in the formation of >4 MeV γ-photons is played by $(n\gamma)$, $(\alpha, p\gamma)$, and $(\alpha, n\gamma)$ processes. An experimental investigation of the reactions $Mg(\alpha, n\gamma)$ and $Al(\alpha, p\gamma)$, in which energetically possible production of γ-photons up to 10 MeV is established, is carried out in order to lend greater precision to the estimates.

Curve 1 in the diagram shows the unscattered flux of photons $\Phi_{unsc}(E_\gamma)$ obtained from a semiinfinite granite slab. All of the γ-radiation from the granite can be placed in two energy intervals in which the integrated flux values contrast sharply: $\Phi_1(E_\gamma < 3 \text{ MeV}) \approx 2.2 \cdot 10^5 \text{ cm}^{-2}/\text{day}$ and $\Phi_2(E_\gamma > 4 \text{ MeV}) \approx 0.8 \text{ cm}^{-2}/\text{day}$. When Φ_{unsc} impinges on a lithium detector (infinite lithium slab), background electrons of density $P(E_e)$ form as a result of the single Compton effect in the lithium slab (curve 2). Comparison of the effect due to neutrino flux from the boron cycle of nuclear reactions on the sun ($\Phi_\nu = 2 \cdot 10^6 \text{ cm}^{-2} \cdot \text{sec}^{-1}$) and the value of $P(E_e)$ shows that the use of electron recording thresholds $E_c^{thr} < 4$ MeV is inadmissible in electronic neutrino detectors, and that normal performance of detectors of this type in an underground mine gallery would be impossible without heavy shielding to absorb the flux of γ-photons of energy $E_\gamma > 4$ MeV at least 10^6-fold to 10^7-fold. This shielding may consist of combinations of pure (uranium and thorium concentrations $\sim 10^{-9}$ g/g) and ultrapure (uranium and thorium concentrations $\sim 10^{-12}$ g/g) materials. This conclusion proves the necessity of an experimental search for shielding materials with an ultralow concentration of uranium and thorium, as well as the need for a detailed analysis of the spectral composition of background radiations in such prospective materials.

DETERMINATION OF THICKNESS OF γ-SOURCES AND ABSORBERS FROM THE DEFORMATION OF THE HARD PART OF THE ENERGY SPECTRUM

V. A. Vorob'ev and Sh. D. Fridman

UDC 539.122:539.173

A method is described for determining the thickness of remote γ-sources and absorbers by taking account of the deformation of the hard part of the energy spectrum of the γ-radiation from distributed sources. This deformation is measured by a quantity ξ defined as the ratio of the intensity of the primary γ-radiation J_0 of energy E_0 to the differential intensity of the hard scattered γ-radiation J_0^S as $E \to E_0$, i.e., $\xi = J_0/J_0^S$.

Relations are presented connecting the function ξ with the thickness of an inactive absorber, and in the absence of an absorber, with the thickness of the radiation source for a plane isotropic source, a uniform half-space, and a uniform layer. Graphs of $\xi(\mu x, \theta)$ have been computed for a vertical collimated detector with a half-angle aperture $\theta \to 0°$, and also for θ equal to 30, 60, and 90° for a range of thicknesses $0.1 \leq \mu x \leq 5.0$.

The method is very sensitive.

Translated from Atomnaya Énergiya, Vol. 30, No. 4, p. 385, April, 1971. Original article submitted May 13, 1970; abstract submitted November 16, 1970.

NEUTRON SPECTRA FROM 0.05 TO 10 MeV IN CERTAIN SHIELDING MATERIALS

A. P. Veselkin, E. V. Voskresenskii, Yu. A. Egorov, Yu. V. Pankrat'ev, and V. I. Piskunov

UDC 539.125.5.164

A fast neutron single-crystal scintillation spectrometer and a He^3 spectrometer were used to measure neutron spectra in hydrogenous materials – lithium hydride and a polyethylene–lead mixture; in materials composed of elements of intermediate atomic weights – graphite, borated graphite, and serpentine concrete; in heavy materials in which the moderation of fast neutrons is mainly by inelastic scattering – titanium, steel, and lead.

The experiment was performed at a water-cooled water-moderated research reactor. The measurements with the He^3 spectrometer were made under conditions close to semiinfinite geometry and those with the scintillation spectrometer under conditions of shield geometry. The experimental results were normalized in the 0.8–1.4 MeV energy region. The experimental error does not exceed 20-30%. As an example the graphs of Fig. 1 show the spectra of neutrons transmitted through iron.

The neutron energy distributions are used to compute the attenuation functions and the relaxation lengths of the neutron fluxes in nine energy groups. The error in determining the relaxation lengths is 5-8%.

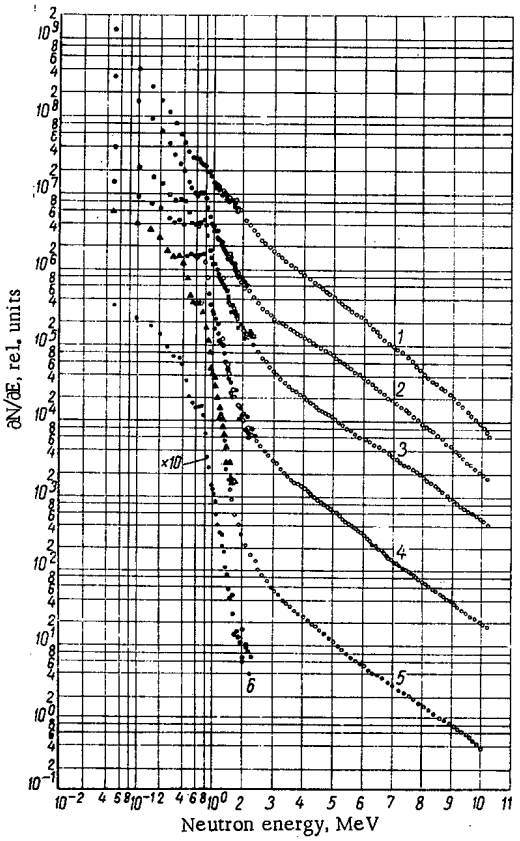

Fig. 1. Spectra of neutrons transmitted through iron (St. 3): 1) outside a 10 cm layer of lead which remains in position; 2) outside a layer of iron of thickness 10 cm; 3) 20 cm; 4) 40 cm; 5) 65 cm; 6) 82 cm.

Translated from Atomnaya Énergiya, Vol. 30, No. 4, p. 386, April, 1971. Original article submitted August 6, 1970.

DISTRIBUTION OF SPONTANEOUS FISSION NEUTRONS FROM URANIUM NUCLEI IN AN ORE BED CUT BY A CYLINDRICAL BOREHOLE

Yu. B. Davydov

UDC 539.125.52:551

The cylindrically symmetrical boundary problem dealing with the distribution of neutrons emitted in spontaneous fission of uranium nuclei in a two-layer infinite medium, with a cylindrical interface, is solved.

The internal medium simulates a borehole, the external medium the ore bed. This ore bed contains neutron sources with a one-dimensional distribution, varying in the direction of the borehole axis. The assumption is that the presence of such sources, i.e., the variation in the chemical composition of the bed, is without effect on the physical properties of the bed responsible for neutron transport (the bed constitutes a quasihomogeneous medium in this sense).

The problem is solved in the two-group diffusion approximation. The solution in the general form is found by the method of integral transformations. The Green's function method is applied in order to find the concrete form of the solution [1].

A formula is derived for the density of thermal neutrons and fast neutrons in the borehole–bed system, with an arbitrary pattern of source density variation. The solution of the boundary problem in the general form serves as the starting expression for a further detailed analysis of the fission-neutron distribution in the cases of greatest practical interest, which are realized in actuality.

As an illustration, the fission-neutron distribution in a system comprising borehole and ore bed of finite thickness with uniform mineralization is considered. Numerical calculations were carried out for an ore stratum made up of porous limestone intersected by a borehole filled with fresh water. It is assumed, in these calculations, that the pores in the limestone become filled up with fresh water.

Analysis of the results of the calculations provide evidence that treatment of the effect of the borehole and intervening host rock can be handled independently in the first approximation, inasmuch as the functions determining the effects of these two factors appeared as cofactors in the final solution. The configuration of the neutron logging curves depends largely on the water content of the bed. Analysis of saturation curves revealed that, as the hydrogen content increased, saturation set in earlier, i.e., at a lower thickness of active ore stratum. It was also successfully demonstrated that, as the radius of the borehole is increased, the fast-neutron density on the borehole axis declines, while a local density rise is observed in the case of thermal neutrons, up to radii of 4-6 cm. This is explained by the anomalously high density of dying-out of fast neutrons in the hydrogeneous medium.

LITERATURE CITED

1. D. Ivanenko and A. Sokolov, Classical Field Theory [in Russian], Gostekhteorizdat, Moscow (1966).

Translated from Atomnaya Énergiya, Vol. 30, No. 4, pp. 386-387, April, 1971. Original article submitted April 21, 1970; abstract submitted July 23, 1970.

DOSE SENSITIVITY OF A RHODIUM NEUTRON DETECTOR

G. M. Obaturov and Yu. K. Chumbarov

UDC 539.12.08

To investigate the possibility of using a Rh^{103} detector for neutron dosimetry we have calculated the average value of its dose sensitivity $\bar{\Gamma}/C$ (barns · neutrons/cm^2 · rad) for various neutron spectra in the energy ranges 0.4 eV–10 MeV, and 0.45–10 MeV.

The results of the calculations are shown in Table 1.

By measuring the activity (A, decays/sec) of a Rh^{103} detector and using the tabulated values of $\bar{\Gamma}/C$ or $\bar{\bar{\Gamma}}/C$ the kerma of the neutrons K can be found from

$$K = \frac{A}{C\,(\bar{\Gamma}/C)},$$

where the constant C is $1.18 \cdot 10^{-7}$ cm^2/barn · sec for 1 g of Rh^{103}.

It follows from Table 1 that dose can be measured with a rhodium detector to an accuracy which is acceptable in practice, particularly if the shield material is known. The lower limit of the measurements is ~1 rad.

TABLE 1. Values of Average Dose Sensitivity of a Rhodium Detector for Various Spectra

Serial No.	Spectrum	$\bar{\Gamma}/C$, barns · neutrons/cm^2 · rad · 10^8	
		0.4 eV–10 MeV	0.45–10 MeV
1	Fission spectrum	2.58	2.72
2	Godiva	2.43	2.62
3	HPRR	2.45	2.65
4	Outside B_4C shield	2.19	2.49
5	BR-1	0.97	2.18
6	Outside Fe shield	1.00	1.88
7	Uranium – graphite reactor	1.79	2.53
8	Vinca	1.80	2.31
9	Outside Pb shield	2.03	2.50
10	Outside C shield	1.98	2.53
11	Critical assembly containing UO_2F_2 solution	2.48	2.70
12	Heterogeneous solution with H_2O moderator	2.23	2.62
	Average $\Gamma/\bar{\bar{C}}$ for all spectra	$2.00^{+29\%}_{-52\%}$	$2.48^{+9.7\%}_{-24\%}$
	Average $\Gamma/\bar{\bar{C}}$ for all spectra except Nos. 5 and 6	$2.2^{+17\%}_{-19\%}$	$2.57^{+5.8\%}_{-10\%}$

Translated from Atomnaya Énergiya, Vol. 30, No. 4, p. 387, April, 1971. Original article submitted February 20, 1970; revision submitted November 30, 1970.

ENHANCING EFFECTIVENESS OF SYNCHROTRON CAPTURE IN BEAM BUNCHING OUTSIDE OF SEPARATRIX

G. G. Gurov, É. A. Myaé,
P. T. Pashkov, and K. A. Yakovlev

UDC 621.384.634

The article cites results of calculations and experimental data on increases in the coefficient of synchrotron capture of particles in the accelerator of IFVÉ [High-Energy Physics Institute]. The nonlinear MN-7 analog simulation computer was used in the calculations. Numerical data on bunching time and the parameters of the radio-frequency program were obtained, and the qualitative pattern of the capture process was examined in relation to cases of beam injection above and below the separatrix.

The rapid phase shift in the accelerating field needed to bring about particle capture experimentally was attained by introducing controlled amplitude and pulse width into the pattern of variation of the ejection frequency. Frequency deviation was measured by a broadband frequency discriminator which was supplied with a signal proportional to the sum of the voltages of the resonators in the accelerator stations.

The pulse spreads of the beam were ±0.2, ±0.24, ±0.3% in the course of the experiments. Injection current varied from 10 to 65 mA. The results of the calculations made with the accelerator operating at low and medium intensities differed only slightly from the experimental results. With a ±0.2% spread in beam pulse at the time of injection, the capture coefficient increased 44% in injection above the separatrix and 38% in injection below the separatrix. At an intensity level of 10^{12} protons/pulse, or higher, the increased capture effectiveness with beam bunching above the separatrix was found to be less than predicted, viz. ~10%. We may assume that particle bunching aggravated the space charge effect of the beam in this case, and this would be important at that intensity level.

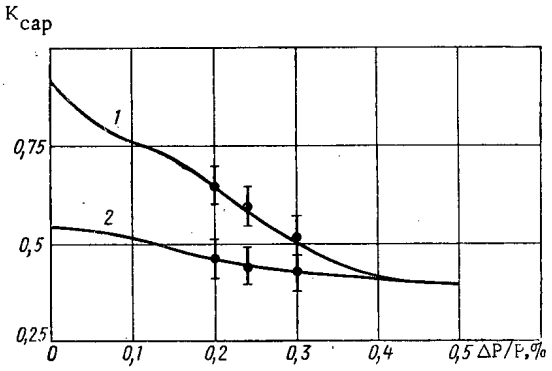

Fig. 1. Dependence of maximum capture on beam pulse spread: 1) capture with bunching; 2) conventional capture (experimental data points indicated on predicted curves).

The calculations performed, and the results of experimental investigations (see Fig. 1), indicate that synchrotron capture effectiveness can be improved well beyond that attainable by injection into a steady-state separatrix, when the IFVÉ accelerator is operated at medium intensity levels (up to $7 \cdot 10^{11}$ protons/pulse). A considerable increase in capture effectiveness can be achieved, by this method, even at the limiting accelerator intensity, it would seem, if the parametric resonance bands are properly corrected.

Translated from Atomnaya Énergiya, Vol. 30, No. 4, p. 388, April, 1971. Original article submitted May 18, 1970; abstract submitted October 12, 1970.

LETTERS TO THE EDITOR

NOTE ON THE PROPERTIES OF THE INTEGRATED REACTOR CHARACTERISTIC K^+

A. I. Mogil'ner

UDC 621.039.5

The integrated reactor characteristic K^+, defined as

$$K^+ = \frac{\text{Average number of neutrons generated}}{\text{Average losses through internal processes}}, \quad (1)$$

has been introduced in some earlier articles [1-3]. By internal processes, we mean those processes taking place without involving any change in coordinates (absorption, slowing-down, scattering, fission). The definition uses neutron worth, an adjoint function, as a weighting factor in the averaging process.

An expression has been derived [2] for K^+ in the diffusion approximation, and it has been shown that this quantity is close to the neutron multiplication factor in an infinite medium K_∞, and the difference in the two quantities alluded to is not below B^4 in order of magnitude, in the two-group approximation, where B^2 is the buckling. Further, a relationship has been established, in the diffusion approximation, between K^+ and S, the total contribution made to the reactivity (total statistical weight) by all the materials included in the composition of the reactor (theorem on the total statistical weight of the reactor materials):

$$S = 2(\rho^+ - \rho),$$

where

$$\rho = \frac{K_{\text{eff}} - 1}{K_{\text{eff}}}; \quad \rho^+ = \frac{K^+ - 1}{K^+}. \quad (2)$$

In a recent paper by Hungarian physicists [4], the above results have been extended to the rigorous Boltzmann equation. In that case, it becomes necessary to add, to the two terms present in the denominator of the ratio K^+ in the diffusion approximation, still a third term.

It was demonstrated [4] that the addition of a third term to $1/K^+$ in the transport equation leaves Eq. (2) unaltered in the many-group approximation of diffusion theory or transport theory, and does not affect the relative conservatism of K^+ with respect to dimensionality. This has been shown in the case of simple one-dimensional geometry.

The purpose of the present note is to shed some light on the physical significance of the dependence of K^+ on the selection of the computational model, and to ascertain some possible limitations to be imposed on the relationship linking K^+ to K_∞.

In diffusion theory, the weight factor (worth or importance) varies at a given point for two reasons: as a result of neutron losses or in response to a change in neutron energy. The two sources of possible losses correspond to the two terms in the formula for $1/K^+$. In the more general case, we also have to deal with changes in neutron worth as the directions of motion (angles) change, leading to the appearance of the third term in $1/K^+$.

Let us show that the similarity between the K^+-characteristic of a real finite reflected reactor to the K_∞-characteristic of a reactor of the same composition (but of unbounded dimensions) is implied by the most general properties of the Boltzmann equation.

The similarity theorem can be formulated as the equivalence of the effect, on the reactivity, of identical relative changes in the density μ and in the dimension R:

Translated from Atomnaya Énergiya, Vol. 30, No. 4, pp. 389-390, April, 1971. Original article submitted March 20, 1970.

$$\mu \frac{\partial \rho}{\partial \mu} = R \frac{\partial \rho}{\partial R}. \tag{3}$$

But the left-hand member of Eq. (3) is equal, by definition, to the total statistical weight of the reactor materials [2]: $S = \mu(\partial\rho/\partial\mu)$. It is convenient to make the substitution of variables

$$B^2 = \frac{C}{R^2} \equiv x, \tag{4}$$

in the right-hand member of the equation; here C is an arbitrary constant, so that $B^2 = x$ has the meaning of the buckling operator. We can then write

$$S = -2x \frac{\partial \rho}{\partial x}. \tag{5}$$

The dependence of the reactivity on the reactor dimensions is a certain function $\rho(x)$ which can be expanded in a power series:

$$\rho(x) = \rho(0) + x \left.\frac{\partial \rho}{\partial x}\right|_0 + \frac{1}{2} x^2 \left.\frac{\partial^2 \rho}{\partial x^2}\right|_0 + \cdots \tag{6}$$

We shall assume that the conditions for differentiation of series (6) are fulfilled, so that, after differentiation, we get

$$\frac{\partial \rho}{\partial x} = \left.\frac{\partial \rho}{\partial x}\right|_0 + x \left.\frac{\partial^2 \rho}{\partial x^2}\right|_0 + \frac{1}{2} x^2 \left.\frac{\partial^3 \rho}{\partial x^3}\right|_0 + \cdots \tag{7}$$

Multiplying the series (7) by x, and taking Eq. (5) into account, we represent the statistical weight S in the form of the series

$$-\frac{S}{2} = x \frac{\partial \rho}{\partial x} = x \left.\frac{\partial \rho}{\partial x}\right|_0 + x^2 \left.\frac{\partial^2 \rho}{\partial x^2}\right|_0 + \frac{1}{2} \left.\frac{\partial^3 \rho}{\partial x^3}\right|_0 + \cdots \tag{8}$$

If we recall that $\rho(0) = \rho_\infty = (K_\infty - 1)/K_\infty$, then we obtain, as a result, a formula for ρ_∞:

$$\rho_\infty = \rho + \frac{S}{2} + \frac{1}{2} x^2 \left.\frac{\partial^2 \rho}{\partial x^2}\right|_0 + \frac{1}{3} x^3 \left.\frac{\partial^3 \rho}{\partial x^3}\right|_0 + \cdots \tag{9}$$

But according to the theorem (2),

$$\rho^+ = \rho + \frac{S}{2}. \tag{10}$$

Substracting the preceding expression from the last one, we obtain the required formula

$$\rho^+ - \rho_\infty = -\frac{1}{2} x^2 \left.\frac{\partial^2 \rho}{\partial x^2}\right|_0 + O(x^3), \tag{11}$$

where

$$O(x^3) = -\sum_{n=3}^{\infty} \frac{1}{n(n-2)!} x^n \left.\frac{\partial^{(n)} \rho}{\partial x^n}\right|_0. \tag{12}$$

The dependence (11) has an important physical meaning, in that it accounts for the importance of the quantity K^+ introduced here. The value of ρ^+ or K^+ is a characteristic of the reactor core material (of its composition), and is a weak function of the reactor dimension (varying as $\sim 1/R^4$) and of the composition of the reactor reflector, since the derivatives in Eq. (11) are taken at x = 0, i.e., for the case of an infinite reactor where the reflector plays no role.

For experimental applications of the statistical weight theorem, the difference between ρ^+ and ρ_∞ can be taken into account by treating the fifth right-hand member of Eq. (11) as a correction calculated on the basis of the dependence of $\rho(x)$ for an unreflected reactor with the same core. Clearly, $\rho^+ = \rho_\infty$ in the one-group approximation, given the absence of any dependence on x^2. The difference between ρ^+ and ρ_∞ shows up starting with the two-group approximation, for which

$$\rho_\infty = \rho + x \frac{M^2}{K_\infty} + x^2 \frac{L^2 \tau}{K_\infty} \tag{13}$$

and

$$\rho^+ - \rho_\infty = x^2 \frac{L^2 \tau}{K_\infty} \tag{14}$$

in conformity with the data reported in [2]. It is clear from Eq. (14) that, in those cases where the two-group approximation is valid, K^+ will be greater than K_∞.

For experimental applications of the total statistical weight theorem, the constants ρ^+ can be obtained from special measurements carried out on "bare" assemblies of the same composition. Comparison of Eqs. (13) and (9) reveals that measurements of the total statistical weight make it possible to determine the migration area approximately:

$$M^2 \simeq \frac{SK_\infty}{2x}. \tag{15}$$

When the values of ρ^+ and ρ_∞ are far apart, we can resort to an estimate:

$$L^2\tau \approx \frac{\rho_\infty - \rho - S/2}{x^2} K_\infty. \tag{16}$$

LITERATURE CITED

1. A. I. Mogil'ner, At. Énerg., 21, 127 (1966).
2. A. I. Mogil'ner, At. Énerg., 24, 78 (1968).
3. A. I. Mogil'ner, V. A. Osipov, and G. N. Fokin, At. Énerg., 24, 42 (1968).
4. G. Kosai and Z. Szatmari, Nukleonik, 12, 243 (1969).

ON THE PHYSICOCHEMICAL REACTION OF HAFNIUM WITH EUROPIUM

E. M. Savitskii, B. G. Arabei,
V. I. Bakarinova, S. E. Salibekov,
N. I. Timofeeva, and V. M. Romashov

UDC 543.2

Hafnium and europium have high chemical activities, the former being a high-melting element, the latter a low-melting element with a high vapor pressure [1, 2]. This explains the difficulty of obtaining alloys of hafnium and europium.

Fusion of the elements by arc melting, and simultaneous heating of hafnium and europium in hafnium containers, gave poor results owing to evaporation of europium. In the case of simultaneous heating, retention at 1800-2000°C led to the appearance of fissures in the containers, through which virtually all the europium escaped by evaporation.

We succeeded in fusing these elements by heating in air-tight molybdenum capsules (diameter 35 mm, height 50 mm, wall thickness 4 mm), filled with hafnium chips (~15 g) and europium metal (~5 g) in an atmosphere of argon. Both elements were degreased before the experiments. These were performed with hafnium iodide (~98.7%), hafnium powder (~99.5%), and europium metal (>99.7%). The capsule cover was sealed by argon-arc welding to make an air-tight joint. The capsules were then annealed in a TVV-4 vacuum furnace at different temperatures in the interval 850-1600°C with a residence time of up to 100 h.

The alloys were subjected to spectral, chemical, x-ray structural, and microscopic analyses. Thin sections of hafnium and its alloys for microscopic analysis were subjected to etching electropolishing at 75-85 V in a 20 : 1 mixture of CH_3COOH and $HClO_4$ with vigorous mixing of the electrolyte. We used a stainless steel cathode.

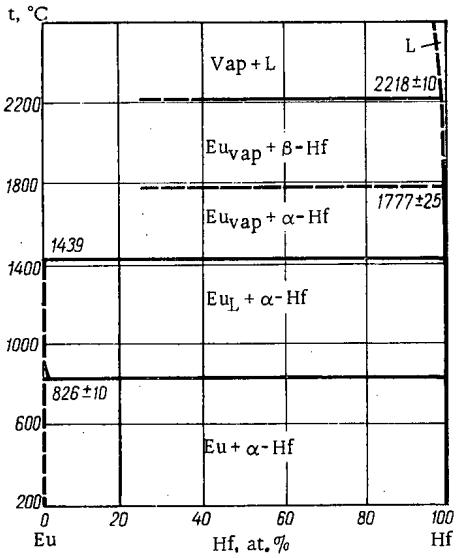

Fig. 1. Hypothetical phase diagram of the system europium–hafnium.

The mutual solubility of hafnium and europium at the investigated temperatures was determined by chemical phase analysis. The capsule was opened and the material immediately treated with a 1 : 2 HCl solution for 24 h at room temperature, then heated for 2 h. In the initial period a vigorous reaction was observed, indicating the presence of europium, which is readily soluble in acids. The hafnium metal remained practically undissolved. The solution was used for determining the europium and hafnium contents by gravimetric analysis (europium by precipitation with oxalic acid, hafnium with phenylarsonic acid). To determine the amount of europium dissolved in hafnium, a weighed sample (~10 g) of alloy chips was treated with HCl, as described above, then dissolved in concentrated HF with heating for 1 h. The europium fluoride precipitate was roasted at 1000°C, treated with 1 : 1 HCl and heated, and europium precipitated as the oxalate by oxalic acid. Table 1 gives the results of chemical phase analysis of europium and hafnium after isothermal boiling.

The mutual solubility of europium and hafnium is negligible. The maximum solubility of hafnium in europium was ~1.7 wt. %

Translated from Atomnaya Énergiya, Vol. 30, No. 4, pp. 390-391, April, 1971. Original article submitted April 27, 1970; revision submitted August 3, 1970.

TABLE 1. Mutual Solubility of Elements of the System Europium–Hafnium from Chemical Analysis Data

Heating temperature, °C (residence time 100 h)	Initial composition, g		Content by analysis, g				Solubility, %	
	hafnium	europium	hafnium		europium		hafnium in europium	europium in hafnium
			free	combined	free	combined		
850	15	4,05	14,83	0,067	3,96	0,0035	1,66	0,025
1200	15	5,17	13,79	0,034	4,97	0,0036	0,68	0,026
1450	15	6,83	13,85	0,045	6,72	~ 0,0047	0,65	~ 0,034
1600	14	4,61	12,89	0,020	2,80	0,0032	0,71	0,025

at 850°C and ~0.7 wt. % at higher temperatures. The solubility of europium in hafnium at all the investigated temperatures was about 0.03 wt. %.

X-ray structural and microscopic analyses of the hafnium-based alloys showed that treatment with HCl did not lead to the appearance of any new phases or structural components. The lattice constants of the alloys were almost the same as those of the initial hafnium, and displayed no change after heating at various temperatures, an increase in temperature leading only to growth of the grains.

The mutual solubility of hafnium and europium at higher temperatures was not investigated owing to possible reaction of the components with the material of the capsule. Microscopic and spectral analyses revealed that >1800°C a reaction occurs in the ternary system Eu–Hf–Mo.

On the basis of our results and data on the pure components [2, 3] and reactions in analogous systems [4-7], and taking into account the marked differences in the atomic radii and melting points, electrochemical properties, and crystal lattices of hafnium and europium, we suggested a hypothetical form of the phase diagram of the system europium–hafnium (see Fig. 1); according to this diagram, europium and hafnium do not form intermediate phases, and their mutual solubility is negligible.

LITERATURE CITED

1. F. Spedding et al., Trans. Metallurg. Soc. AIME, 212, 379 (1958); Problems of Present-Day Metallurgy, No. 3, 130 (1959).
2. F. Spedding and A. Daane, Metallurgical Reviews, 5, No. 19, 297 (1960).
3. D. E. Thomas and E. T. Hayes, The Metallurgy of Hafnium [Russian translation], F. M. Perel'man (editor), Metallurgiya, Moscow (1967).
4. R. Lesser and E. Erben, Metall., 15, 30 (1961); Problems of Present-Day Metallurgy, No. 3, 146 (1961).
5. M Wright et al., Paper No. P/696, in: Proc. of the Second United Nations Intern. Conf. on the Peaceful Uses of Atomic Energy, Vol. 5, IAEA, Geneva (1958), p. 390.
6. R. Elliott, Constitution of Binary Alloys, Suppl. I, McGraw-Hill (1965), p. 412.
7. I. Obinata et al., Trans. Amer. Soc. Metals, 52, 1097, 1072 (1960).

NOTES ON MEASUREMENT OF Tc^{99m} ACTIVITY

Kh. Shtefan, V. A. Bazhenov,
V. V. Bochkarev, Yu. M. Golubev,
and T. N. Sokolova

UDC 621.039.5

To date, the activity of Tc^{99m} has been measured primarily by a relative method, making comparisons with the isotope Co^{57}. The $4\pi\beta-\gamma$-coincidence procedure has been used [1] in precision measurements. This article presents a method for measuring Tc^{99m} activity with the aid of a $4\pi\beta$-counter to within ±2% error (95% confidence interval).

The decay scheme of Tc^{99m} is shown in Fig. 1. For convenience, the same scheme notation is used here as in [1]: a is the transition probability, energy 2 keV; α_1, α_2, α_3 are the internal conversion coefficients of the corresponding γ-lines; ε_{β_1} is the sensitivity of the $4\pi\beta$-counter to radiation related to the 2 keV transition; ε_β is the sensitivity of the $4\pi\beta$-counter to conversion electrons of the 140 keV and 142 keV transitions; $\varepsilon_{\beta\gamma}$ is the sensitivity of the $4\pi\beta$-counter to γ-emissions at 140 keV and 142 keV; ε_γ is the sensitivity of the scintillation sensor to γ-emissions at 140 keV and 142 keV.

We can write

$$N_\beta = N_0\left\{a\varepsilon_{\beta_1} + a(1-\varepsilon_{\beta_1})\varepsilon_\beta\frac{\alpha_2}{1+\alpha_2} + \varepsilon_\beta\frac{(1-a)\alpha_3}{1+\alpha_3} + a(1-\varepsilon_{\beta_1})\frac{1}{1+\alpha_2}\varepsilon_{\beta\gamma} + (1-a)\frac{1}{1+\alpha_3}\varepsilon_{\beta\gamma}\right\};$$

$$N_\gamma = N_0(1-\varepsilon_{\beta\gamma})\varepsilon_\gamma\left(\frac{a}{1+\alpha_2} + \frac{1-a}{1+\alpha_3}\right);$$

$$N_c = N_0 a\frac{1}{1+\alpha_2}(1-\varepsilon_{\beta\gamma})\varepsilon_\gamma\varepsilon_{\beta_1}.$$

for the count rates in the β- and γ-channels and in the coincidence channel.

Hence, assuming $\alpha_2 \approx 0.1$, $\alpha_3 \approx 30$ [2], $\varepsilon_{\beta\gamma} < 5\cdot10^{-4}$, $\varepsilon_{\beta_1} < 0.5$, and neglecting terms introducing less than 1% distortion in the sum of the results, we obtain the approximate Goodier–Williams formula [1]:

$$\frac{N_\beta N_\gamma}{N_c} \approx N_0\left[1 + \frac{1-\varepsilon_{\beta_1}}{\varepsilon_{\beta_1}}\varepsilon_\beta\left(\frac{a\alpha_2}{1+\alpha_2} + \frac{(1-a)\alpha_3}{1+\alpha_3}\right)\right].$$

Figure 2 shows extrapolation curves obtained when ε_{β_1} is varied, in the coordinates

$$y = \frac{N_\beta N_\gamma}{N_c};\quad x = \frac{1-\varepsilon_{\beta_1}}{\varepsilon_{\beta_1}}.$$

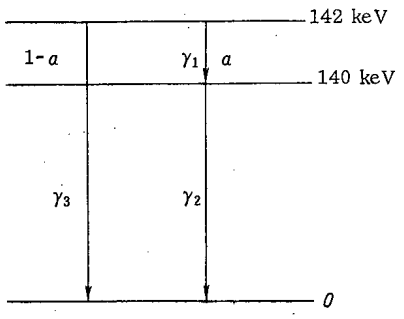

Fig. 1. Decay scheme of Tc^{99m}.

Curve 1 is borrowed from [1], while curve 2 was taken by the authors. The Tc^{99m} was obtained from a Mo^{99}-generator. The Mo^{99} was absorbed, in the form of sodium phosphomolybdate, on aluminum oxide. Proceeding along the axis from zero 3.5 times closer than in [1] made it possible, to begin with, to use NH_4Cl to wash off the Tc^{99m}, with subsequent decomposition of the ammonium chloride upon heating, and dissolution of the residue with the Tc^{99m} in HNO_3. Secondly, use of a layer of gold for reflecting the electrons derived from the 2 keV transition aided this purpose.

The coating of the source, applied to film 15 $\mu g/cm^2$ thick, in films of total thickness ~60 $\mu g/cm^2$ thick on both sides, rendered

Translated from Atomnaya Énergiya, Vol. 30, No. 4, pp. 392-393, April, 1971. Original article submitted May 12, 1970.

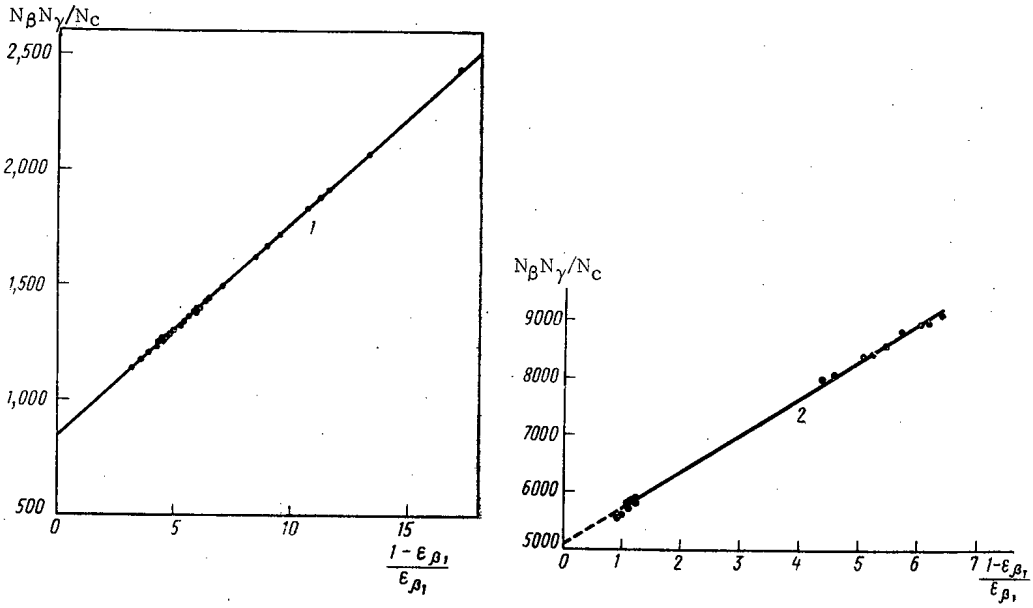

Fig. 2. Dependence of $N_\beta N_\gamma / N_c$ on $1-\varepsilon_{\beta_1}/\varepsilon_{\beta_1}$.

possible absorption (~10^3-fold) of the radiation associated with the 2 keV transition, while the conversion electrons from the 140 keV and 142 keV transitions underwent practically no absorption. The count rate of the $4\pi\beta$-counter for radiation from a sealed source is

$$N_\beta = kN_0,$$

where

$$k = \varepsilon_\beta \left[\frac{a\alpha_2}{1+\alpha_2} + (1-a)\frac{\alpha_3}{1+\alpha_3}\right].$$

By measuring N_0 by the extrapolation method, using $4\pi\beta-\gamma$-coincidences and subsequent measurements of the count rates N_β from those same sources sealed on both sides by layers 60 $\mu g/cm^2$ thick, we found

$$\left[\frac{a\alpha_2}{1+\alpha_2} + (1-a)\frac{\alpha_3}{1+\alpha_3}\right] = 0{,}1193$$

to within ±2% error in a 95% confidence interval.

Using the value so found, we measured the Tc^{99m} activity with ease, with the aid of a $4\pi\beta$-counter, and using the formula

$$N_0 = \frac{N_\beta}{0.1193\varepsilon_\beta},$$

where N_β is the count rate of the $4\pi\beta$-counter intercepting radiation from a source sealed on both sides by layers 60 $\mu g/cm^2$ thick, and corrected for background and dead time; ε_β is the recording effectiveness of the $4\pi\beta$-counter for conversion electrons from the 140 keV and 142 keV transitions, and is usually close to unity.

LITERATURE CITED

1. I. Goodier and A. Williams, Nature, 210, No. 5036, 614 (1966).
2. R. Growther and J. Eldridge, Nucl. Phys., 66, No. 2, 272 (1965).

CONSTRUCTION OF CERTAIN INJECTORS FOR EXPERIMENTS WITH RADIOACTIVE INDICATORS

J. Dobzhansky, K. Korbel, and T. Ovsjak

UDC 621.039.85

The constantly increasing use of tracer atoms in scientific research and technological measurements compels experimental research workers to develop new types of injector construction. In this paper we shall describe the construction of injectors in two cooperating Cracow institutes, the Institute of Nuclear

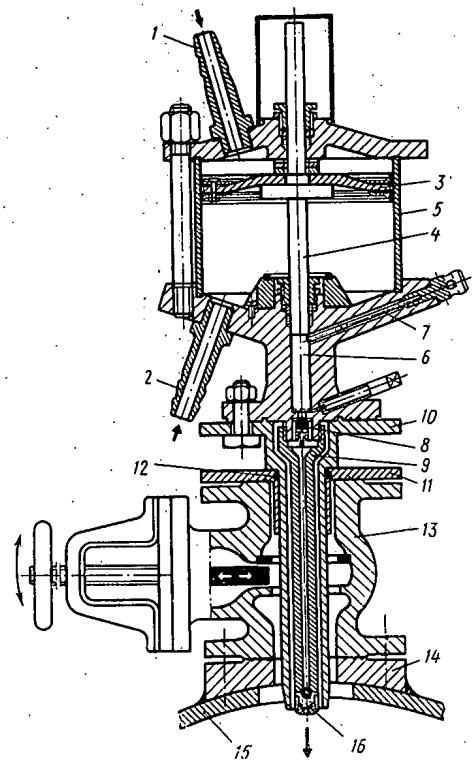

Fig. 1

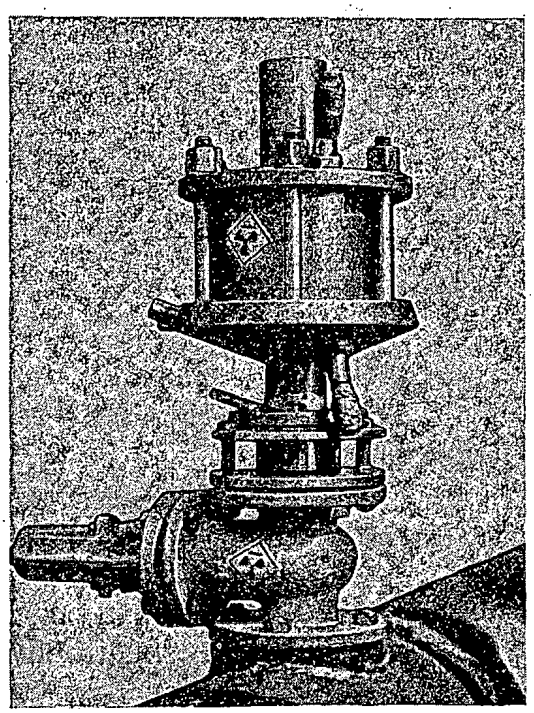

Fig. 2

Fig. 1. Section of a rapid-pulse injector: 1, 2) channels for supplying compressed air; 3) piston; 4) axis of piston; 5) cylinder of pneumatic drive; 6) injection chamber; 7) channel inserting indicator; 8) first reciprocating valve; 9) injector nozzle; 10) sheath of extension system; 11) leading flange; 12) seal of the "0" type; 13) slide-valve; 14) flange; 15) transporting pipeline; 16) reciprocating valve of the extension system.

Fig. 2. General view of the rapid-pulse injector mounted on the pipe-line.

Institute of Nuclear Technology of the Mining and Metallurgical Academy, Cracow, Poland. Institute of Nuclear Physics, Cracow, Poland. Translated from Atomnaya Énergiya, Vol. 30, No. 4, pp. 393-396, April, 1971. Original article submitted June 1, 1970.

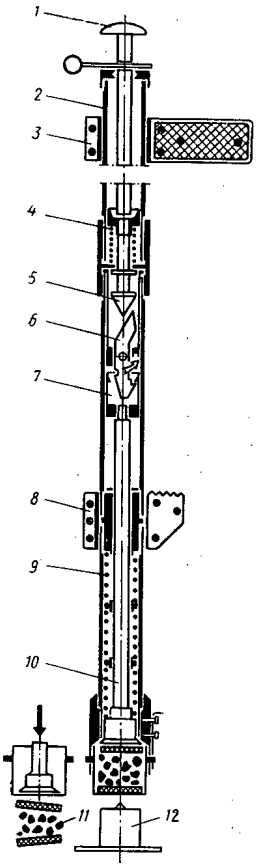

Fig. 3

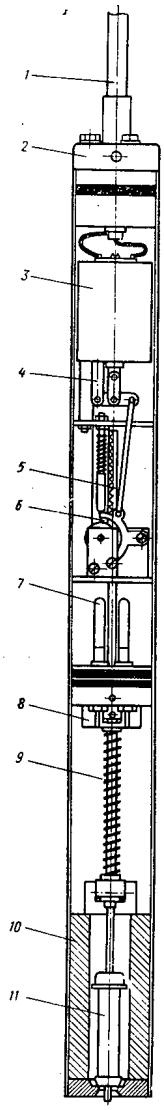

Fig. 4

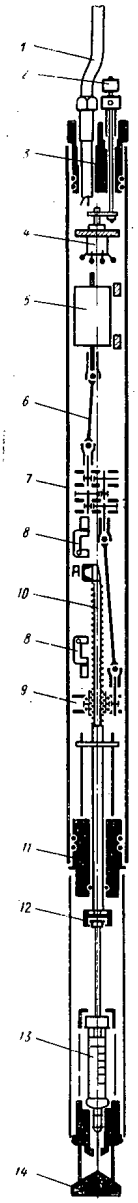

Fig. 5

Fig. 3. Throwing-in injector: 1) release rod; 2) sheath; 3) holder handle; 4) rotating spring of the release mechanism; 5) cone of the release mechanism; 6) lever; 7) injector rod catch; 8) pedal; 9) set of springs; 10) axis of injector; 11) radioactive indicator; 12) block for tightening the injector spring.

Fig. 4. Bore-hole pulse injector (simplified): 1) cable; 2) upper end piece; 3) electromagnet; 4) system of levers; 5) rack and pinion; 6) release (traveling) wheel with dog; 7) rubber compensators; 8) lower end piece; 9) working spring; 10) lead sheath; 11) syringe.

Fig. 5. Bore-hole injector with a constant outflow of the indicator: 1) carrier cable; 2) gear lever; 3) upper end piece; 4) electric switch; 5) electric motor; 6) universal shaft; 7) distributor box; 8) end switches; 9) gear-wheel drive; 10) push rod; 11) control device; 12) channel connecting the syringe with the push rod; 13) interchangeable syringe; 14) protective stem.

Technology of the Mining and Metallurgical Academy and the Institute of Nuclear Physics. These injectors are intended for measuring the velocity of liquids and hydraulic mixtures under two conditions: 1) in pipelines; 2) in bore-holes associated with hydro-geological and geophysical investigations. For the first problem, rapid-pulse and "throwing-in" injectors have been designed, for the second, pulse and continuous injectors.

The Rapid-Pulse Injector. This was designed in order to introduce a tracer substance into the medium under investigation (the medium moving through a pipeline) in a very short period of time so as to be uniformly distributed over the whole cross section of the flow. Figures 1 and 2 show a section and a general view of the injector; the construction of this satisfied both the foregoing requirements.

The injector consists of three main elements: 1) a two-chamber cylinder 5 with a piston 3, serving as a pneumatic drive for the injector; 2) an injection chamber 6; 3) an injection nozzle 9 furnished with reciprocating valves 8 and 16. The two chambers of the pneumatic-drive cylinder 5 and the injection chamber 6 are arranged in series, facilitating the incorporation of a single common coaxial system. The piston 3 in the drive cylinder 5 is reinforced by means of leather sleeves which automatically contract during the operating period. The piston has a greater working area in the upper region; in alternate working cycles, compressed air from a compressor is forced against this through channels 1 and 2 by means of distributor valves. The working cross section of the piston in the injection chamber 6 is some 100 times smaller; thus a comparatively low pressure (3 atm) easily overcomes the internal pressure acting in the pipeline, ensuring a high rate of injection. Three channels lead into the injection chamber. Two of these (the second is not shown in the figure) communicate with the upper part of the chamber and serve to introduce portions of tracer substance into the injector. These channels are opened each time before filling, and after filling are firmly closed by means of special slides. The working volume of the chamber 6 was decided by considering the activity of the portion of indicator needed in order to match a specified sensitivity of the detectors, and also by considering the practically feasible activities of the materials available. The volume in question approximately equalled 12 cm^3. The outlet of the injection chamber 6 was made in the form of a jet 5 mm in diameter with a reciprocating valve 8. The injector was mounted on the pipeline by means of a flange sealed to the latter. During the fitting of the injector the pipeline accordingly had to be evacuated, which in practice caused many difficulties. In order to avoid this, an additional attachment was designed so as to allow the injectors to be fitted during the normal operation of the pipeline. This consisted of a slide valve 13, a flange 11 with a seal of the "0" type, an extension system comprising a tube 9 terminating in the injector nozzle, and also a sheath 10. The slide 13 was mounted on the pipeline during an interruption in the technological process (in the closed position). During the measurements, the injector proper was attached to the slide, then the injector was moved up to the support through the open channel of the slide and connected into a single whole.

The Throwing-In Injector. Figure 3 illustrates the specially designed throwing-in injector for measuring the velocity of multiple-component hydraulic mixtures. The injector serves to introduce several different indicators into the inlet of the pipeline at the same time, simulating various granulometric fractions of the solid phase of the hydraulic mixture; it also serves to inject the liquid phase of the hydraulic mixture. The injector is made from a steel tube with an outer diameter of about 30 mm and a length of about 3 m. The injection of a portion of indicator (earlier prepared in the capsule 11) is effected as follows: after introducing the device 12 into the holder of the injector, the pedal 8 is depressed with the foot and the rod 10 is let down until the catch 7 connects with the lever 6. At the same time the pin enters into the rod 1, which protects the system from any chance ejection of the charged capsule. Then the capsule, closed on both sides by rubber pistons, is inserted into the bayonet holder of the injector. In order to eject the capsule, the pin is removed by applying pressure to the head of the striking rod and the rod is set in axial motion. The cone 5 seated on the end of the rod rotates the lever 6 and releases the catch 7. The springs 9 expand, moving the piston, which expels the contents of the capsule together with the rubber stoppers.

The Bore-Hole Pulse Injector. The bore-hole pulse injector (Fig. 4) has been specially developed for measurements in bore holes, in which it is essential to provide for repeated injection after the simultaneous installation of the measuring probe. An injector of this type consists of two chambers: a closed and an open one. The closed chamber is closed at the top with an end piece 2 accomodating a sealed cable 1, and at the bottom with an end piece 8, carrying a compensator to compensate for the volume of the glycerin filling the chamber. A rod with a spring 9 passes into the lower end piece through an appropriate gasket. Inside the closed chamber is an electromagnet 3, which, on receiving pulses along the cable 1,

operates the catch of the release wheel 6. The wheel in turn is connected to the rack and pinion 5, and when the spring 9 is released it produces forward motion in the plunger of the syringe 11. The open chamber constitutes a space in direct contact with the medium under examination. This accomodates the lead sheath 10 and the working spring 9, together with the plunger of the syringe 11, which squeezes out approximately 0.7 cm^3 of the substance. The volume of the syringe is approximately 20 cm^3, which provides for some 27 injections. The next filling of the syringe is effected after removing the sheath 10.

This injector may also be used in hydro-geological installations for measuring the velocity and direction of motion of waters in open reservoirs. Practice has shown that, in the case of a small outlet cross section of the syringe, no spontaneous outflow occurs; hence there is no need for a reciprocating valve in the apparatus.

Bore-Hole Injector with a Steady Outflow of Indicator (Fig. 5). Like the injector which we have just been describing, this is intended for measurements in bore holes and in hydro-geological research. In contrast to the pulse-type injector, which always inserts the same volume, this injector provides for continuous injection with a constant (steady) efflux of indicator. The injection time is changed by smoothly regulating the period of operation of the drive motor. The operating principle of the injector is as follows: when the gear lever is set in "reverse," the rod 10 moves to the position A until the upper end switch 8 operates. After a brief manipulation (associated with the fixing of the injector 13), the injector is connected to the channel 12. Then the gear lever is set in the "forward" position, after which (in accordance with the time of starting the drive motor) the indicator ejected by the injector plunger starts flowing out. Motion is transmitted from the motor to the indicator plunger in the following manner: the motor 5 is connected with the distributor box 7 by way of the universal shaft 6; the motion is transmitted from the box 7 by a drive system 9, which operates through a rack and pinion to produce forward motion of the rod 10 and the indicator plunger 13. When the indicator is completely discharged, the lower end switch 8 starts operating. After the gear lever has been returned to the "reverse" position, the next portion of indicator passes into the injector from an auxiliary container.

DEPENDENCE OF BUILDUP FACTOR ON POSITION OF SHIELD BETWEEN BREMSSTRAHLUNG SOURCE AND DETECTOR

V. P. Kovalev, V. P. Kharin,
V. V. Gordeev, and S. P. Filipenok

UDC 539.12.08:539.122

From a consideration of the process of transmission of radiation through a shield it follows that a change in the position of a shield between a source and a detector alters the conditions under which radiation scattered in the shield is incident on the detector and therefore changes the dose buildup factor [1, 2]. Flattening absorbers of various materials are commonly used to produce uniform dose distributions of bremsstrahlung from electron accelerators. A study of the dependence of the buildup factor on the position of the shield permits the location of the optimum position of the absorber between the target and the irradiated object. The buildup factor for an isotropic γ-source and a semiinfinite absorber may reach values of several units [1]. If the angular distribution of the bremsstrahlung has a peak in the direction of motion of the electrons and the absorbers are finite in size the buildup factor will be smaller.

We have measured the dependence of the dose on the position of the absorber between a bremsstrahlung source and a detector for electron energies of 12.5, 15.7, and 21.8 MeV. The work was performed with a type LYÉ-25 linear electron accelerator [3] using a tungsten target 1.8 radiation lengths thick. The angular distribution of the bremsstrahlung from the target at selected values of the electron energy are shown in

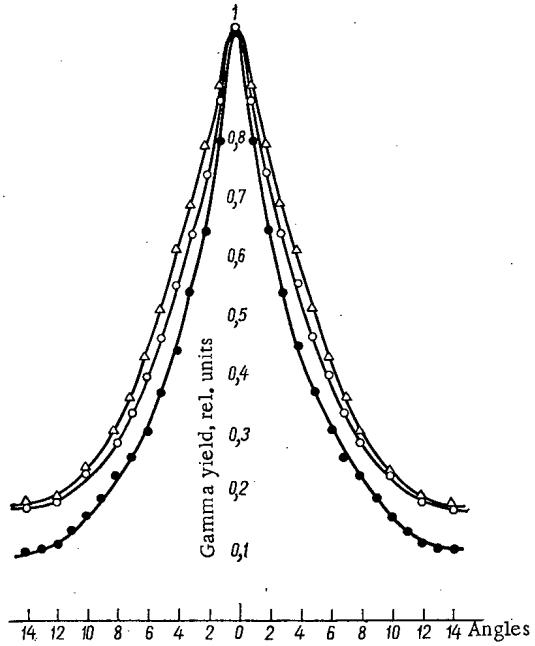

Fig. 1

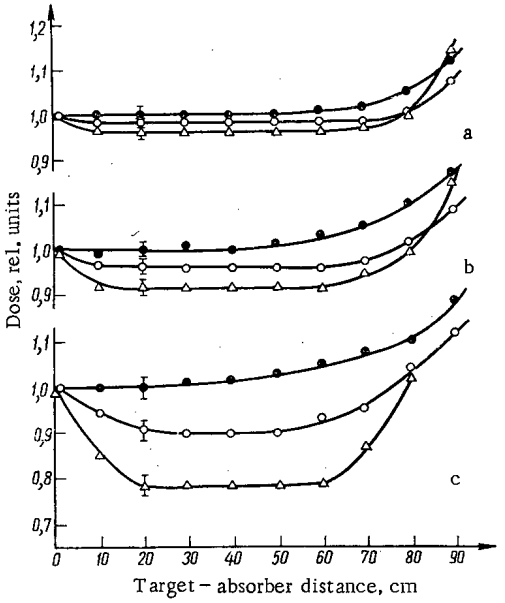

Fig. 2

Fig. 1. Angular distributions of bremsstrahlung from a tungsten target for electron energies of 22 (•); 15 (○); and 12.8 (Δ) MeV.

Fig. 2. Dose as a function of position of aluminum absorber of diameter: a) 50; b) 80; c) 120 mm for electron energies of 21.8 (•); 15.7 (○); and 12.5 (Δ) MeV.

Translated from Atomnaya Énergiya, Vol. 30, No. 4, pp. 396-397, April, 1971. Original article submitted April 6, 1970.

Fig. 1. Aluminum, copper, and lead absorbers of various sizes were used. The detector was a thimble chamber with a plastic lining 16 mm thick. The detector was 1 m from the target.

Figure 2 shows the results for aluminum absorbers. The figure shows that the maximum value of the buildup factor occurs for the minimum electron energy of 12.5 MeV when the absorber is placed close to the target. The buildup factor decreases with increasing electron energy and increases as the absorber diameter increases. Thus for aluminum absorbing cylinders 120, 80, and 50 mm in diameter and 100 mm high the differences in dose, depending on the position of the absorber between the source and detector, are respectively 23, 8, and 4% for electron energies of 12.5 MeV.

The buildup factor also increases when the absorber is close to the detector. However, it is difficult to make a quantitative estimate in this case because of the contribution to the dose made by secondary electrons from the absorber.

Similar results were obtained for equivalent thicknesses of copper and lead. No significant change in the buildup factor with the atomic number of the absorber was observed.

LITERATURE CITED

1. D. P. Osanov, in: Instruments and Methods for Radiation Analysis [in Russian], Vol. 3, Gosatomizdat, Moscow (1962), p. 53.
2. Yu. A. Kazanskii et al., Information Bulletin of the Nuclear Data Center [in Russian], No. 2, Atomizdat, Moscow (1965), p. 305.
3. V. I. Ermakov et al., Atomnaya Énergiya, 29, 206 (1970).

THE USE OF A (p, γ) REACTION TO DETERMINE THE CONTENT OF LIGHT ELEMENTS IN THIN SURFACE LAYERS OF SAMPLES

S. S. Vasil'ev, Yu. A. Dzhemard'yan, G. I. Mikhailov, and L. P. Starchik

UDC 539.1.06:621.039

Resonance reactions (p, γ) permit the detection of the presence of light elements in very thin surface layers of samples [1], as well as the establishment of their depth distribution in the investigated layer [2, 3] or sample [4].

For thick layers, the yield of γ-quanta Y is determined by the function (the number of reactions per incident proton)

$$Y = \frac{\mu_a \tau_a}{\Omega_0} C_a + Y_b, \quad (1)$$

where $\mu_a = (\pi/2)(N_{Av}\sigma_{aR}\Gamma_r)/A_a$; N_{Av} is Avogadro's number; Γ_r is the true width of the resonance level r of the compound nucleus; C_a and A_a are the content and atomic weight of the element to be analyzed; τ_a is the occurrence of the isotope, on the nuclei of which the reaction used is observed; $\Omega_0 = \sum_i \Omega_i C_i$; Ω_i and C_i are the stopping power ($eV \cdot cm^2/mg$) and content of the i-th element present in the sample; σ_{aR} is the cross section in resonance, determined by the element to be analyzed; Y_b is the yield of γ-quanta due to the matrical elements, considering the constant background of the pickup.

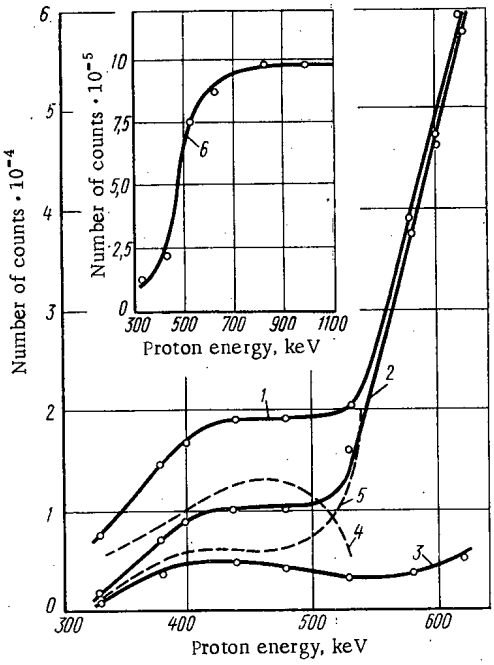

Fig. 1. Excitation functions obtained by proton irradiation of targets of silicon, tantalum, and carbon (graphite): 1, 2) samples of silicon; 3) tantalum target; 4) excitation function of carbon; 5) excitation function of silicon (without carbon impurity); 6) excitation function of graphite.

Translated from Atomnaya Énergiya, Vol. 30, No. 4, pp. 397-398, April, 1971. Original article submitted April 6, 1970; revision submitted May 4, 1970.

The content of the element to be monitored, found in a thin layer (the energy loss by the protons is comparable with the width of the resonance level $\Delta E_p \approx \Gamma_r$), can be found by determining the area A (ε) of the resonance peak:

$$A(\varepsilon) = \varepsilon (Y - Y_b) = \nu \mu_a \tau_a C_a. \quad (2)$$

In this expression ν is the thickness of the layer in g/cm^2, while ε is the thickness of the layer in energy units with the corresponding resonance energy of the protons. If the width of the real resonance peak $\Gamma_{experim}$ and the width of resonance on a "thick" target Γ_T are known, then

$$\varepsilon = \sqrt{\Gamma^2_{experim} - \Gamma^2_T}. \quad (3)$$

The largest yield of the (p, γ) reaction in the case of thin targets is observed when

$$E_p = E_{res} + \frac{\varepsilon}{2}. \quad (4)$$

An experimental verification of the method of analysis of the composition of thin layers was conducted for the determination of the contamination with carbon of the surface of eight samples of semiconductor silicon, subjected to various stages of technological treatment (cutting, grinding, diamond and chemical polishing). An electrostatic accelerator was used to accelerate the protons. The cross-sectional area of the beam incident on the target was ~1 cm^2; the current of the beam did not exceed 3 μA.

The determination of the carbon content was based on the use of the reaction C^{12}(p, γ)N^{13} ($T_{1/2}$ = 10.1 min, $E_{\beta+}$ = 1.19 MeV, $E_\gamma \approx$ 2.4 MeV). Since samples of silicon in which the impurities did not exceed 1% were investigated, it may be considered that the value of $\Omega_0 \approx$ const.

Figure 1 presents the experimental excitation functions of two samples of silicon 1 and 2, graphite 6, and tantalum 3. The presence of carbon in the surface layer of silicon can be concluded according to the shape of the excitation functions 1 and 2, which was confirmed by an investigation of the curve of the decomposition of one of the irradiated samples. On the basis of the excitation functions obtained in the irradiation of samples of silicon (with the least positron activity) and tantalum, with the aid of theoretical calculations we constructed the excitation function of hypothetically pure silicon 5, corresponding to the conditions of this experiment. Deducting the function 5 from the function 1, we obtained the function of excitation of carbon 4. On the basis of graph 4 we found the value of $\Gamma_{experim}$, and on the basis of the curve of escape due to pure graphite, 6, we found Γ_T. It was determined according to formula (3) that $\varepsilon \approx$ 100 keV. This corresponds to a layer of a silicon sample contaminated by carbon atoms, $\lesssim$0.4 mg/cm^2 thick. Since there is no noticeable displacement of the strong resonance (620 keV) of the reaction Si^{30}(p, γ)P^{31}, it may be concluded that a layer $\lesssim$0.4 mg/cm^2 is not a solid carbon film, but a layer of silicon with a small admixture of carbon. This is also confirmed by a calculated comparison of the yield of γ-quanta due to the presumed carbon film, with the escape of γ-quanta that actually occurs.

The spectra of γ-quanta were also obtained after irradiation of one of the samples of silicon with protons with two energies, 530 and 950 keV. Although a peak due to γ-quanta with $E_\gamma \approx$ 2.4 MeV is clearly distinguished in the first case, it is absent in the second. This once again confirms the fact that carbon at the level of the threshold sensitivity (0.01-0.02%) contaminates only a thin surface layer.

The contamination of the surface layers of samples of semiconductor silicon with carbon was determined by a method of comparison with a standard, as which we used the sample with the largest carbon content (0.6%). The carbon content in the sample was found by two methods: 1) according to the formulas (1) and (2), considering the excitation function of pure graphite; 2) by comparison of the yields of the products of the reaction C^{12}(p, γ)N^{13}(γ and β^+) due to the investigated and specially prepared samples. The contamination of the surface layers with carbon reached 0.2-0.4% in certain samples.

LITERATURE CITED

1. S. Rubin, T. Passell, and L. Bailey, Analyt. Chem., 29, 736 (1957).
2. M. I. Guseva, E. V. Inogin, and S. P. Tsytko, ZhÉTF, 36, 3 (1959).
3. N. A. Skakun and O. N. Khar'kov, At. Énerg., 27, 351 (1969).
4. E. Möller and N. Starfelt, Aktiebolaget Atom-Energi, Report No. 237, Stockholm (1966).

THE USE OF ACCELERATED CHARGED PARTICLES (α AND p) TO DETERMINE THE CONTENT OF CERTAIN LIGHT ELEMENTS

K. A. Baskova, S. S. Vasil'ev,
Yu. A. Dzhemard'yan, G. I. Mikhailov,
and L. P. Starchik

UDC 543.53+539.125

Reactions excited by charged particles of low and medium energies, produced on accelerators, can be used to determine the content of light elements. Thus, protons with an energy of 6.25 MeV and α-particles with an energy of 25 MeV, produced on a cyclotron, have been used to determine the content of boron and oxygen in semiconductor silicon.

Samples of silicon 20-30 mm in diameter and 0.5-1.5 mm thick were irradiated with a flux of particles corresponding to a current of the beam of 1-2 μA. The number of charged particles bombarding the sample, which was set up in a Faraday cylinder, was measured with a current integrator.

To record the induced positron activity we used a $\gamma\gamma$-coincidence spectrometer on two crystals of NaI(Tl), with dimensions 40 × 40 mm.

Boron was determined according to the induced activity, due to the isotope C^{11} with half-life 20.4 min, which is formed according to the reaction $B^{11}(p, n)C^{11}$, which possesses a threshold of 3 MeV [1]. The isotope C^{11} can also be formed according to the reaction $N^{14}(p, \alpha)C^{11}$, with a threshold of ~3 MeV; however, an appreciable yield of this reaction is observed only at proton energies >4 MeV. If the boron and nitrogen contents in the sample are equal, then the ratio of the activity induced on account of boron to the activity on account of nitrogen at a proton energy of 4 MeV is equal to 10^3, and at a proton energy of 5 MeV it is equal to 10^2 [2, 3].

To eliminate the influence of nitrogen, the proton energy was lowered to 4.5 MeV with the aid of aluminum foils. The reaction $O^{18}(p, n)F^{18}$ with a threshold 2.58 MeV can occur on nuclei of the isotope O^{18}, leading to the formation of F^{18} with a half-life of 110 min. After irradiation of a sample of semiconductor silicon, a portion characterizing the presence of the isotope F^{18} can be clearly distinguished on the decay curve. However, as was shown by the investigations, when a surface layer ~10 μ thick is removed after irradiation of the sample, no activity due to F^{18} is observed in the silicon matrix. This indicates a substantial contamination of the surface layer of the silicon by oxygen. Therefore, the surface layer must be removed before measuring the activity of the sample.

Samples of silicon containing 10^{18}-10^{19} atoms/cm^3 of boron were used as the standards. The time of irradiation of the sample and standard was selected at 20 min, time of cooling 40 min, time of count of induced activity 40 min. The threshold sensitivity of the determination of boron was 10^{-6}%.

Oxygen was determined according to the isotope F^{18} with half-life 110 min, formed according to the reaction $O^{16}(\alpha, d)F^{18}$ and $O^{16}(\alpha, pn)F^{18}$ with thresholds 20.4 and 23.2 MeV, respectively [4, 5]. At an α-particle energy of 25 MeV, the reactions $B^{10}(\alpha, n)N^{13}$, $C^{12}(\alpha, n)O^{15}$, and $N^{14}(\alpha, n)F^{17}$ occur on the nuclei of impurity atoms. The positron-active nuclei N^{13}, O^{15}, and F^{17} have half-lives of 10.1, 2, and 1.1 min, respectively. When the sample is cooled for 40 min in the absence of boron, all the activity in it will be due to F^{18}. An analysis of the distribution of oxygen through the depth of the sample indicated that in a layer ~10 μ thick, the oxygen content is an order of magnitude higher than in the matrix. Just as in the case of the determination of boron, a layer 10 μ thick was removed from the surface of the sample before the measurement.

Translated from Atomnaya Énergiya, Vol. 30, No. 4, pp. 398-399, April, 1971. Original article submitted April 6, 1970; revision submitted May 4, 1970.

TABLE 1. Threshold Sensitivities (Analysis according to the height of the step on the yield curve)

Element	Composition of sample	Proton energy, keV		Energy of γ-quanta	Dose of irradiation, μCi	Threshold sensitivity, %	Threshold sensitivity at a dose of irradiation of 10^5 μCi
		E_{p_1}	E_{p_2}				
B	$B_2O_3 + Li_2O$	500	900	9,5—12,3	1000	0,15	$1{,}5 \cdot 10^{-2}$
Li	$Li_2O + B_2O_3$	300	500	16,5—20,0	1000	$1{,}0 \cdot 10^{-2}$	$1{,}0 \cdot 10^{-3}$
Li	$Li_2O + SiO_2$	300	500	14,0—20,0	1000	$8{,}0 \cdot 10^{-3}$	$8{,}0 \cdot 10^{-4}$

Optical quartz was used as the standard. The time of irradiation of the sample was 110 min, time of count of the induced activity 110 min. The sensitivity of the determination of oxygen was equal to $5 \cdot 10^{-6}$%. In the presence of boron in the silicon, the activity of the sample was measured 2 h after irradiation. The sensitivity of the determination of oxygen in this case was 10^{-5}%. The reproducibility of the results in the case of repeated measurements was no poorer than 20%.

Under the action of ~1 MeV protons on the nuclei of light elements, there are (p, γ) and (p, αγ) reactions, having a pronounced resonance character, which substantially facilitates the possibility of their selective determination. The determination of lithium [6], beryllium, boron [7], fluorine, and other elements has been performed according to the yield of γ-radiation of these reactions. The threshold sensitivities at a dose of irradiation (total of the charges of the protons bombarding the target) of the order of 10^3 μCi are n(10^{-2}–10^{-5})%.

The light elements can be determined selectively according to the height of the resonance steps, which are observed in the plot of the excitation functions. The height of the steps is proportional to the concentration of the element to be analyzed. Thus, by irradiating a sample with protons with energies below and above one of the concrete resonances of the given element, information can be obtained on its quantitative content. This method of analysis has been used to determine the content of lithium and boron. The sensitivities of the determination are cited in Table 1.

LITERATURE CITED

1. S. P. Kalinin, A. A. Ogloblin, and Yu. M. Petrov, At. Énerg., 2, 171 (1957).
2. H. Rommel, Analyt. Chim. Acta, 34, 427 (1966).
3. C. Engelmann and G. Cabane, International Conference on Modern Trends in Activation Analysis, Texas College Station, USA (1965), p. 331.
4. T. Nozaki et al., Nature, 190, 4770, 45 (1961).
5. K. Saito et al., Int. J. Appl. Rad. and Isotopes, 14, 357 (1963).
6. S. S. Vasil'ev et al., At. Énerg., 25, 328 (1968).
7. S. S. Vasil'ev et al., Zavod. Lab., No. 3, 299 (1969).

PRODUCTION OF STRONG, HIGH-ENERGY NEUTRON FLUXES IN A CYCLOTRON BY IRRADIATING THICK LITHIUM AND BERYLLIUM TARGETS WITH 22-MeV DEUTERONS

V K. Daruga and N. N. Krasnov

UDC 621.384.633

Data relating to the neutron yield and the energy and angular distribution of the neutrons obtained in the Li + d reaction were presented earlier [1]. The deuteron bombardment of a thick target composed of a low-z material gives a fairly strong flux of neutrons with energies of 10 MeV or over, suitable for solving various practical problems in neutron physics and technology.

In analyzing the results of the earlier paper [1], the characteristics of the ZnS(Ag) + Plexiglas detectors employed were taken from another reference [2]. Subsequent checks showed that these characteristics were inapplicable to the scintillator blocks employed, which consisted of ZnS(Ag) + Plexiglas (standard B-2 type). A refinement of the earlier data [1] carried out with due allowance for the true characteristics of this threshold detector showed that the average effective threshold was equal to ~1.8 MeV, so that all the absolute values given earlier [1] should be increased by a factor 1.25 times.

In the present investigation we measured the absolute yields of neutrons of all energies in the direction $\Theta = 0^0$ (relative to the irradiating deuteron beam) from thick lithium, beryllium, niobium, and uranium targets, using an "all-wave" detector with a BF_3 counter of the SNM-5 type (Table 1). The deuteron energy equalled 22 ± 1 MeV.

As in the earlier case [1], we used a stilbene scintillation spectrometer for measuring the neutron spectra (at an angle of $\Theta = 0°$) from the lithium and beryllium targets. The accuracy of normalization of the spectrum was ±15% or better. The average energies of the spectra are shown in Table 1, together with estimates of the neutron yields for various energy groups. The ZnS(Ag) + Plexiglas threshold detector was used to measure the yield ratio $Y(0°)/Y(90°)$ of neutrons with energies of over 1.8 MeV (Table 1) and to estimate the angular distribution for $E_n > 4$ MeV (Fig. 2).

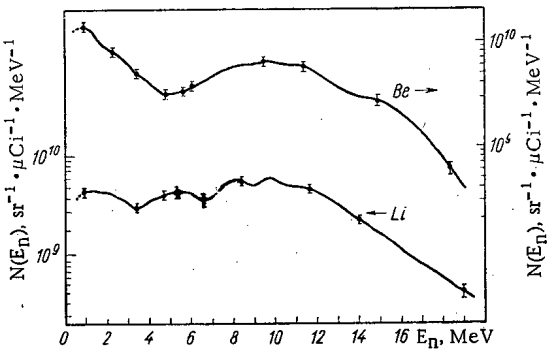

Fig. 1

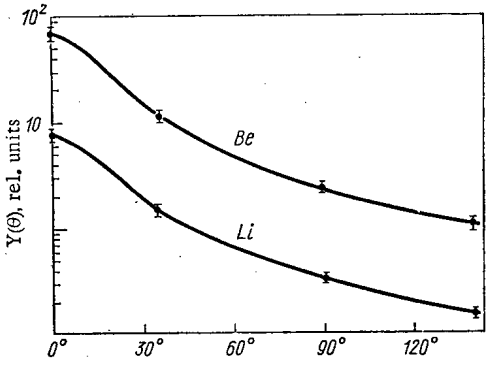

Fig. 2

Fig. 1. Neutron spectra for lithium and beryllium targets.

Fig. 2. Angular distribution of the neutrons obtained from lithium and beryllium targets.

Translated from Atomnaya Énergiya, Vol. 30, No. 4, pp. 399-400, April, 1971. Original article submitted April 6, 1970.

TABLE 1. Neutron Yields, Neutrons/sr · μCi (at Θ = 0°)

Target	$E_n > 0$	$E_n > 4$ MeV	$E_n > 10$ MeV	$E_n > 14$ MeV	$\bar{E}_n$, MeV	Y (0°) /Y (90°)
Li	$7{,}3 \cdot 10^{10} \pm 8\%$	$5{,}7 \cdot 10^{10}$	$2{,}7 \cdot 10^{10}$	$0{,}9 \cdot 10^{10}$	9,1	11
Be	$9{,}1 \cdot 10^{10} \pm 8\%$	$5{,}5 \cdot 10^{10}$	$2{,}7 \cdot 10^{10}$	$0{,}8 \cdot 10^{10}$	7,3	12
Nb	$1{,}0 \cdot 10^{10} \pm 10\%$	—	—	—	—	5
U	$8{,}4 \cdot 10^{9} \pm 8{,}5\%$	—	—	—	—	4

The authors wish to thank V. A. Dulin, E. S. Matusevich, and N. N. Pal'chikov most sincerely for help in this work, and also A. E. Romanchenko and A. A. Ognev for preparing the cyclotron used in the experiments.

LITERATURE CITED

1. V. K. Daruga et al., At. Énerg., 24, 66 (1968).
2. S. F. Degtyarev et al., Bulletin of the Information Center for Nuclear Data [in Russian], No. 3, Atomizdat, Moscow (1966), p. 459.

METHOD OF EXPERIMENTALLY DETERMINING THE MAGNETIC-WELL DEPTH IN A SYSTEM WITH MINIMUM B

V. M. Glagolev, Yu. V. Skosyrev, and A. A. Shmarin

UDC 533.9.01,621.039.61

At the present time, one of the basic requirements imposed on magnetic systems intended for the stable thermal isolation of a plasma is that the systems have a minimum B. The condition of hydrodynamic stability of a low-pressure plasma derived by Rosenbluth and Longmire [1] and considered in detail by Kadomtsev [2] reduces to the requirement that the quantity $\int (dl/B)$ decrease, where the integral is taken along a force line of the magnetic field B, with a transition from the interior force lines to exterior force lines. Methods for obtaining minimum B essentially reduce to the application of specially selected transverse fields to the longitudinal fields [3-6].

Since a regime with minimum B usually occurs with rigorously defined field relations, it is important to establish the existence of a magnetic well in a real magnetic system. Presently there is no known universal experimental method for determining the depth of a magnetic well. The method proposed here is suitable for determining the magnetic-well depth in systems that have regions on which the distribution of the magnetic field over the cross section of the magnetic surfaces is known. The minimum B can be determined in that case, in particular, if there are homogeneous-field regions (e.g., in a Stellarator with cylindrical symmetry).

The authors determined the minimum B in Glagolev's proposed system with homogeneous-field regions [5].

In this trap a magnetic well is created in stabilization sections owing to the extension of central lines of force. This situation occurs because of the superposition on the homogeneous longitudinal field of transverse harmonically varying fields that depend on the azimuthal angle θ in the transverse cross section of the cylindrical chamber as $\sin\theta$, $\sin 2\theta$, and $\sin 3\theta$, respectively.

The model of a stabilization section on which we conducted our measurements had a system of windings intended for obtaining fields of the first, second, and third harmonics; the model is schematically shown in Fig. 1. The order of arranging the multipole windings along the longitudinal z axis of symmetry that coincides with the direction of the external homogeneous magnetic field was as follows: we first set up the quadrupole lens (2), and then in the slots of the coaxial cylinders of the insulation material we put up the windings that establish the field of the first (1) and third (3) harmonics, i.e., the dipole and hexapole magnetic lenses. The stabilization section had a symmetry plane P perpendicular to the z axis. The currents in the adjacent or symmetrically positioned windings of each of the harmonics are in opposite directions (indicated by arrows in Fig. 1). Therefore, each line of force that belongs to a certain cylindrical surface at the input of the stabilization section is deflected away from the cylindrical surface by the fields that act on one side of the plane P exactly as much as it is deflected towards this surface by the fields on the other side of the plane P. Because of this situation, the magnetic surfaces along both sides of the stabilization section have a circular cross section in the absence of cylindrical symmetry.

The system of stabilizing windings was positioned on the surface of a 150-mm-diameter cylindrical vacuum chamber.

Translated from Atomnaya Énergiya, Vol. 30, No. 4, pp. 401-403, April, 1971. Original article submitted March 26, 1970; revision submitted August 11, 1970.

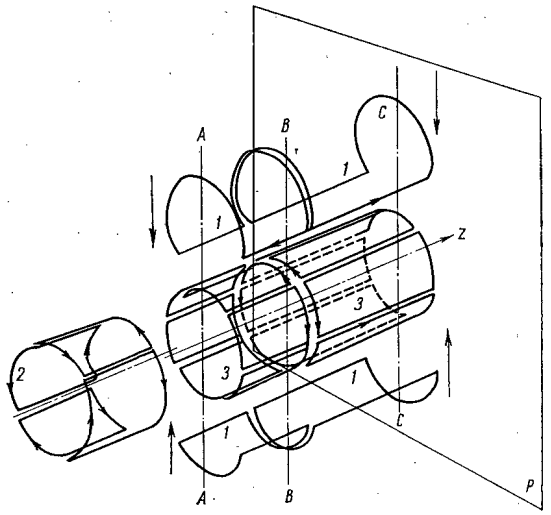

Fig. 1

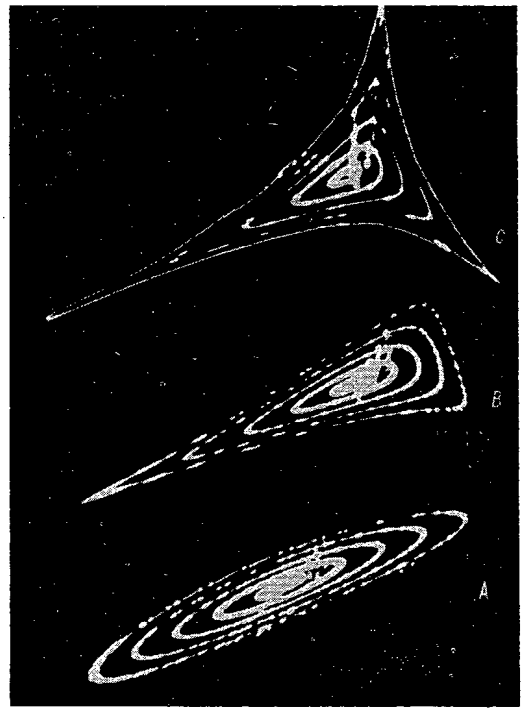

Fig. 2

Fig. 1. Diagram of a stabilization section: 1) conductors that create the first harmonic of the magnetic field (dipole lens); 2) conductors that create the second harmonic of the magnetic field (quadrupole lens); 3) conductors that create the third harmonic of the magnetic field (hexapole lens).

Fig. 2. Cross sections of the magnetic surfaces formed as the gun is rotated.

An electron gun was placed at one end of the vacuum chamber; at the other end there was an aperture through which one could photograph the Plexiglas screen that was covered with a luminescent compound. The screen could be moved along the z axis. By turning the gun with respect to the longitudinal axis of the chamber, at the input to the stabilization section one could separate a family of force lines belonging to the magnetic surface of a closed configuration with a sufficiently large number of sections, which had the form of a circular cylinder at the gun. We were able to observe the motion of the screen along the chamber axis due to the motion of the force lines along the system and the deformations of the original circular cross section of the magnetic surface under the influence of the stabilizing fields.

Figure 2 shows the experimentally obtained cross sections of the magnetic surfaces in planes perpendicular to the z axis at the points marked A, B, and C in Fig. 1

Derivation of the Calculation Formula and Measurement Results

The depth of a magnetic well $\delta U/U$ is characterized by the change in the ratio $\Delta V/\Delta\Phi$ (the ratio of the volume of the magnetic surface to the longitudinal flux) in the transition from interior surfaces to exterior surfaces [4].

We consider the enclosed magnetic surfaces having volumes V_0, V_1, and V_2, and fluxes Φ_0, Φ_1, and Φ_2.

Then

$$\frac{\delta U}{U} \approx \frac{\frac{\Delta V_1}{\Delta\Phi_1} - \frac{\Delta V_2}{\Delta\Phi_2}}{\frac{1}{2}\left(\frac{\Delta V_1}{\Delta\Phi_2} + \frac{\Delta V_2}{\Delta\Phi_1}\right)},$$

where

$$\Delta V_2 = V_2 - V_1,\ \Delta V_1 = V_1 - V_0;\ \Delta\Phi_2 = \Phi_2 - \Phi_1;\ \Delta\Phi_1 = \Phi_1 - \Phi_0.$$

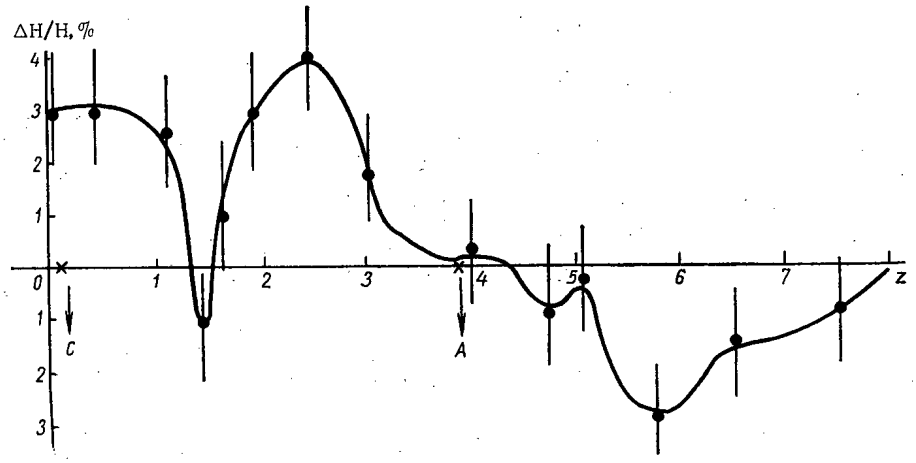

Fig. 3. Distribution of the relative variation of the average magnetic field in a stabilization section.

We represent the volume of a magnetic tube in the form $V = \sum_i S_i \Delta Z_i$, where S_i is the cross-sectional area of a volume cut by planes perpendicular to the axis at the point Z_i. From the law of conservation of magnetic flux inside a tube it follows that $\Delta\Phi_1 = H_0\Delta S_1^0$ and $\Delta\Phi_2 = H_0\Delta S_2^0$, where ΔS_1^0 and ΔS_2^0 are the cross sections of the volumes ΔV_1 and ΔV_2 in the region of the homogeneous field H_0. Assuming that the screen moves in steps of ΔZ = const, we have

$$\frac{\delta U}{U} \approx \sum_i \left(\frac{\Delta S_{1i}}{H_0\Delta S_1^0} - \frac{\Delta S_{2i}}{H_0\Delta S_2^0}\right)\left[\frac{1}{2}\sum_i \left(\frac{\Delta S_{1i}}{H_0\Delta S_1^0} + \frac{\Delta S_{2i}}{H_0\Delta S_2^0}\right)^{-1}\right].$$

Taking $N = L/\Delta Z$, where L is the length of a stabilization section, we obtain

$$\frac{\delta U}{U} \approx \frac{1}{N}\sum_i \frac{\Delta S_1^0}{\Delta S_2^0}\left(\frac{\Delta S_2^0}{\Delta S_1^0} - \frac{\Delta S_{2i}}{\Delta S_{1i}}\right),$$

where N is the number of measurements, since $\Delta S_1 \approx \Delta S_1^0$ and $\Delta S_2 \approx \Delta S_2^0$ with accuracy to within 1%. Thus, an approximate measurement of minimum B in the system reduces to a measurement of the ratio of the cross-sectional area of magnetic surfaces to the motion of the screen along the longitudinal axis of the chamber. A photograph of the cross sections of the magnetic surfaces was enlarged 10 times. The cross-sectional area was measured with a planimeter.

Measurement Results and Calculation of Errors

Figure 3 shows results of measuring minimum B. The given data correspond to values of transverse fields for which the maximum magnetic surface has a diameter of 40 mm at the input. Since only the ratio of the areas enters into the calculation formula, we did not analyze the systematic errors. The random errors in measuring the area of the magnetic surface were determined by processing the systematic data after several repetitions of all the operations (establishing the currents in the windings, photographing, drawing the contour of the surface, and measuring the cross-sectional area). The relative error in the measurements of the area was 0.5%.

The accuracy of the result was estimated by finding the root-mean-square error and determining the reliability of the result by the Student–Fisher method for a small number of measurements. The final result can be represented in the form

$$\frac{\Delta H}{H} = \left(\frac{\Delta H}{H}\right)_{\text{rms}} \pm A\sigma \left(\frac{\Delta H}{H}\right)_{\text{rms}},$$

where the coefficient of the limiting deviation A = 5.84, the reliability of the result α = 0.99, i.e., the depth of the magnetic well on the part of the stabilization section AC is $\Delta H/H$ (2 ± 0.25) with reliability 99%. After allowance for the effect of the lens, we found that the quantity $\Delta H/H$ in the system was 0.5 ± 0.25.

LITERATURE CITED

1. M. N. Rosenbluth and C. L. Longmire, Ann. Phys. (N. Y.), 1, 120 (1957).
2. B. B. Kadomtsev, in: Reviews of Plasma Physics, Vol. 2, Consultants Bureau (1966), p. 153.
3. L. S. Solov'ev, V. D. Shafranov, and É. I. Yurchenko, Paper CN-24/B-2 at the Conference on Controlled Thermonuclear Fusion, Novosibirsk (1968).
4. J. M. Green and J. L. Johnson, Phys. Fluids, 4, 875 (1961).
5. V. Glagolev, Plasma Phys., 1, 621 (1969).
6. H. P. Furth and M. N. Rosenbluth, Phys. Fluids, 7, 764 (1964).

NEWS

VIENNA OCTOBER 1970 IAEA SYMPOSIUM ON COST ASPECTS OF NUCLEAR POWER STATION HOOKUP TO POWER GRIDS

A symposium on the cost aspects of hooking up nuclear electric power generating stations to national power grids was held in Vienna in October, 1970. This symposium was organized under joint sponsorship of IAEA and the UNO Economic Commission for Europe. Present at this symposium were 250-odd delegates from 42 countries and 11 international organizations. Fifty-two papers were presented.

A typical feature of the symposium was the fact that the overwhelming bulk of the papers presented came from power firms and organizations generating electric power. An appreciable portion of the reports dealt to some extent with forecasts of national power development in general, and nuclear power development in particular, covering periods of varied length all the way to the year 2020.

The reports read at the panel sessions grouped around the following general topics: 1) special features of nuclear power stations relating to the operating costs of the stations in the national power system; 2) general planning problems encountered in hooking nuclear power stations up to the national power grids; 3) use of analytical techniques and simulation techniques in the planning and operation of national power systems incorporating nuclear power stations; 4) cost outlook for incorporation of nuclear power stations in national power networks; 5) effect of international and regional collaboration on the economics of nuclear power station hookup to national power grids. This division of the agenda is highly arbitrary, since the topics were touched upon simultaneously in overlapping fashion in the reports, in quite a few instances.

The group of papers associated with the first topic dealt with operating experience of major nuclear power stations and how their characteristics correspond (now, and in the future) to the operating conditions in the overall power system. Reports in this group dealt with various aspects and goals. Stress was laid either on possibilities for adjusting reactors or requirements of power stations now and in the future (e.g., reports on British and West German power stations), or on conscientious descriptions of operating experience, servicing, repair and maintenance, and handling of accidents (e.g., the Chinon power station, the Julich reactors). It was emphasized that there is no point to covering up accidents occurring at nuclear power stations, for no matter how embarrassing or troublesome the fact of an accident at a nuclear power station may be, the experience gained in overcoming the accident and shedding as much light as possible on its causes and ways of coping with the problem make it possible to accumulate valuable information for mutual benefit.

The second group of papers dealt more with topical problems concerning power systems and related ways of overcoming different complications in operating conditions stemming from daily and seasonal fluctuations in power demands. Technical difficulties in solving the problem of covering peak power demands, complicated further by the enormous variety of specific conditions prevailing in each country, generated any number of proposals on methods for solving this problem. These include building combined nuclear-fueled and fossil-fuel electric power stations with heat-power turbines with the load-handling patterns based on heat-power demand; possible discrepancies between heat-power demand peaks and electric-power demand peaks would then render the whole problem easier. The concept of an aviation type turbine working in tandem with a nuclear reactor belongs to the same category of solutions. The gas generated in the aviation turbine in this tandem arrangement would be cycled to heat the feedwater for a SGHWR type reactor, so that electric power could also be obtained from the gas turbine during hours of peak electric power demand, while the reactor is being run at its top electric power output rating. Another approach to solving this type of problem relies on the use of steam accumulators.

All of these concepts are at the stage of proposals yet to be tried out, and reflect research directions considered in various countries, while still a long way from actual realization.

Translated from Atomnaya Énergiya, Vol. 30, No. 4, pp. 404–405, April, 1971.

Two reports from the USA, in this grouping, are of independent interest, however, and stand apart from the others. The first deals with processing cost data on the building of 41 nuclear power stations with LWR type reactors in the USA. The report deals with derivation of formulas for approximating the numerous, often contradictory, and constantly varying, data on nuclear power plant construction costs in the USA. The second report dealt with uranium demands for nuclear power stations, and the needed capacities of uranium processing plants. The author of that report stated that the USAEC is adopting natural uranium, termed "Daval" type, for diffusion enrichment with uranium-235, with a concentration of 0.2 in the process tailings. Processing with a higher concentration in the tailings would be economically unfeasible, and will not be attempted.

One conspicuous omission in the topics treated at the symposium was any mention of nuclear power stations utilizing natural uranium.

Foreign papers presented on the second topic can be divided arbitrarily into two basic groupings: problems in the planning and operation of several nuclear power stations incorporated in a national power grid, and the problem of siting the power plant and operating conditions for a particular country's first nuclear power plant (in the case of developing nations). Reports in the first group shared much in common in terms of approach to the solution of the problem and technique. As a rule, an estimate of the income and outlay branches of the fuel–power balance was attempted, with estimates of power demand trends, attention to internetwork relationships and their development, anticipated fluctuations in power demands, and cost optimization in relation to incorporation of a group of nuclar power stations into the national power grid, and their operating conditions. Reports of this type were presented by Italy, West Germany, and Great Britain. Reports in the second group contain analyses of the geographical and power situations in the developing countries, as a basis for proper siting of nuclear power plants and arriving at unit power output of a nuclear reactor station having a reactor of some specified type (mostly PWR or BWR). These reports of course reflect the power situation inside the country, with a reactor already developed and tested in other countries being imported. Reports of this type were presented by Turkey, Thailand, Mexico, etc.

Reports on the next topic dealt with the methodology of calculations of cost indices for large systems (incorporating groups of nuclear power stations), with treatment of the developmental dynamics of nuclear power ratings. Reports on this subject were presented by the USA, Great Britain, Poland, the Netherlands, Belgium, and Yugoslavia. Naturally, the reports on this topic originating in the western countries were based on the familiar "present worth" method reflecting the social essence of the functioning of the capitalist economy. All the reports on this topic contained either data and technique prerequisites for computer processing or computer results. Results of calculations on nuclear power development were presented most exhaustively in one paper presented by the USA delegation. This paper cited various developmental power models with the total electric power generating capacities of the country brought up to the year 2000 at a level of 1300 million kW (with nuclear power stations accounting for 1 billion kW), and to the year 2020 at a level of 3 billion kW (all of it accounted for by nuclear power stations).

A novel approach in technique to the selection of unit power ratings for blocks of nuclear power stations in a developing nuclear power network was applied in one of the papers presented by the French delegation. The problem was solved by a negative method, i.e., by estimating and proportioning economic losses incurred when nuclear power stations are taken off the line, and when there is a need to cover a shortage of electric power by resorting to standby power courses exhibiting a variety of cost indices.

Papers on the fourth topic were in a variety of formats. These papers dealt preponderantly with the role and economic outlook of nuclear power stations, and the problem of incorporating them successfully in the national power grid, and were based to some extent on engineering cost studies of both existing and planned fuel–power balances in the respective countries. Such reports were presented by Czechoslovakia, Hungary, Yugoslavia, Poland, Spain, Japan, and Mexico.

A Swiss report falling within the fifth topic is of special note. This report dealt with a way of overcoming difficulties stemming from costs in building nuclear power stations which are often excessive to small countries (and one of the overriding conditions in judging cost feasibility in such instances), and the problem of cooperation between firms and between governments. The report went into the organizational experience in arranging international exchanges of electric power has already been accumulated. Exchange of power and smoothing of complications attendant upon the introduction of nuclear power stations to the economy and power networks of the countries involved were discussed in a British paper. Finally, a USA

paper dealt with organizational principles and goals concerning a unified power network for all power sources on the northeastern seaboard of the USA. Lack of organizational ties between power networks is causing difficulties in the handling of power resources and regulation of performance of electric power stations in that part of the country.

Four Soviet papers were presented at the symposium. A report by Yu. D. Arsen'ev discussed utilization of two turbines combined in a single power unit with a reactor, to enhance the reliability of nuclear power stations while at the same time cutting operating costs. Techniques and calculations based on the methodology proposed were the subject of a paper submitted by A. A. Beschinskii, K. P. Kislov, and Ya. I. Khainson on the discovery of a nonuniform portion of power load charts for major power networks, under conditions where nuclear power stations become part of the national power picture on a major scale. A report by Yu. I. Koryakin and A. V. Bakanov on the comparative cost picture of nuclear power stations operating as part of the national power grid covered similar ground. The ultimate purpose of these papers was to shed light on the comparative pattern of economic losses when the regulating functions in the national power system are performed by different types of power sources. Finally, a paper submitted by E. Z. Borodyanskii, I. M. Vol'kenau, and A. P. Zeilinger was devoted to increasing the power output of power generators and of the power station in major power networks.

It should be stressed that the lively discussion following presentation of the reports was a characteristic feature of this symposium. Clearly, this was a consequence of the timeliness of the topics covered. The proceedings of the symposium will be published by IAEA in the first half of 1971.

GRENOBLE SEPTEMBER 1970 INTERNATIONAL CONFERENCE ON MAGNETISM

V. I. Ozhogin

The commission on magnetism of the International Union of Pure and Applied Physics (IUPAP) schedules international conferences on magnetism once every three years, and these have steadily become better attended and more representative. The Grenoble September 1970 conference was the seventh in the series, and drew 1191 participants from 31 countries. A total of 493 papers were heard, 48 of these being "invited" papers. Soviet scientists presented 38 of these reports. Interest was stimulated by the "invited" paper of A. S. Borovik-Romanov entitled "Static and resonance properties of antiferromagnetic material with "light plane" type anisotropy," and by two papers on birefringence in magnetic crystals submitted by Leningrad physicists (and presented by R. V. Pisarev), and others.

On the whole, the current distribution of interests and efforts in the science of magnetism, and its various trends, were reflected by the topics covered in the "invited" papers. For example, constant attention was given by the countries "most highly developed in magnetism" to investigations of spin waves (magnons) in magnetic materials of the most varied types, and above all to their mutual interactions and interactions with other elemental excitations in crystals. A large group of reports dealt with a comparatively new phenomenon of great importance, metal–dielectric phase transitions in compounds of the transition metals (first discovered in V_2O_3). Intensive investigations of trace magnetic impurities in various types of host matrices are continuing, and papers submitted by J. Schrieffer, G. Gladstone, A. Higer H. Suhl, and others were devoted to this topic. Interest in transport phenomena (heat, charge) in magnetic materials remained quite high. Special attention is being given to the steadily expanding investigation of such new materials as ferromagnetic semiconductors (particularly the chalcogenide spinels), which include substances exhibiting high magnetic Q and similar electrical properties.

Work done by French physicists at Saclay, reported on by A. Abraham, of unquestionable importance (and equal complexity) although disputed, was met with lively interest. The report dealt with observations of a state exhibiting antiferromagnetically ordered spins of F^{19} nuclei in CaF_2, with special techniques (remotely reminiscent of adiabatic demagnetization) developed to bring about conditions equivalent to a temperature of 10^{-6}°K.

The conference demonstrated once again that the widespread use of nuclear physics techniques in the investigation of magnetic materials has unquestionably become a characteristic feature of the contemporary physics of magnetic phenomena. For example, of the total number of papers presented at the conference, 70 reported on results of neutron diffraction research, and another 35 dealt with Mössbauer investigations. Another trend in this area is the development and utilization of methods based on inelastic scattering of polarized neutrons, which make it possible to study not only these and other energy transitions in the scattering system, but also accompanying changes in spin (report by T. Riste, Norway). The Mössbauer experiments also show promise in the utilization of polarized Mössbauer emission.

The percentage yield of results in physical research in the sphere of new engineering applications continues to be large, as before, and is still on the increase. One striking example is that of orthoferrites of the rare earths ($RFeO_3$), which in past were investigated purely academically as antiferromagnetic materials exhibiting weak ferromagnetism, and which are now attracting close interest in physics and engineering as materials displaying record-high rates of motion of domain walls (e.g., the mobility of the walls in YFeO at 77°K is 50,000 cm/sec·Oe, according to a report by F. Russell from Bell Telephone). A no less

Translated from Atomnaya Énergiya, Vol. 30, No. 4, pp. 405-406, April, 1971.

striking example is provided by a combination of two "magnetic" groups of elements: 3d and 4f, which began to undergo study years ago from a purely theoretical vantage point. The results of this research are detection of $SmCo_5$ type compounds, which can be used, with the aid of specially engineered processing, in the fabrication of permanent magnets with record characteristics: $BH_{max} = 2 \cdot 10^7$ G·Oe and higher (reports by D. L. Martin and M. Wentz from General Electric Co., by K. Strnat and A. Raye from the University of Ohio, and others).

By analogy with this example, we can point out the purely physical research, not dealt with broadly at the conference, on compounds of elements with an unfilled 5f-shell (these include all the actinoids), with representatives of other "magnetic" groups that have been studied in greater detail. This trend seems to promise some pleasant surprises, the more so in that some of the intermetallic compounds of the actinoids (for instance, of uranium, as reported on by B. Matthias from Bell Telephone), are also superconductors, as research has revealed.

The construction of Europe's largest magnetism research laboratory, the National High Magnetic Fields Laboratory at Grenoble, work on which was started in January 1970, is a new development. The laboratory's task will be to investigate solid state physics under extreme physical conditions (constant magnetic field to 200 kOe, pressures 100-500 kbar, ultralow temperatures to 10^{-2}°K). The first water-cooled 200 kOe solenoid (diameter of effective opening 30 mm) is to be ready in July 1971. The laboratory is being built on the basis of the experience acquired with a similar operation, the National Magnetic Laboratory of the USA. But a single-section solenoid arrangement has been selected to generate the peak magnetic field (200 kOe or higher), rather than a three-section arrangement. This became possible only recently with the appearance on the scence of a new type of insulating material (capton) which is still very expensive and highly unavailable. Use of this material, along with other improvements, has enabled French engineers to utilize a 5 MW solenoid at a level of 350 V, rather than 200 V as in the USA, and has thereby facilitated the solution of several attendant electrical engineering problems.

The organization of the conference was generally on a very high level. Special attention was given to facilitating exchanges of views between delegates outside the main auditorium. There was much interest in an exhibit of up-to-date scientific and technical equipment manufactures by the leading French and foreign firms, which was organized at the conference. The delegates were provided with ample data reproduction facilities for making their own copies of material made available at the conference. The complete texts of the reports presented at the conference will be published in an early 1971 issue of Journal de Physique.

A VISIT TO CULHAM LABORATORY

L. I. Artemenkov

A delegation of Soviet scientists visited Culham Laboratory in October 1970, as part of the fulfillment of an agreement on scientific collaboration and exchange of visits between Great Britain and the Soviet Union in the field of thermonuclear fusion research.

The program of the visit, as suggested by the administration of Culham Laboratory, covered familiarization with the work in progress at this research center, and more detailed familiarization with advances in the field of design of superconducting solenoids and automatic data processing systems.

In addition to their visit to Culham Laboratory, the members of the Soviet delegation also stopped off at the Rutherford Laboratory, where the NIMROD proton synchrotron is in operation. This visit was interesting from the standpoint of familiarization with superconducting technology and computer techniques. A portion of the delegation paid a visit to the C. T. L. computer firm, which manufactures computers for Culham Laboratory. The delegation also visited the laboratory at Harwell, where a demonstration was given of how the CAMAC modular system works, and how complex measuring instruments, such as multichannel pulse-height analyzers, can be designed.

The visit took place after the European plasma physics conference (Rome, September, 1970), so that the major plasma physics research findings were already reported, and the members of the Soviet delegation focused their interest rather on new experiments and new research facilities.

The "High-β toroidal experiment" facility has now been finished at Culham Laboratory, and is already in operation. Investigations on this machine are a logical extension of the work commenced on the ZETA facility. A dozen or so minor experiments on other facilities are underway to back up this program. Specifically, diagnostic work on measurement of the magnetic field in a high-β plasma with the aid of Thomson scattering is being performed. Experiments on stabilization of θ-pinch plasma instabilities by feedback are being prepared.

Construction work on the superconducting Levitron installation has been in progress for several years, in the hands of the Sweetman group, and low-force work is being done on the Phoenix-2 machine. The Levitron is scheduled for completion before the end of 1971, at an estimated cost of half a million pounds sterling. The levitating ring and several other coils are made of superconducting material.

Construction of the new CLEO stellarator will be completed within the next two to three years. This is in essence a toroidal facility, which will be operated in the tokamak mode and in the stellarator mode. A hot plasma is to be generated in the tokamak mode, and confinement of that plasma by a stellarator field will be studied.

Superconducting solenoids are being fabricated from round multicore wire at the Culham and Rutherford laboratories. The diameter of one superconducitng core made of niobium and titanium alloy is not greater than 30 μ. This small dimension of the superconducting cores, combined with the large number of such cores (as many as a thousand), has made it possible to use a small amount of copper to attain a high current density with stabilization. The area ratio of the cross sections of copper and superconductor is three to one. A coil is wound from this combination wire to a specified profile. The winding is encapsulated in a special epoxy resin which resists cracking even when cooled all the way down to 4°K and heated back to normal temperature. It took three years to work out this technology. A monolithic block of superconductor is produced in the technology. The coils are cooled by helium in the vapor phase, rather than the liquid phase, thereby simplifying fabrication technology and functioning of the cryogenic system.

Translated from Atomnaya Énergiya, Vol. 30, No. 4, pp. 406-407, April, 1971.

The design current density in the solenoids fluctuates from 10,000 to 25,000 A/cm^2, depending on the dimensions of the solenoids. Windings 1200 mm in diameter with a 60 × 40 mm cross section, and 260 kiloampere-turns, were demonstrated. These coils were fabricated for the Levitron machine.

An extensive program on fabrication of a new variant of accelerator with superconducting magnets is planned for the Rutherford Laboratory, and a large bubble chamber several cubic meters in volume, with a superconducting solenoid, is also in planning and design stages.

The KDF-9 central digital computer which has been an old standby at Culham Laboratory was backed up in 1970 by the installation and commissioning of a new and more powerful ICL-4/70 computer. To date small machines of the PDP-8 and LINC-8 types have been working on line with the experimental research facilities. Five new machines of the Modular One type manufactured by C. T. L. have now been acquired in addition. The Modular One computer is faster and, better yet, more flexible than the PDP-8. All of the new experiments, such as the "Toroidal pinch," Levitron, and CLEO are being supplied with new Modular One type computers.

As we know, analog-digital converters (ADC) play an important role in automating thermonuclear experiments. ADC units with a 200 nsec minimum time between measurements have been developed at Culham Laboratory on the basis of utilizing CAMAC integrated-module systems. This converter yields 256 time points and 128 intensity gradations for a single measurement channel. Fifty fast ADC connected to physical sensors have been installed for the "Toroidal pinch" experiment. In addition, there are another 50 channels with a slower converter for monitoring the process variables. This monitoring action is available before the experiment starts, so that the computer can give the OK for going ahead with the experiment.

A lot of work has been done at Culham on developing programs for effective complex functioning of small computers and of the central computer serving twenty distinct subscribers. Culham Laboratory has a direct telephone line to London University, where a large computer is installed. The rates for computations using this machine are four pounds sterling per hour.

In the next two years, new computer hardware referred to earlier in this article will be put into operation at the laboratory, and at that time Culham Laboratory will attain the level of the best modern nuclear physics laboratories in terms of its level of automatic processing capabilities for experimental data.

At the end of the visit, discussions on future scientific contracts were held on the initiative of the administration of Culham Laboratory. The laboratory administration specifically expressed the wish to continue the participation of British physicists in the tokamak experiments underway at the I. V. Kurchatov Institute of Atomic Energy.

RESONANCE TRANSFORMER FOR MINIATURE ACCELERATOR FACILITIES

B I. Al'bertinskii, A. T. Ermolaev,
Ya. Ya. Pil'kevich, and G. I. Polyakova

An experimental prototype of a resonance transformer with a voltage rating of 1 MV has been developed and tested at the D. V. Efremov Electrophysical Equipment Research Institute [NIIÉA]. The transformer is intended to supply an accelerator tube in a miniature transportable or stationary accelerator facility. Depending on the type of anode assembly in the tube, the facility may be used either as a source of accelerated electrons for irradiating various materials and objects, or as a source of x-rays in nondestructive testing.

The general design features of the resonance transformer and the accelerator based on it are well known. A magnetic baffle with the cooling system of the equipment, the transformer primary and secondary coils (Fig. 1b), the high-voltage electrode and the accelerator tube with its power supplies and cathode controls, are housed in a steel tank (Fig. 1a). The anode assembly of the tube protrudes out from the tank, where the focusing coil is located, and the electron beam scanning and starting system can be located there should the need arise.

The use of compressed dry nitrogen with 10% electronegative gas or Freon-12 added, at an operating pressure of 10 kg/cm^2 in the tank, as the basic insulation, and voltage of heightened frequency (430 to 500 Hz) used as the supplies, not only made it possibly to shrink the size of the equipment down in design, but also to lessen the total weight of the equipment appreciably. As a consequence, the resonance transformer together with the accelerator tube and the power supply pack could be fitted in a tank 912 mm in

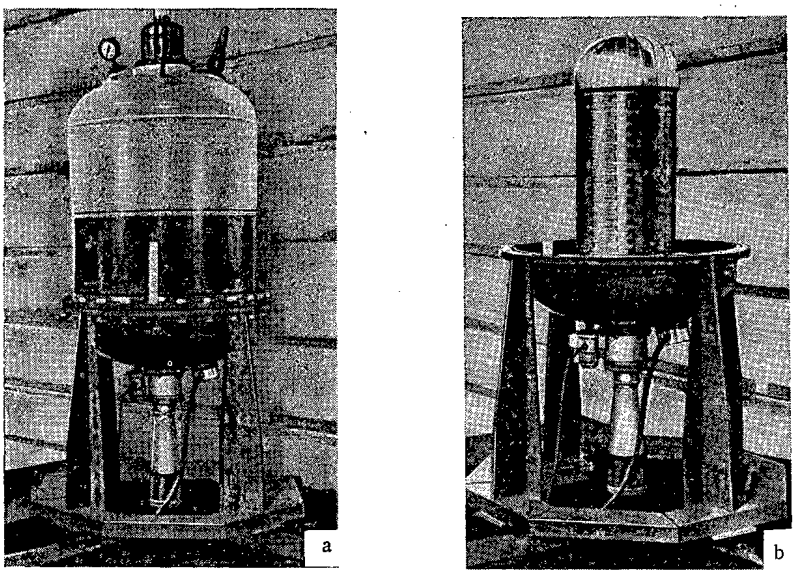

Fig. 1. X-ray equipment, 1 MeV, based on resonance transformer and mounted on test stand: a) as assembled; b) with part of high-pressure vessel removed.

Translated from Atomnaya Énergiya, Vol. 30, No. 4, pp. 407-409, April, 1971.

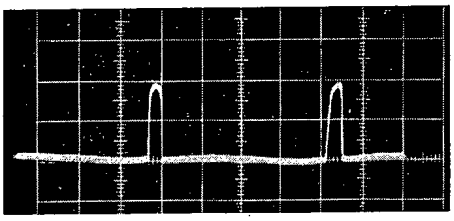

Fig. 2. Shape of load current curve of resonance transformer (U = 1000 kV; I_{max} = 27 mA; f = 470 Hz).

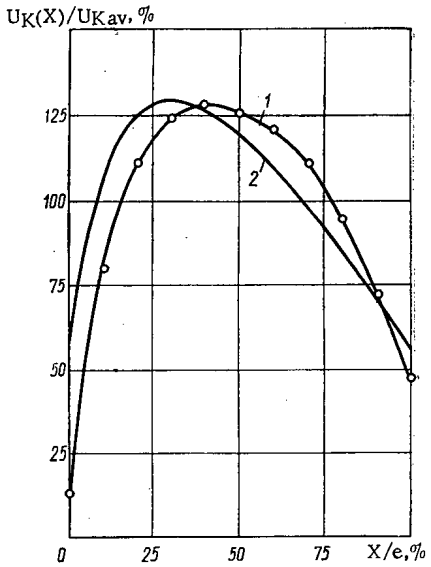

Fig. 3. Voltage distribution over the length of the secondary winding of the resonance transformer: 1) experimental data; 2) predicted data.

diameter and 1450 mm in length (without the ventilator hood), with that part of the facility weighing 740 kg.

The use of supply voltage at elevated frequencies, and the consequent increase in the reactive power of the transformer, entail an increase in the load current rating of the facility. In particular, a beam of accelerated electrons with a maximum current of 27 mA in a burst (Fig. 2) was obtained when the equipment was tested in the x-ray variant. No distortions in the shape of the secondary voltage curve of the resonance transformer were detected. Estimates showed that the load current of the equipment could be stepped up to 30-50 mA when power supplies of suitable output are used.

Certain difficulties due to the need to achieve a uniform voltage distribution over the basic sections of the accelerator tube, and the need to achieve appropriate focusing potentials across the tube electrodes in the initial phase of acceleration, showed up when the resonance transformer was perfected as a high-voltage source for accelerator facilities. Calculations demonstrated that the voltage distribution over the secondary coil of the resonance transformer is not uniform. Measurements carried out with the aid of specially embedded probe turns on an operating transformer, over a voltage range from 20 to 700 kV, confirmed the design calculations (Fig. 3). Moreover, these measurements removed the danger that the voltage distribution over the transformer winding may vary depending on the output voltage of the equipment. This in turn opens up the possibility that any required distribution over the 12 sections of the accelerator tube can be attained by utilizing dense compartmentalization of the transformer secondary (120-130 sections). It should be pointed out that the focusing quality of the electron beam in the accelerating tube, in a resonance transformer, does not depend quite as much, as in the case of other facilities, on the ratio of voltages across the first accelerating electrodes (which are essentially focusing electrodes). The reason is that the accelerating tube is located on the axis of the transformer secondary solenoid, and the magnetic field established by this winding, even though modest in magnitude, enhances beam focusing because of the almost ninety-degree phase shift resulting.

One of the important characteristics of an accelerator facility designed especially for use under production conditions or pilot-plant conditions, is operational reliability. In the case in point, this operational reliability is determined to an appreciable extent by the operational reliability of the resonance transformer per se. It was found, during the tests, that the short-term electrical strength of the resonance transformer itself was not less than 1400 kV provided the insulating gas mixture was properly desiccated. The electrical strength of the transformer was tested additionally by operating it for six hours continuously at 1200 kV. The absence of discharges, of any disproportionate increase in idling losses, and of any other abnormalities in the course of this experiment testified to the adequate reserve of electrical strength possessed by the equipment at the rated voltage of 1000 kV.

The investigations performed made it possible to develop a miniature 1 MV transportable x-ray equipment on the basis of the resonance transformer. When this equipment is provided with the necessary starting and scanning devices, it is capable of functioning as a powerful, reliable, and inexpensive source of accelerated electrons for industrial use on a broad basis.

THE KVANT DATA TRANSFER SYSTEM

I. N. Ivanov, V. V. Eldashev,
and V. V. Filippov

The Kvant ("Quantum") data transfer system is designed to facilitate automatic readout of data from multichannel analyzers of types AI-1024 and AI-4096, and transfer of that data to the rapid-access memory of a Minsk type computer via a regular communications cable.

The system is designed in the form of two stands (one for transmitting and one for receiving) and an outboard control panel. The transmitting stand is placed near the analyzer. It incorporates a matching device linking up with the analyzer, a translator (transmitter), a device for data readout from a page teletype apparatus, and power supplies.

Data is transferred from the analyzer to the computer via multicore telephone cable. The data can also be read out of the analyzer via a RTA-60 page teletype (on punched tape with simultaneous printout on paper), or via a PL-150 tape puncher or PL-80 tape puncher (on the receiving stand). Data punched out in M2 telegraph code comes with all the accessory punch symbology (beginning of data field, gaps, end of data field, etc.). The system operates as an automated unit.

Data can be transferred manually to selected MOZU memory cells of the computer by using the keyboard on the outboard control panel of the Kvant system. Accuracy of the data transferred is monitored by appropriate visual signals on the control panel.

The modular functional design principle in the system allows utilization of data readout units separately, on the PL-150 and on the RTA. Also built into the system is the option of communicating with other types of computers or analyzers, when the appropriate modifications are made in the matching devices.

The system can be operated continuously for 12 h out of the day. It is supplied from ac lines at 220 V ± 10%. The power intake is not greater than 300 W.

The Kvant data transfer system is usable with communications extending 1000 m in cable length. The transfer code for data readout from multichannel analyzers is an 18-digit binary code, and data transfer from VPU devices is based on a 20-digit binary-decimal code. The transfer rate on the communications cable is 30,000 bits per second, the data readout rate onto punched tape via the PL-150 tape puncher is ~20 bits/sec, or ~10 bits/sec via the PL-80 tape puncher ~1 bit/sec via the RTA-60 page teletype. The operational reliability of the system is characterized by one malfunction (at maximum) per 20,000 bits.

Translated from Atomnaya Énergiya, Vol. 30, No. 4, p. 409, April, 1971.

MINIATURE HYDRAULICALLY POWERED CENTRIFUGAL EXTRACTOR

G. I. Kuznetsov, M. F. Pushlenkov, and G. N. Yakovlev

A miniature centrifugal extractor, MTsÉ-300 model [1], with a 300 cm^3 compartment volume has been built (Fig. 1). A hydraulic motor 1 is employed in this extractor with the object of enhancing the reliability of the power drive under severe radiation loads. The engineering characteristics of the MtsÉ-300 are: size 340 × 340 × 400 mm; capacity 200 liters/h; volume of mixing chamber 100 cm^3; separation chamber volume 150 cm^3; phase contracting time 1.8 sec; diameter of extractor compartment 115 mm; phase carryover not greater than 0.02%; efficiency not less than 99%; shaft rotation speed 2800 rpm; power output of drive hydraulic motor (G15-2) 260 W; reducing gear transfer ratio 1.1; basic structural material Kh18N10T steel; total weight of extractor and hydraulic motor combined 64 kg.

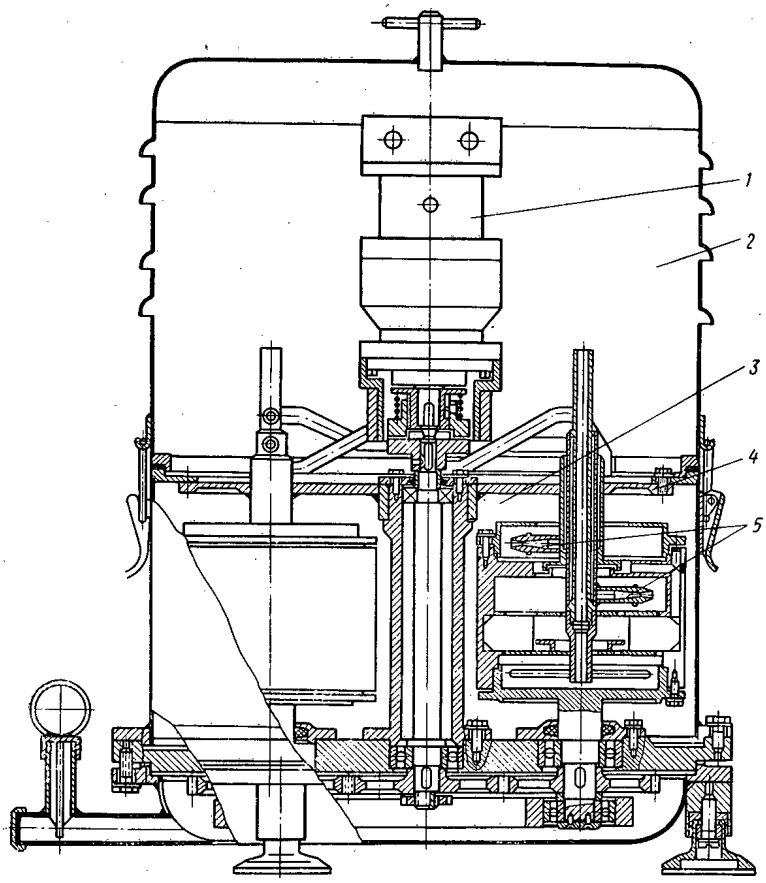

Fig. 1. MTsÉ-300 miniature centrifugal extractor powered by G15-2 hydraulic motor.

Translated from Atomnaya Énergiya, Vol. 30, No. 4, pp. 410-411, April, 1971.

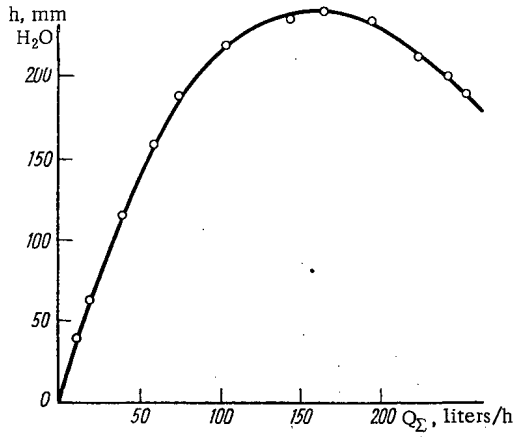

Fig. 2. Dependence of rarefaction in MTsÉ-300 operating region on total throughput.

TABLE 1. Dependence of Basic Characteristics of G15-2 Hydraulic Motor and the Number of Motors Serviced by One ÉMN-1, 25/100

Basic characteristics of hydraulic motors	Number of hydraulic motors				
	13	10	8	7	6
Oil flowrate, liters/h	400	800	1300	1700	2100
Shaft speed, rpm	500	1000	1500	2000	2500
Power, W	20	60	125	180	260

The hydraulic motor zone 2 is separated off from the extractor zone 3 by a hermetically sealed membrane 4. A rarefaction of 250 mm H_2O is brought about in the extractor zone by the operation of the bleeding valves 5 (see graph, Fig. 2). This not only eliminates loss of slurry through evaporation, but also keeps radioactive aerosols from getting into the surroundings.

The hydraulic motor is caused to rotate through momentum imparted to mineral oil of viscosity 4-12 E supplied by an ÉMN-1, 25/100 electric screw pump. Experimental data on tests of the arrangement with several built-in hydraulic motors in series supplied by a single pump are given in the accompanying Table 1. The oil pressure at the inlet to the first hydraulic motor was 50 atm. The tabular data indicate that a single ÉMN-1, 25/100 hydraulic (oil) electric screw pump is capable of energizing six four-compartment MTsÉ-300 extractors.

Tributylphosphate was also used as the hydraulic fluid in testing the arrangement of hydraulic motors alluded to. The basic hydrodynamic characteristics of the pump and hydraulic motors were the same in this case as when mineral oil was used as hydraulic fluid.

LITERATURE CITED

1. MTsÉ-150, At. Énerg., 28, 244 (1970).

PROXIMATE ANALYSIS OF FIELD WORK GEOLOGICAL SAMPLES WITH PORTABLE NEUTRON GENERATORS

V. A. Kasatkin, D. I. Leipunskaya,
S. I. Savosin, and Yu. G. Chulanov

Successful prospecting and exploration of occurrences of natural minerals depend to a considerable extent on capability, accuracy, and precision in analytical laboratory and field work. Methods of rapid ultimate analysis suited to applications directly in field work can render valuable assistance here. Promising groundwork for arriving at an efficient method of proximate analysis in field work is seen in neutron activation analysis using portable neutron generators (E_n = 14.5 MeV).

A transportable equipment set incorporating a portable neutron generator [1, 2] was devised with the object of shedding light on the possibilities for developing field methods of proximate analysis of geological samples. This entire set of equipment is accommodated in the closed body of a truck. The set includes a neutron generator with a sealed-off accelerating tube (NGI-1, NGI-4, or NGI-5) and neutron yield of 10^8 to $3 \cdot 10^8$ neutrons/sec, a system for monitoring neutron flux, dosimetric inspection instruments, a pneumatic conveying device for displacement of the specimens, and recording equipment capable of carrying out measurements of γ-activity and β-activity, and taking spectra of γ-emission, $\beta - \gamma$-coincidences, and $\gamma - \gamma$-coincidences. The measuring equipment includes two scintillation counters enclosed in a lead castle. Spectrometric NaI(Tl) crystals sized 70 × 70 mm and FÉU-56 or FÉU-82 phototube multipliers are employed to record the γ-emission.

The equipment is designed for use with a combined fast-flow coincidence sampling arrangement. The resolving time of the fast coincidence circuit is $5 \cdot 10^{-8}$ sec, and the resolving time for the slow coincidence circuit is $4 \cdot 10^{-6}$ sec.

Investigations carried out under field conditions showed that the following types of analysis can be carried out with the existing parameters of the equipment: 1) simultaneous determination of contents of aluminum and silicon in different alumosilicate rocks and in untreated aluminum ore; 2) determination of copper content in cupriferous ores; 3) analysis for phosphorus, fluorine, aluminum, and silicon in phosphorites and apatites. Determination of aluminum and silicon is handled by activating those elements through the reactions $Al^{27}(n, p)Mg^{27}$ ($T_{1/2}$ = 10.0 min) and $Si^{28}(n, p)Al^{28}$ ($T_{1/2}$ = 2.3 min). Gamma-radiation due to the induced activity is recorded in two energy ranges: 0.75 to 0.95 (Mg^{27}) and 1.65 to 1.95 (Al^{28}) MeV. The silicon content is determined from the integrated count in the energy range mentioned, while the aluminum content is determined from the difference count (by the method of subtracting the Compton contribution from the γ-emission of the isotope Al^{28} in the energy range from 1.65 to 1.95 MeV). At a neutron emission intensity of $2 \cdot 10^8$ neutrons/sec and sample weight of 10 g, the sensitivity of the analysis is $n \cdot 10^{-1}\%$ Al_2O_3 and $n \cdot 10^{-2}\%$ SiO_2. It takes about 10 min to complete the entire analysis.

The use of the NGI-4 portable neutron generator made it possible to work out a procedure for precision determination of silicon, which is an especially important advance for analysis of standard rock species. Weighed portions of pulverized silicon used in the fabrication of semiconductors, and weighed portions of optical grade quartz, were used as reference standards. The relative rms error for a single SiO_2 analysis was 1.2% when the total SiO_2 content was 40-50%. An accuracy of 0.25% was achieved in the analysis in a run of 26 measurements.

The need to develop a method for determining phosphorus in phosphorites with the aid of neutron generators is dictated by the fact that existing proximate methods of analysis are based on the correlation

Translated from Atomnaya Énergiya, Vol. 30, No. 4, pp. 411-413, April, 1971.

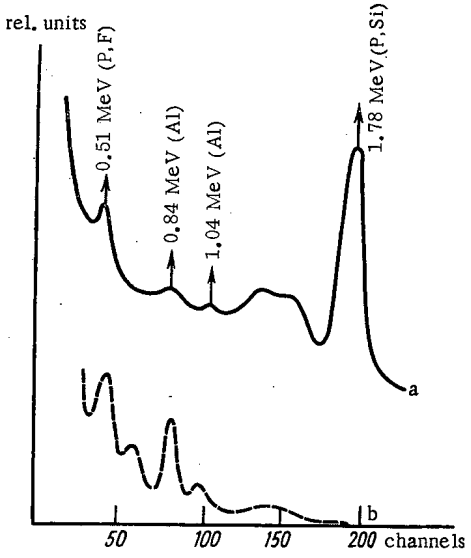

Fig. 1

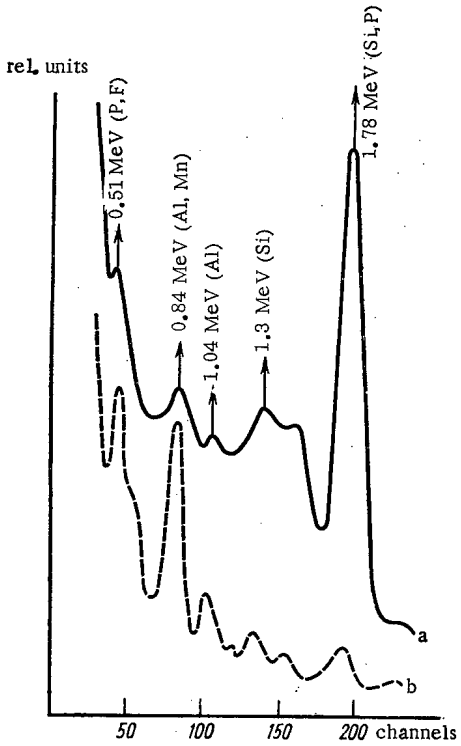

Fig. 2

Fig. 1. Spectrum of γ-emission from induced activity of a sample of phosphorite rock (weighing 1 kg) irradiated by the portable neutron generator: a) "cooling" time 1 min; b) "cooling" time 22 min.

Fig. 2. Spectrum of γ-radiation due to enhanced activity in a block of sandstone –phosphorite rock (weighing about 50 kg) irradiated by the portable neutron generator: a) "cooling" time 8 min; b) "cooling" time 25 min.

relationship between phosphorus and fluorine, or between phosphorus and uranium. But there are occurrences of phosphorites where rigorous correlation relationships do not obtain, and indirect methods are practically unfeasible in those instances.

The reactions $P^{31}(n, 2n)P^{30}$ and $P^{31}(n, \alpha)Al^{28}$, which yield short-lived radioactive isotopes, are of greatest interest from the standpoint of direct analysis for phosphorus. Practical phosphorus determinations in rocks can be achieved only through the (n, 2n) reaction. The reason is that silicon responding to activation by fast neutrons through the (n, p) reaction yields the isotope Al^{28}, and is present in significant quantities in all rocks. The radioactive isotope P^{30} forming via the (n, 2n) reaction is a positron emitter, and the line of this isotope, $E_\gamma = 0.511$ MeV, shows up in general very weakly over the entire γ-energy spectrum against the Al^{28} background. The use of the fast–slow coincidence sampling arrangement makes it possible to reduce the background by more than 10^3 times, while at the same time improving selectivity of the measurements in the selected energy range about 40 times.

A serious disturbance in recording emission from the P^{30} in the coincidence method is the contribution due to formation of pairs generated by hard γ-radiation, in particular by silicon. The masking contribution due to the pair formation effect was taken into account by running parallel measurements of the radiation intensity in the region of the 1.78 MeV photopeak, and the γ–γ-coincidences were sampled in the 0.42 to 0.62 MeV energy range.

Fluctuations of the neutron flux and instability in the performance of the equipment were corrected for in the light of data on sequential measurements of copper standards irradiated at the same time as the field sample.

The procedure was tried out on phosphorites from various types of occurrences. The sensitivity was 0.5% P_2O_5. The accuracy of the analysis depends on the silicon content, and is 5-7% in the case of ores containing 5-15% P_2O_5 and 3-5% in the case of ores containing more than 15% P_2O_5.

A similar procedure was applied to copper analysis on cupriferous ores. The reaction $Cu^{63}(n, 2n)Cu^{62}$ was utilized for that purpose. Copper determinations were carried out in different types of copper, copper–lead, and copper–molybdenum ores. Sensitivity was $5 \cdot 10^{-2}$% Cu. The accuracy of the analysis corresponds to requirements imposed on laboratory analysis of samples in tallying of copper ore reserves.

In copper determinations carried out in ores with an enhanced zinc content, a systematic bias raising the copper content findings was detected, and attributed to activation of the zinc through the reaction $Zn^{64}(n, 2n)Zn^{63}$ ($T_{1/2}$ = 38 min). When the copper content and zinc content are equal, the Zn^{63} activity is found to be one-tenth that of the Cu^{62}, and the systematic error is not so troublesome in the case of copper–zinc ores in which the copper content is far greater than the zinc content, in which case the bias can be eliminated through reliance on special standards.

When zinc content is high, the masking effect of the zinc can be coped with by utilizing the results of a repeated measurement carried out after the Cu^{62} atoms have almost all decayed (in about 1 h).

It is important to estimate the ultimate composition in representative samples before the comminution stage within a very short time, in analysis of geological field samples in ore assay work. Depending on the type of mineral and mode of mineralization, the weights of the representative samples will fluctuate anywhere between a few hundred grams and tens of kilograms.

Figure 1 shows the γ-ray spectrum of induced activity of a sample of phosphorite rock weighing 1 kg irradiated by the portable neutron generator.

Figure 2 shows the γ-ray spectrum of a sandstone–phosphorite rock irradiated and measured in a barrel (about 50 kg). In this case, the enhanced peak in the 0.84 MeV region, after a 25 min "cooling" period, testifies to the presence of manganese activated via the reaction $Mn^{55}(n, \gamma)Mn^{56}$ (2.56 h) by neutrons slowed down while traversing the bulk of rock with a high moisture content. Analysis of the small sample showed that the iron present in this case makes no appreciable contribution to the activity of the Mn^{56}.

The development of hardware for neutron activation analysis in the field, and in particular the use of portable neutron generators with a higher neutron yield (10^9 to 10^{10} neutrons/sec) expands the area of application of the method considerably.

LITERATURE CITED

1. B. G. Egiazarov et al., At. Énerg., 20, 252 (1966).
2. A. K. Berzin et al., in: Proc. of the Sci.-Engng. Conf. on Activation Analysis Equipment, TsIFI, Budapest, 1968 [in Russian], COMECON Secretariat, Moscow (1969), p. 196.

BRIEF COMMUNICATIONS

A conference of specialists from COMECON member-nations on production of radioactive medicinal preparations was held in October, 1970, in Budapest, as part of the program of the Permanent Commission of COMECON on the peaceful uses of atomic energy.

The conference discussed findings of engineering cost research on production of these following items in the COMECON countries: tagged mercury isotopes, selenium-75-labeled *l*-selenomethionine, cobalt-labeled vitamin B_{12}, and medicinal preparations for research in vitro. The possible volumes of production capable of meeting the demands of COMECON member-nations in these products were determined, and the characteristics of the preparations were also considered. Suggestions on specialization in the production of various specific medicinal preparations were drawn up at the conference.

* * *

A delegation of Swedish specialists on reactor materials visited the Soviet Union from November 23 through December 4, 1970. The five-person delegation visited the I. V. Kurchatov Institute of Atomic Energy, the Power Physics Institute, the Khar'kov Physics and Engineering Institute, and the Atomic Reactor Research Institute (Melekess). The Swedish scientists discussed a number of topics relating to reactor materials, and of general interest, with Soviet specialists.

Translated from Atomnaya Énergiya, Vol. 30, No. 4, p. 413, April, 1971.

A. M. Petros'yants

FROM SCIENTIFIC RESEARCH TO ATOMIC INDUSTRY*

Reviewed by A. F. Tulinov and O. P. Shevchenko

The list of Soviet popular scientific literature on the utilization of atomic energy is enriched by this new book. The author of this book is well acquainted with the state of the art in this branch of the national economy, so that the presentation of the material is distinguished by its breadth and historical reliability.

The red thread running through the entire book is the concept of displaying to the maximum the practical feasibility and applicability of atomic energy. The dynamic character evident in the book's title was not chosen randomly, and reflects the author's basic underlying concept: a gradual and at the same time exceptionally rapid transformation of the first results of scientific research in the field of nuclear physics, undertaken several decades back, into a major branch of industry, an extensive complex of trends and developments in science and engineering.

We have to admit that it is impossible to find other examples in the history of science where a slow development of one of its "pure" scientific research trends, that of nuclear physics, supported by the creative zeal of individual enthusiasts of that branch of knowledge, flowered forth in such consequences and results capable of exerting such a sweeping effect on the life of literally all of humanity. It is precisely in the attempt to demonstrate this entire vast array of modern practical applications of atomic energy and the scientific trends in its development that the principal difficulties tackled by the author come to light. On the one hand, the breadth of the range of readers to whom the book is addressed calls for a presentation made as interesting, or "entertaining," if you will, as possible. On the other hand, the seriousness and complexity of the subject matter concerning applications of atomic energy and the related sciences rule out simplified popularized treatment, not to mention the fact that the Soviet readership, fairly well developed in terms of scientific and technical understanding, would not welcome any attempts in that direction. Finally, the author posed himself the task of generalizing and reviewing technical information strewn over a large number of scattered publications. In other words, the scope, and to a certain extent, the reference character of some of the material covered in the book in themselves constitute a burden difficult for any author to shoulder.

Satisfaction of all these contradictory requirements is no simple task, and the author nevertheless managed to come out on top. To a certain extent, success in coping with this problem can be credited to the fact that the author of the book has ample experience behind him in the publication of scientific and popular articles.

As stated earlier, the book encompasses a wide range of topics. There is not sufficient space to detail them all. But the book material can be grouped under the following headings: history of nuclear physics research, accelerator techniques, thermonuclear fusion, reactor engineering (research, electric power, and propulsion aspects), isotopes and their applications, atomic scientific research centers in the USSR and their activities, and international aspects of the utilization of atomic energy.

Naturally, in keeping with the actual state of affairs in this area, a different scale has to be assigned to treatment of the various topics. Nuclear power, for instance, given the enormous weight and results associated with it in its place in the national economy, gets a lion's share of the attention and space. There is a detailed survey of the evolution of the technical characteristics of power reactors, and ample treatment

*Atomizdat, Moscow, 1970, 310 pp.

Translated from Atomnaya Énergiya, Vol. 30, No. 4, pp. 414-415, April, 1971.

of the contents and underlying thinking of Soviet nuclear power policies, governed by a number of competing factors in the existing and anticipated fuel–power balance of our country.

In covering most of the trends in scientific and engineering research, the author does not limit his treatment to a retrospective glance or to the present state of affairs in a particular branch of knowledge, but rather seeks out the interesting concepts and viewpoints relating to future trends along various lines. Sufficient sensitivity and sense of proportion are manifested, since attempts at a popular treatment of the future of atomic energy are invariably attended by hazards of ungrounded fantasy and blue-sky prospects. At the same time, the author does not take on the task of forecasting, since the area of prognosis has become an independent and complex scientific discipline which is only in its rudimentary stages, in the Soviet Union as well as elsewhere.

Especially noteworthy is the moderate and refreshing "dilution" of the book's material by spacing it out with descriptions of several episodes from the routine life of the author when they provide excellent illustrations of the technical matters covered. The author draws upon a vast store of personal impressions based on personal encounters with leading Soviet and foreign specialists in the field of atomic energy. For that reason, the presentation of these episodes in the course of discussing certain topics renders the book more interesting, and in fact quite lively.

The author proceeds correctly in "dropping" an extended list of names of scientists and specialists working in the field of atomic energy, with outstanding results to their credit. The personal aspects of the book constitute a tribute and paying of due respect to those whose work has been in large measure responsible for the advances of Soviet atomic science and atomic industry in the case of practical utilization of nuclear energy. Unfortunately, this ethical side is too often ignored in other publications of the type.

Some critical comments could be advanced as well. But not a single one is sufficiently serious to merit detailed discussion. On the whole, then, the book deserves only kudos. It will be read with interest and profit by the readers to whom it is addressed.

A. I. Abramov, Yu. A. Kazanskii, and E. S. Matusevich

FUNDAMENTALS OF EXPERIMENTAL NUCLEAR PHYSICS TECHNIQUES*

Reviewed by A. F. Tulinov and O. P. Shevchenko

This book is a textbook for students taking the course on experimental nuclear physics techniques at higher educational institutions, and given in many institutes and universities throughout the country. The first, introductory, portion of the book takes up the properties and parameters of radiation sources, the basic processes of interaction between radiation and matter, and information on statistical laws and distributions needed in the processing of experimental data.

The second part of the book describes various detectors of nuclear radiation, with the main stress placed on analysis of the characteristics which govern the feasibility of applications of those detectors in a particular nuclear physics experiment (efficiency, speed of response, shape of curve, etc.).

The third part is devoted to spectrometry of nuclear radiation. Methods of spectrometry of charged particles, γ-photons, and neutrons are discussed. The fourth, and last, part deals with methods for taking various nuclear physics measurements (activity of sources, neutron cross sections).

*Atomizdat, Moscow, 1970, 395 pp.

It should be pointed out that the book was written by experimental physicists working in a scientific research institute, who in addition to their regular work have been giving lectures in nuclear physics at the Obninsk branch of MIFI for several years. This experience has had a positive effect on the level of presentation of the material, from both a basic scientific standpoint and from a pedagogical standpoint. Apparently, this is what predetermined the clear "bent" visible in the direction of neutron research, a bias which is more of an asset to the book than a liability, since it is precisely neutron physics which lies at the basis of most practical applications of atomic energy, and the number of specialists being trained with heavy emphasis in that area is particularly large.

Nevertheless, from our vantage point we find it more useful to give more detailed treatment to methods of nuclear spectroscopy (and not solely to methods for measuring the energies of particles, as done in Chapters 10-12), and also methods of studying photonuclear reactions and reactions brought about by charged particles. Furthermore, it would have been helpful to discuss statistical techniques of measurements which have gained popularity in recent years in the study of neutron spectra, in some nuclear-reactor investigations, and in many other applications. These remarks may be taken into account in future editions of the text.

It could also be pointed out that the book is well edited, and the illustrative material contained in it is capable of providing much material of a reference nature not only for students, but also for instructors and specialists working in nuclear physics laboratories.

ERRATA

To the article "Subbarrier neutron fission of Pu^{238}" by S. B. Ermagambetov and G. N. Smirenkin (Vol. 29, No. 6, pp. 1190-1192, December, 1970):

Reference [9] was erroneously cited in the caption to Fig. 1. The data denoted by open squares in that figure was taken from an article by É. F. Fomushkin and E. K. Gutnikova [Yadernaya Fizika, 10, 917 (1969)]. The reference [9] mentioned in the text of the article is correct.

Translated from Atomnaya Énergiya, Vol. 30, No. 4, p. 403, April, 1971.

TOPICS IN MATHEMATICAL GEOLOGY

Edited by **M. A. Romanova**
and **O. V. Sarmanov**
Laboratory of Mathematical Geology, Leningrad, USSR

Translated from Russian

Contains papers by eminent authorities on applications of mathematics to geology ranging from the most complex investigations to the simplest applications of mathematics to geological problems. Topics covered include experimental petrology, regional lithology, tectonics, methods of computing reserves, and selection of computers. The book is of interest to geologists, geophysicists, and geochemists at all levels.

CB Special Research Report
Approx. 281 pages 1970 $37.50

PLENUM PUBLISHING CORPORATION
Plenum Press • Consultants Bureau • IFI/Plenum Data Corporation
227 WEST 17th STREET, NEW YORK, N. Y. 10011

In United Kingdom: Plenum Publishing Co. Ltd., Donington House, 30 Norfolk Street, London, W.C. 2.

Far-Infrared Properties of Solids

Edited by **S. S. Mitra** and **S. Nudelman**
Department of Electrical Engineering
University of Rhode Island

This book provides an excellent account of recent studies relating far-infrared radiation to properties of solids. Because it both indicates the scope of the subject and examines important areas in depth, it serves as an invaluable source book for researchers and graduate students in the field of optical physics.

Careful organization and a thorough treatment of material further insure its usefulness. The first six chapters present experimental considerations for recording measurements in the far-infrared spectral region, while they also provide a helpful introduction to the subsequent chapters which deal with theoretical areas in the study of far-infrared properties of solids. Important reference material is included in the body of the work. Placing a continuation order for the series guarantees delivery of this and other volumes **immediately** upon publication.

Proceedings of a NATO Advanced Study Institute, held in Delft, Netherlands, August 5-23, 1968

Approx. 515 pages Plenum Press 1970 **$25.00**

SBN 306-30491-0

PLENUM PUBLISHING CORPORATION 227 WEST 17th STREET, NEW YORK, N. Y. 10011
Plenum Press • Consultants Bureau • IFI/Plenum Data Corporation

In United Kingdom: Plenum Publishing Co. Ltd., Donington House, 30 Norfolk Street, London, W C 2.